A MACH 1.95 FREE-JET FACILITY FOR EXPERIMENTAL INVESTIGATION OF INJECTANT FLOW PATTERNS

by

John Richard Mills

Thesis submitted to the faculty of the

Virginia Polytechnic Institute and State University

in partial fulfillment of the requirements for the degree of

MASTER OF SCIENCE

in

Mechanical Engineering

APPROVED:

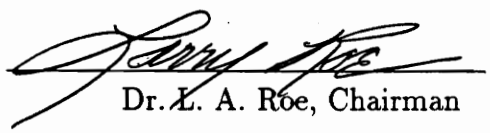

Dr. L. A. Roe, Chairman

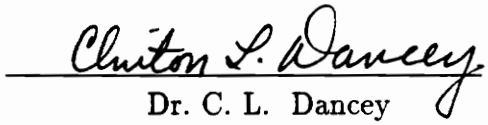

Dr. C. L. Dancey

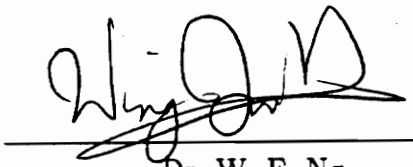

Dr. W. F. Ng

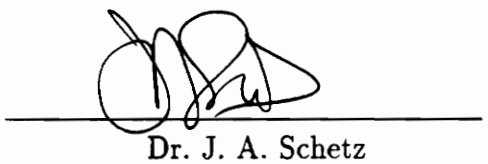

Dr. J. A. Schetz

October 1991

Blacksburg, Virginia

A Mach 1.95 Free Jet Facility for Experimental Investigation of Injectant Flow Patterns

by

John Richard Mills

Dr. Larry A. Roe, Chairman

Mechanical Engineering

(ABSTRACT)

Inspired by the need to study injectant flow patterns near the test surface, a supersonic free-jet facility was designed and constructed. This facility provides a Mach 1.95 flow over a test section area of 6.35 cm by 5.08 cm. The facility was thoroughly tested and proved that it is durable, versatile and capable of providing repeatable test conditions. When compared to the main supersonic tunnel at VPI & SU, the free-jet facility has many advantages, including greater optical and spatial access, longer available test durations and less time needed between tests for the storage tanks to be refilled. As a part of the project several diagnostic techniques were evaluated in the facility. Normal, sonic injection of helium through a circular injector was studied as a way to evaluate nanoshadowgraph photography, oil flow photography and infrared imaging as qualitative flow visualization methods. Quantitative measurements of the local helium concentration within the boundary layer were taken to evaluate the effectiveness of an existing hot-film concentration probe. The tests showed that oil flow visualization is a very effective technique in the free-jet facility, producing clear photographs that could be directly scaled. Nanoshadowgraph photography also produced clear photographs of the flow field, although this method was more difficult to implement in the free-jet facility than in the main supersonic tunnel.

Finally, infrared imaging, which was not possible in the main supersonic tunnel without major hardware reconfigurations, showed great promise as a method for studying normal injection. Although the tests revealed no conclusive information about injectant flow patterns in the boundary layer, a heat transfer analysis showed that it may be possible in future studies to use this technique as a way to quantitatively measure local helium concentration at the surface. Helium concentration was measured for test cases with both air and helium injection. The measurements were taken at two axial locations with the probe positioned a distance of 0.1 injector diameters above the test surface. The air injection tests showed helium concentration levels up to 30 percent mole fraction, which is erroneous, since no helium was present in the flow. Based on these results it was concluded that the existing probe was ineffective in the free-jet facility, with an uncertainty level of no less than 25 percent mole fraction helium. The cause of the high uncertainty and overall ineffectiveness was most likely the probe calibration and data reduction methods.

Acknowledgments

I wish to express my sincere appreciation to my academic advisor and friend, Dr. Larry Roe, for his guidance, patience, and support during my graduate career. Many thanks are also due to my committee members, Dr. C. L. Dancey, Dr. W. F. Ng and Dr. J. A. Schetz, for their helpful suggestions. I would also like to thank Dr. C. Hurst for his contributions to the design of the sound insulation room and Dr. D. Nelson for his help with the infrared imaging system.

Many thanks are in order for the entire Mechanical Engineering Shop, especially Jerry Lucas and Johnny Cox. I also received a great deal of support from Frank Shelor, Jake Frazier and Kent Morris of the Aerospace Engineering Shop. My appreciation also goes to Gary Stafford, who provided assistance throughout the entire project. All of these people contributed greatly to my educational experience.

I am especially grateful for the tremendous support that was offered during the difficult and exhausting process of building the free jet facility and running the experiments. Much appreciation is extended to Jeff Collie, Ken Chadwick, Rodney Bowersox, Chuck Wood, Eric Fuller, Olivier Ferrandon, Matt Barber, Richard Mays, Kurt Schaubach, Vince Hatcher, Tracey Shea, Stacy Johnson, Bill Westerman, Becky Herrmann, Jane Walsh and Maz Zeinali. All of these people graciously contributed their time, ideas and resources throughout the entire project.

Table of Contents

List of Figures

List of Symbols

a - calibration constant for concentration probe

b - calibration constant for concentration probe

C_D - injector discharge coefficient

C_p - specific heat

d - jet diameter

γ - ratio of specific heats

h - convective heat transfer coefficient

i - current supplied by arc welder

k - thermal conductivity

l - hot film sensor length

m - calibration constant for concentration probe

$\dot{m}$ - mass flow rate of injectant

M - Mach number

Nu - Nusselt number

P - static pressure

P_T - total pressure

Pr - Prandtl number

q - heat flux

ρ - density

R - gas constant

R_b - effective radius (nondimensional parameter)

R_c - electrical resistance of injectant supply coil

R_s - electrical resistance of CTA bridge

R_w - electrical resistance of sensor

Re - free stream Reynolds number

t - thickness of injector block

T - static temperature

T_i - temperature of inner surface of injector block

T_o - temperature of outer surface of injector block

T_T - total temperature

T_w - sensor temperature

u - flow velocity

V - sensor voltage

x - axial distance downstream of the injection point

y - lateral distance from the jet centerline

z - distance from the test surface

Subscripts:

∞ - free stream property

CH - choked flow property

j - injectant property

1 Introduction

Injection of a gaseous jet into a supersonic crossflow is a very important topic in fluid dynamics. This problem has become even more critical with the continuing development of hypersonic, airbreathing flight vehicles, that will be propelled by supersonic combustion ramjet (scramjet) engines. Because the typical residence time in a scramjet combustor is on the order of milliseconds [1], effective mixing of the fuel and air is critical. Poor mixing will result in incomplete combustion, which will significantly reduce the engine's efficiency. Many supersonic injection experiments aim to simulate the injection of gaseous fuel in scramjet combustors. These experiments not only provide a means to compare different injection schemes, but they also provide a data base used to validate the computational fluid dynamics (CFD) research being done in this area. Various injection schemes have been experimentally investigated, including transverse injection, tangential injection through wall slots and various combinations of the two. Thomas, et al. [2] provide an excellent review of relevant injection experiments.

One problem found in many normal injection experiments is that a comparison between the mass flow rate of injectant downstream and the measured mass flow rate at the point of injection usually shows some discrepancy. The downstream mass flow rate is determined by a numerical integration technique that relies on the sampled mean flow data. Typically, the integrated mass flow

rate is 10 to 20 percent less than the measured value. Rogers [3,4] studied normal injection of hydrogen through injectors with a circular cross section for both a single injector [3] and an array of injectors [4], using an intrusive sampling probe to collect flow samples at various points in space. The hydrogen concentration in the samples was determined using a process gas chromatograph, while an orifice meter was used to measure the mass flow rate of the injectant. A typical result of the mass balance performed is given in Figure 1. Rogers concluded in both experiments that the apparent discrepancy was caused by large concentration gradients that reduced the accuracy of the numerical integration. He also noted that as the axial distance downstream of the injector increased, the gradients decreased, leading to better agreement.

Torrance [5] studied normal injection of various gases with molecular weights ranging from 2 (hydrogen) to 40 (argon). Like Rogers, he used an intrusive sampling probe to collect samples, a process gas chromatograph to analyze the samples and an orifice meter to measure the injectant flow rate. Torrance found the maximum mass flow deficiency from the numerically integrated data to be 20 percent of the measured mass flow rate. He also noted that, in general, the larger discrepancies occured when the injectant was helium or helium-air mixtures. Cohen, et al. [6] also found mass balance discrepancies in their normal injection studies.

Thomas, et al. [2] addressed the problem of mass imbalances in these early studies by postulating that the discrepancies may be due, in part, to selective sampling of the flow. Selective sampling occurs when a bow shock stands off from the tip of the sampling probe, causing spillage around the probe. If the flow sampled is a mixture of two gases, as many injection studies are, the lighter of the

two gases will be deflected by the spillage more than the heavier gas. The result is that a lower concentration of the lighter gas is sampled. Reis and Fenn [7] provide a more extensive study of the selective sampling process.

One way to avoid the selective sampling problem is to eliminate the bow shock at the probe tip. Ng, et al. [8] designed and used an aspirating, hot-film concentration probe that was designed with an internal divergence upstream of the sensor location and a choked orifice downstream of the sensor to eliminate the bow shock at the probe tip. This geometry causes a normal shock to be located inside the diverging tip, effectively swallowing the bow shock, and allowing for an undisturbed stream tube, equal in area to the probe inlet, to be sampled. Because most early experiments did not employ such concentration probes, it is likely that selective sampling had an effect on the results. This is one possible explanation for the sampled mass deficiencies found in the work cited earlier.

Most current injection studies employ a shock swallowing concentration probe or some non-intrusive method to determine injectant concentrations to avoid selective sampling. Recently, Wood [9] studied low angle helium injection using an aspirating, hot-film probe similar to the one designed by Ng, et al., while using an in-line flowmeter to measure the mass flow rate of the injected helium. Surprisingly, the results show an average sampled mass flow deficiency of roughly 20 percent. Other experiments using the same probe also show significant mass imbalances [10], which indicate that selective sampling may not have been the only cause of discrepancies in earlier work. One hypothesis to explain the discrepancies is that a portion of the injectant is entrained into a recirculation region upstream of the injector, and then passes around the jet core region within the boundary layer. The recirculation zones that result from normal injection are

illustrated in Figure 2.

Early indications of the recirculation region can be found in the analytical work of Schetz and Billig [11]. Schetz and Billig performed an analysis of normal injection into a supersonic crossflow by extending subsonic solid body modeling. This analysis includes a distinct separation zone upstream of the injector, the size of which is largely dependent on the ratio of the jet pressure to the effective back pressure, a concept they introduced. As this ratio is increased, the size of the separation region increases. The results of this analysis compare favorably with results from later experiments performed by Schetz, et al. [12].

The recirculating nature of the separated region is proven in more recent analytical and numerical studies. Weidner and Drummond [13] studied normal injection of hydrogen and helium using a computer code that solved for turbulent mixing, as well as the combustion of hydrogen and air. Non-reacting injection of both gases was studied, in part as a code validation, and revealed that a recirculation pattern exists within the separated region. Shuen and Yoon [14] also developed a CFD code for the study of turbulent mixing and chemically reacting flows in scramjets. Their study included transverse injection of helium, as well as the mixing and combustion of a transverse hydrogen jet. The non-reacting transverse injection cases clearly show a recirculation zone upstream of the injector. In fact, Shuen and Yoon make note of this region for its superior flame holding characteristics. Other studies that show a distinct recirculation zone include the work of Harloff and Lytle [15] and McDonough and Catton [16].

Many recent numerical simulations of non-reacting transverse injection show that a distinct amount of injectant is entrained into the recirculation region. Uenishi and Rogers [17] used a numerical code to study transverse injection of air

into a Mach 2 cross flow for three different injector configurations. Their results showed that, in all cases, a small amount of the injectant was entrained upstream. A later study by Uenishi, et al. [18] also showed this trend. Mao, et al. [19] performed numerical simulations for seven experimental injection configurations using the Langley Research Center SPARK family of CFD codes. The configurations included both normal and angled injection of hydrogen and helium. In all seven cases, upstream entrainment of the injectant was evident. The results from the simulation of hydrogen injection into a Mach 4.05 free stream are presented in Figure 3, which shows a plot of the hydrogen mass fraction contours. Carpenter [20] also studied many different injection schemes using the SPARK family of codes, with similar results.

The final persuasion for studying injectant flow in the boundary layer away from the jet core comes in the form of experimental results. Thomas and Schetz [21] studied normal injection of liquid and slurry jets into a Mach 3 cross flow. An erosive slurry was used to polish all surfaces in contact with the injectant, which resulted in a representative flow pattern of the injectant at the test surface. A sketch of the erosion pattern from one test case is presented in Figure 4. The results clearly show that a small amount of the injection is entrained upstream of the injector, and then is swept downstream far on either side of the jet core.

Typically, flow sampling proceeds laterally from the injector centerline outward until no more injectant is detected. Because this procedure only samples within the jet core region, it is possible that small amounts of the injectant may pass outside of this region, escaping undetected. Additionally, due to restrictions imposed by conventional, enclosed wind tunnels, sampling within the boundary

layer is often not possible. These are two of the hindrances that have limited studying the injectant flow patterns within the boundary layer away from the jet core region.

Hollo, et al. [22] studied normal injection of air into Mach 2 and 2.9 cross flows, measuring the injectant concentration using the planar laser-induced iodine flourescence technique. The results from these tests show that some of the injectant was entrained into the recirculation zone upstream of the injector. In fact, Hollo, et al. note this, and postulate that the entrained injectant may escape around the jet core region within the boundary layer. A similar study by Abbitt, et al. [23] shows similar trends.

This review of previous experimental and analytical work emphasizes the need to further investigate two areas of the flow: the area outside the jet core region and the area within the boundary layer. Whether the experimental means used are intrusive sampling techniques or non-intrusive optical techniques, the rigidity of a confined test section facility may become a limiting factor. Because of this, the goal of this research project was to design and construct a supersonic free-jet facility and evaluate diagnostic techniques to further study normal injection.

Free-jet facilities have many advantages over conventional confined test section wind tunnels, one of which is greater optical access, and thus are a useful addition to experimental facilities [24]. The present facility was designed with three specific flow visualization techniques in mind: nanoshadowgraph (and schlieren) photography, surface oil flow photography and infrared imaging. Each method benefits from not having any windows in the optical path, which become dirty and may distort the images. One drawback of the confined tunnel at VPI &

SU is that, due to the location of the windows, oil flow photographs may be taken at an angle no greater than about 60 degrees to the test surface, which makes interpreting and scaling distances in the photographs difficult. The free jet facility was designed to allow the photographs to be taken normal to, and at any distance from the test surface.

Perhaps the biggest motivation for developing a free-jet facility is the potential of using infrared imaging as a flow visualization technique. As of late, this technique has proven to be a useful way to evaluate surface flow patterns in subsonic [25,26], transonic [27] and supersonic [28,29] flows. Due to the structure of the confined tunnel at VPI & SU, infrared imaging of the test surface is not possible without many expensive and time consuming changes. First and foremost, since ordinary glass or plastic windows are opaque to infrared radiation, special windows made of sapphire or zinc selenide would be required. Secondly, because the available infrared imaging system has a liquid nitrogen cooled sensor, the camera cannot be positioned at an angle more than about 30 degrees from horizontal [30]. Because the test surface in the main supersonic tunnel is positioned in the horizontal plane, this restriction reduces the effectiveness of the technique. The free-jet facility avoids these problems by eliminating windows entirely and by positioning the test surface in the vertical plane, allowing for infrared images to be taken normal to the surface.

In addition to having greater optical access, the free-jet system also adds greater spatial versatility, which is an advantage when using intrusive methods for flow measurements. The main supersonic tunnel at VPI & SU is currently configured to allow sampling at only three axial locations, with limited range in the lateral direction. Also, due to spatial limitations, probes cannot easily sample

within the boundary layer or traverse in directions other than vertically without major reconfigurations. The free-jet facility allows for probes to traverse with virtually unlimited range in all directions. Sampling at the test surface is also possible because of the unrestricted nature of the facility.

Inspired by these advantages, the purpose of this research was to evaluate techniques applicable to normal injection studies in a free-jet faciltity by examining the flow within the boundary layer. The first part of the project was spent designing, constructing and testing a Mach 1.95 free-jet facility. The next major task was to evaluate three flow visualization techniques to determine their effectiveness in studying normal injection in the facility. Finally, measurements of the injectant concentration at the test surface were taken with an existing hot-film concentration probe to determine the effectiveness of the probe in the free jet facility. The circular injector used by Barber [31] in his investigation of normal injection was used in this research. Additionally, many of the test parameters and methods used in this work are similar to those used by Barber.

2 Free Jet Facility

All tests were conducted in the VPI & SU Mach 1.95 free-jet facility. Since this test system was constructed as a part of the project, it will be discussed in detail. A major criterion in the design process was to maximize the use of existing hardware. The most important components of the facility are the supersonic nozzle, the injection plenum and the test surface. Together these components are referred to as the test section.

2.1 Test Section

2.1.1 Mach 1.95 Nozzle

To provide the supersonic flow, a converging-diverging nozzle with a rectangular cross section was designed. A drawing of the nozzle is provided in Figure 5. The nozzle dimensions are:

Entrance Area	=	6.35 by 6.35 cm (40.3 sq cm)
Exit Area	=	6.35 by 5.08 cm (32.3 sq cm)
Throat Area	=	6.35 by 3.05 cm (19.4 sq cm)
Length	=	30.5 cm

The nozzle contour was calculated by the method of characteristics using a design code developed at the Naval Ordnance Laboratory in White Oak, Maryland [32]. The code provided 113 points to describe the two dimensional nozzle contour from the throat to the exit plane; the contour from the inlet to the throat was described by an additional 112 points. The dimensions of the nozzle were chosen considering many factors, including the mass flow rate required to operate the

nozzle at design conditions. Plumbing hardware limitations made a nozzle with a low flow rate most desirable. Another consideration in the design was the exit flow area, which must be large enough to insure that the existing injector model can be used. Considering these tradeoffs, a Mach 1.95 contour was chosen because it provides a flow well within the supersonic range, at a minimal flow rate and over a large enough flow area to use the existing injector model. Any additional increase in the nozzle Mach number would increase the pressure requirements for nozzle operation, which is not desirable. The depth of the nozzle was chosen as 6.35 cm to provide an adequate exit flow area. The nozzle inlet geometry was chosen to be a square to ease in the fabrication of the transition piece from the 15 cm diameter settling chamber.

The nozzle was machined from aluminum using a numerically controlled milling machine. The contour was cut by milling a linear, point-to-point path between the supplied coordinates. Once the nozzle contour was machined to the desired depth of 6.35 cm, a 1.9 cm thick aluminum plate was used to enclose the nozzle. This plate was secured by eight $\frac{5}{16}$ - in bolts and sealed with two o-rings to prevent any leakage during facility operation. Finally, a rectangular flange with ten $\frac{5}{8}$ - in bolt holes was secured to the inlet side of the nozzle to make connection to the facility plumbing easy. This modular construction method will make any future changes to the facility much easier to implement.

2.1.2 Plenum Chamber and Test Surface

The injection plenum serves mainly as a stagnation chamber for the injectant. The plenum was designed to be used interchangeably with the plenum chambers used in the main supersonic tunnel, and has a volume of 2160 cu cm. The plenum is equipped with a pressure tap and a mounted thermocouple to

monitor injectant conditions. Additionally, the top surface of the plenum serves as the test surface, and was designed so that injector models can be flush mounted, providing a flat test surface. The design is such that the injector models used in the main supersonic tunnel can be interchangeably used with the free-jet facility. The length of the surface is 12.5 cm in the flow direction and 23.7 cm in the lateral direction, although only 6.35 cm of this width is useful test surface area. Figure 6 shows a photograph of the entire free jet section. The coordinate system used to describe positions in the test section is shown in Figure 7.

2.2 Air Handling System and Facility Plumbing

The free jet is a blowdown facility that uses the same compressor, filters and dryer employed by the main supersonic tunnel. Figure 8 provides a schematic of the air handling system and facility plumbing. The air is compressed by an Ingersoll Rand Type 40 watercooled, reciprocating compressor. Before being sent to the storage tanks, the air is first passed through a series of filters and dryers. The free jet facility uses a separate air supply line than that used for the main tunnel. The supply line is 2 - in nominal diameter, schedule 80 black iron pipe, which is rated to handle 51 atm of non-shock pressure.

From the storage tanks, the air is passed through a Grove Model 412 F dome pressure regulator that reduces the inlet pressure from 38 atm down to 6.7 atm. The system must operate with such a high inlet pressure to insure that the mass flow rate through the regulator orifice is sufficient to operate the facility at design conditions [33]. By adjusting the regulator reference pressure, the free jet total pressure can be adjusted to provide an exit static pressure equal to the local atmospheric pressure, which eliminates any strong exit shocks or expansion waves

that otherwise may be present.

The next component of the system is a 4 - in nominal diameter manual gate valve (Milwaukee Valve Co. Model P-905). This on/off valve serves to initiate and end all free jet tests. For safety purposes a high pressure, stainless steel ball valve is located in-line at the storage tank exit flange. Directly downstream of the gate valve, the plumbing diverges into a 6 in nominal diameter settling chamber that is 47.6 cm in length. From here the air is sent to the nozzle inlet through a circular to square transition piece. All plumbing components are connected by standard threaded pipe fittings, which are sealed with an anaerobic pipe sealant, and bolted flanges. For economic reasons, only the components upstream of the regulator (on the high pressure side) are rated for 51 atm or better.

The entire facility rests on two angle iron support racks, each bolted to the floor. The support racks are also used to secure other items, including compressed gas cylinders and pressure transducers. A photograph of the entire facility, excluding the test section is given in Figure 9.

2.3 Sound Insulation Room

Because the noise level during facility operation was about 140 decibels, a sound insulation room enclosing the test section was built. The room was designed using a muffler theory of parallel baffles described by Beranek [34], which was chosen because it allows the muffler design to be tailored to attenuate sound in a specific frequency range. The construction of a parallel baffle muffler was also more practical than implementing other muffler types. The target frequency for attenuation was chosen as 1500 Hz, based on several spectral analyses performed using a Spectrascope Model SD330A real time analyzer.

Figure 10 shows the results from a typical analysis, with the relative sound pressure level plotted against the frequency.

The sound insulation room is 2.45 m on each side, with the side opposite the nozzle left open to exhaust the free jet. Equipment and materials can be moved into the room through a 0.1 by 2.1 m hinged door. Two small utility openings, one near the test section and one in the door, allow for instrumentation lines to pass into the room. The room contains six baffles constructed from 0.9 cm thick plywood, each spaced 32 cm apart, as shown in Figure 11. The baffles are 2.44 m high and 1.22 m in length, and are supported by sliding tracks, which allow easy installation and removal. The baffles are covered with standard 8.9 cm thick fiberglass insulation, that is secured by stapled chicken wire with the paper side facing against the plywood. The porous nature of fiberglass gives the insulation excellent sound attenuating properties.

To prevent the baffles from being destroyed by the force of the free jet, a large flow deflector is located immediately downstream of the test section. The deflector consists of a perforated plate welded to a 2.5 - in nominal diameter pipe. The entire assembly is bolted to the floor and the support rack. The plate is 0.8 cm thick with overall dimensions of 25 by 61 cm. There are 162 - 1.0 cm diameter holes, spaced 2.5 cm apart, on the plate. The deflector also serves to support the traversing system. The deflector can be seen in Figure 6.

The attenuation provided by the sound insulation room was measured with a Columbia Research Lab Model SPL-103 sound pressure level meter. This hand held instrument allowed readings to be taken at various locations. Comparing similar measurements taken both before and after the construction of the room shows a noise attenuation of roughly 15 decibels. The measurements also indicate

that, outside of the building, the noise level from the free-jet facility, with the sound room, is about 90 decibels, which is not significantly louder than the main supersonic tunnel.

3 Description of the Experiment

3.1 Overall Description

All tests were conducted in the free-jet facility at the following free stream conditions:

$$\begin{array}{lcl} M_\infty & = & 1.95 \\ P_{T\infty} & = & 6.7 \text{ atm} \\ T_{T\infty} & = & 300 \text{ K} \\ Re_\infty & = & 85 \text{ x } 10^6 \text{ / m} \end{array}$$

The Mach number was determined from the ratio of the exit static pressure to the free stream total pressure. Note that a total pressure of 6.7 atm corresponds to an exit static pressure equal to the local atmospheric pressure (94 kPa), which eliminates any strong exit shocks or expansion waves that otherwise may be present. This facility provided test durations of up to 25 seconds.

The goals of the experiment were to:

1. Evaluate the performance of the free jet facility.
2. Evaluate three flow visualization techniques as methods for examining normal injection in the free-jet facility.
3. Evaluate the effectiveness of an existing hot-film concentration probe in the boundary layer.

To achieve these goals, normal injection of both helium and air through a circular cross-section injector was studied. The experimentation was divided into two parts, an evaluation of the qualitative flow visualization techniques and an evaluation of quantitative helium concentration measurements taken with the probe. The three flow visualization techniques tested were nanoshadowgraph

photography, surface oil flow photography and surface infrared imaging. For the nanoshadowgraph and oil flow visualization tests, the injectant total pressure was varied to correspond to values of 1.20, 1.45 and 1.70 for the expansion ratio. During the infrared imaging tests, the expansion ratio was held constant at 1.45. The expansion ratio is defined as the ratio of injectant static pressure to the minimum injectant static pressure required to choke the flow through the injector [31]. The injectant total temperature was 300 K during the oil flow and nanoshadowgraph photography experiments. For visualization with the infrared imaging system, the injectant was heated to a maximum temperature of 320 K. This was done to create different temperature gradients between the injectant and the free stream, to provide contrasts in the infrared images.

To study the effectiveness of the existing hot-film concentration probe, helium concentration measurements were taken at the test surface. The probe was capable of traversing laterally from $\frac{y}{d}$ = -10 to $\frac{y}{d}$ = + 10 (see Figure 7). Measurements were taken at two axial positions, $\frac{x}{d}$ = 6.9 and $\frac{x}{d}$ = 10.9. The coordinate system used to describe positions in the test section is shown in Figure 7. Although the diameter of the circular injector was listed by Barber as 3.45 mm, during an insulation process (described in Section 3.2.1), the diameter was inadvertently widened to its present diameter of 3.76 mm. The injectant total pressure was varied to correspond to expansion ratio values of 1.20, 1.45 and 1.70 for helium injection and values of 1.30, 1.57 and 1.85 for air injection. The following tables list the jet total pressures, mass flow rates and discharge coefficients for helium and air injection through the circular injector. The injection parameters are discussed in detail in Section 3.4.2. These tables only include information for the injector after it was insulated. The injectant total

temperature was 300 K for all concentration tests.

Mass Flow Parameters - Helium Injection

P_{Tj} (atm.)	Expansion Ratio	$\dot{m}$ (kg/s)	C_D
3.67	1.20	0.0029	0.77
4.44	1.45	0.0035	0.77
5.20	1.70	0.0042	0.77

Mass Flow Parameters - Air Injection

P_{Tj} (atm.)	Expansion Ratio	$\dot{m}$ (kg/s)	C_D
3.67	1.30	0.0078	0.81
4.44	1.57	0.0095	0.81
5.20	1.85	0.0111	0.82

3.2 Equipment

3.2.1 Injector Model

The circular injector model was designed to inject normal to a flat plate flow. The model consists of an injector block, that serves as part of the injection plenum, and a circular injector insert, which is shown in Figure 12. The injector block was designed so that all of the injector inserts used in the main supersonic tunnel can be used in the free-jet facility. The injector is simply a 3.76 mm

diameter hole drilled into an injector insert, which was designed to be flush mounted into the injector block, providing a flat plate test surface. The injector insert is held in place by four screws and is sealed with an o-ring to prevent any injectant leakage. This arrangement was leak tested before all experiments.

The purpose of the infrared imaging experiments was to evaluate the feasibility of using this technique to visualize the injectant flow patterns on the test surface. By heating the injectant, a contrast between images taken of unheated and heated injection is provided, which may lead to conclusions about the surface flow patterns. For this to be successful, a significant temperature difference between the injectant and free stream must exist during the heated injectant tests, causing detectable temperature gradients on the test surface, which are the basis for this flow visualization technique. During preliminary tests, it became apparent that heat from the injectant within the plenum was rapidly being conducted to the test surface, causing distorted images of the surface flow patterns. To solve this problem, the inside surface of the injector insert was insulated with Teflon, which was chosen because of its machinability and relatively high thermal resistance. A numerical heat transfer analysis showed that insulation with Teflon would significantly reduce the heat flux through the injector block to the test surface. The Teflon coating is secured in place with epoxy and is 3.2 mm thick. During the insulation process, the injector diameter was inadvertently widened from its original size of 3.45 mm to 3.76 mm.

3.2.2 Injectant Supply System

Air and helium were supplied by single, standard compressed gas cylinders that were secured to the facility support racks. Figure 13 shows the injectant supply system. The injectant pressure was controlled by a high flow Airco

compressed gas mechanical regulator. From the regulator, the injectant was passed through a single coil of $\frac{3}{8}$ - in diameter stainless steel tubing that is 3.5 m in length. The injectant is routed through a flowmeter and into the plenum chamber via a single $\frac{1}{2}$ - in diameter copper tube.

During the infrared imaging experiments, the injectant was heated by passing an electric current through the stainless steel coil. Stainless steel was chosen over cheaper and more workable alternatives, such as copper, because of its relatively high electrical resistance. The current was supplied by attaching the leads of a Lincoln Type SAE 150 arc welder to each end of the coil. Typical welder settings were 100 amps at 50 volts. The temperature rise of the injectant is given by the following equation:

$$\Delta T = \frac{i^2 R_c}{\dot{m} C_p} \tag{3.1}$$

where $\dot{m}$ is the mass flow rate of the injectant and C_p is the specific heat of the injectant. The resistance, R_c, of the stainless steel coil was measured with an ohmmeter and i is the current supplied by the welder. The total temperature of the injectant ranged up to 320 K, depending on the welder settings and the duration of the coil pre-heating.

3.2.3 Traverse System

The sampling probe was raised and lowered along the test surface in the lateral (y) direction (see Figure 7) by a traversing system. This system consists of a rack and pinion driven by a Hurst model GA synchronous motor. The single-speed motor is equipped with a gearbox that reduces the pinion speed to one RPM. This translates to a traversing speed of 2.6 mm/sec. The motor is capable of both clockwise and counterclockwise rotation, which allows for bi-directional

traversing. The system was manually controlled by a toggle switch.

3.2.4 Vacuum System

Because helium concentration measurements were taken using an aspirating probe, a vacuum system was necessary. The system consisted of a Cenco Corporation Model 91482 vacuum pump and a tank. The tank was used as a buffer between the pump and the probe, to damp any undesirable pressure oscillations. The tank was equipped with a pressure tap to monitor the vacuum pressure.

3.3 Instrumentation

3.3.1 Pressure Measurements

During all experiments at least three pressures were measured: injectant total pressure, free jet total pressure and free jet exit static pressure. When using the concentration probe, a fourth pressure measurement was required (see Section 3.3.3). The free jet total pressure was measured using a Pitot tube located in the settling chamber. This pressure was monitored using a Marsh Instruments Model 103 analog pressure gage that had a range from 0 to 10.9 atm. The injectant total pressure was measured using a Pitot tube mounted in the plenum chamber. This pressure was converted to a voltage signal by a Genisco Tech Model PB-923 absolute pressure transducer with a range of 0 to 6.8 atm. The free jet exit static pressure was measured using a static pressure tap located in the nozzle 0.95 cm from the exit. Because the nozzle area changes very little from this point to the exit, the static pressure at this location is a good approximation of the exit static pressure. An Alinco Model 151-EBU-1 absolute pressure transducer with a range of 0 to 1.02 atm converted the pressure to a voltage signal.

The signal from each transducer was amplified by a Gould Model 13-4312-00 differential DC amplifier. Excitation voltage to the transducers was provided by a Hewlett Packard Model 6220-B DC power supply. After amplification, a Frequency Devices Model 9002 programmable filter was used to low-pass filter the signals. The cutoff frequency of these Butterworth filters was set at 50 Hz. The cutoff frequency was intentionally set below 60 Hz because of the high level of electronic noise being emitted by the compressor motor. During the flow visualization experiments, both the injection total pressure and the exit static pressure were monitored using analog pressure gages. The gages used were a Heise Model CMM-1112C analog pressure gage with a range from 0 to 6.8 atm for the injectant pressure and a Heise Model C-53331 analog pressure gage with a range from 0 to 2.7 atm for the exit static pressure.

3.3.2 Temperature Measurements

The injectant temperature was monitored during all experiments. When using the concentration probe, an additional temperature measurement was required (see Section 3.3.3). The total temperature of the free jet was not continually monitored, but was assumed to be 300 K, based on selected initial measurements and results from the main supersonic tunnel. The injectant temperature was measured with a Type K (Chromel-Alumel) thermocouple mounted in the plenum chamber. No filtering of the analog signal was performed, instead the data were digitally filtered after the experiments. During the flow visualization tests, the injectant temperature was monitored using an Omega Model HH-71K2 hand held thermometer.

3.3.3 Concentration Probe

An aspirating, hot-film probe (Figure 14) based on the design by Ng, et al. [8], was used to measure helium concentration in the flow field as a means of evaluating its effectiveness. This is necessary because the existing probe was specifically designed to operate in a two-dimensional free stream, not positioned against a surface, as in the free jet experiments. This positioning may have a bearing on whether or not the probe swallows the stand-off shock, if one exists in the boundary layer. The operation of the probe is based on differences in the convective heat transfer from the hot film sensor under different flow conditions. The probe is designed with a choked orifice downstream of the sensor, as a reference point, to provide information about the mass flow rate of the sampled gas. Given this information, a gas dynamics analysis provides the sensor voltage as a function of gas composition, pressure and temperature. Ninnemann [35] provides a discussion on hot film techniques as a means for helium concentration measurement.

The probe is equipped with a diverging tip, which eliminates the selective sampling problem. The tip is removable to facilitate the removal and installation of the sensor. The sensor used was a TSI Model 1220-20 mounted hot film. The sensor was connected to a Dantec Model 55M10 Standard Constant Temperature Anemometer (CTA) Bridge, which was used in conjunction with a Dantec Model 55M01 Main Unit. The output from this unit was low-pass filtered by a Frequency Devices Model 9002 programmable filter, with the cutoff frequency set at 10 Hz to minimize the effects of the noise produced by the compressor motor.

Local pressure and temperature in the sensor plane were measured. The sensor pressure was converted to a voltage by a Genisco Tech Model PB-923

absolute pressure transducer with a range from 0 to 6.8 atm and was filtered by a Frequency Devices Model 9002 programmable filter. The low-pass cutoff frequency was set at 50 Hz. The sensor temperature was measured using a Type K (Chromel-Alumel) thermocouple mounted into the sensor plane with an epoxy. The thermocouple was wired directly into the EXP-16 expansion multiplexer (see Section 3.3.5) with no analog filtering.

3.3.4 Position Measurement

The lateral position of the concentration probe was measured using a Circuit Instruments Type 121080 rotational potentiometer that was gear driven by the traverse motor. An excitation voltage of +5 VDC was provided by a Hewlett Packard Model 6220-B DC power supply. The signal was low-pass filtered, with a cutoff frequency of 50 Hz, by a Frequency Devices Model 9002 programmable filter, which was also used to amplify the signal. The linearity of the potentiometer is ± 0.5 percent, however because of deflections in the traverse system during tests, the lateral position measurement had an uncertainty of ± 2 mm (0.5 injector diameters).

During experiments, the movement of the probe caused light scratches on the test surface, indicating its exact path of travel, which were used to determine the axial position of the probe. The post-run measurements were made with calipers. Because of deflections in the traverse system, the axial position varied up to 3 mm (0.8 injector diameters) during testing. The surface marks also verified that the probe was traversed directly on the test surface. Bearing this in mind, the position of the center of the probe tip was determined to be 0.4 mm from the test surface ($\frac{z}{d} = 0.1$).

3.3.5 Data Acquisition System

Conditioned voltages from the transducers, the position potentiometer and the hot-film sensor were read by a Metrabyte DAS-16F, high speed, analog-to-digital conversion board (ADC). Figure 15 shows a schematic of the data acquisition system. The DAS-16F is a successive approximation converter, which allows for very high conversion rates, but also has a high sensitivity to noise. For this reason, it was imperative to filter the analog inputs. The board is installed in an IBM PC computer equipped with two floppy disk drives, as well as a hard drive. The DAS-16F can convert up to eight differential channels, with a resolution of 0.0024 V (based on a 0 to 10 volt range). In addition to the DAS-16F, a Metrabyte EXP-16 expansion multiplexer was used for the thermocouple inputs. The EXP-16 is equipped with an on-board cold junction temperature sensor and built in amplification, which eliminated the need for thermocouple calibrations.

Labtech Notebook, a data acquisition software package, was used to assist in the data collection process. This menu-driven software converts the binary numbers from the ADC to real data and stores the information to the hard disk. The package has many convenient features, including variable sampling rates for each input channel and programmable offset and scale factors. The total sampling rate available with the system is about 300 Hz. The sampling rate is limited by many factors, including the data filing to the hard disk and real-time graphics displays.

3.3.6 Flow Rate Measurement

A Brooks Instrument Division Type 1231-1110 flowmeter was used to

measure the volumetric flow rate of injectant. The flowmeter was placed in line, downstream of the stainless steel coil. To determine the mass flow rate, corrections were required for the pressure, temperature and specific gravity of the injectant. The meter was monitored visually during the experiments.

3.3.7 Nanoshadowgraph Photography

Nanoshadowgraph photography was one method of flow visualization that was examined in the free-jet facility. This method shows the second derivative of the flow density [36]. The light source used for these photographs was a Xenon Novatron Model 739-B nanopulse lamp, powered by a Xenon Model 437-B nanopulser. This system provided a variable intensity light pulse of 30 nanoseconds. The point light source was passed through a simple lens on to a parabolic mirror, which reflected a collimated light beam through the flow area and on to the film plane. The images were recorded on Polaroid Type 57 high speed instant film which was processed by a Polaroid Model 545 film holder/processor.

3.3.8 Oil Flow Photography

Oil flow photography was evaluated as a way to visualize the surface flow patterns of the injectant/free stream interaction. The procedure involves placing drops of a mixture of Dow Corning 500 cs oil and Dayglo A-14-N orange flourescent pigment on the test surface, just upstream and downstream of the injector. Upon running the test, the oil highlighted the separation zones around the injector. A single ultraviolet lamp was used to enhance the appearance of the oil/pigment mixture. Still photographs of the surface patterns were taken with a Nikon F Series 35 mm camera, equipped with a Vivitar 2X teleconverter. ASA

1000 color film was used for all photographs.

3.3.9 Infrared Imaging

Infrared imaging was evaluated as another method to visualize the surface flow patterns. Previous work using this technique has been aimed at detecting boundary layer transition [26,27]. These experiments relied on the difference in heat transfer properties between laminar and turbulent flow, which resulted in surface temperature differences between the laminar and turbulent regions that were easily detectable. Similarly, the injection of helium into the flow will cause certain areas to have different heat transfer properties. Certain areas that may be distinguishable are regions of separated flow and vortical flow caused by the injection. Additionally, by performing experiments with both heated and unheated injectant, the contrasting images may lead to more information about the surface flow patterns. The experiments were dependent on whether or not the differences in heat transfer characteristics would translate into detectable surface temperature differences, and also, whether or not these images could be interpreted to determine injectant flow patterns. To insure the integrity of the images, the aluminum test surface was painted flat black. The infrared image of a painted surface will more closely indicate the actual surface temperature, while the bare aluminum surface will display mostly an image of reflected surrounding temperatures.

The infrared imaging system used was an Inframetrics Model 600 infrared imaging radiometer. This system provided longwave (8 to 14 μm wavelength) spectral response. The scanner was designed to use interchangeable filters and telescoping lenses, however these items were not necessary for the injection studies. During tests, the scanner was mounted on an optical bench

approximately 0.5 m from the test section. The signal from the system was run directly to a VCR and then to a standard color monitor. Figure 16 shows a schematic of the system.

This setup allowed for near real-time monitoring of the surface image, as well as recording capabilities. All tests were recorded on a standard VHS video cassette. Photographs of the recordings were taken directly from the color monitor. These photographs were taken with a Nikon F Series 35 mm camera.

3.4 Experimental Methods

3.4.1 Instrument Calibration

During all concentration measurement experiments, pressure data was obtained using electronic transducers, which were calibrated by exposing them to a range of known pressures and recording the corresponding output voltage. This data was used to relate transducer voltage to pressure by a least squares linear curve fit. The calibration pressures were provided by an Amtek MK100 pneumatic pressure tester connected to a compressed air cylinder. This dead weight tester provided a range of pressures from 1 to 4.5 atm in 0.7 atm increments. Because the transducer used to measure the exit static pressure has a limited range (zero to 1.02 atm), it was calibrated with a different setup. In this case, the calibration pressures were provided by a pressure vessel evacuated by a Cenco Corporation Model 91482 vacuum pump. A Heise Model C-5331 analog pressure gage was used to measure the tank pressure. This system provided a range of pressures from 0.15 atm to 0.9 atm. Voltages were amplified, filtered and digitized with the same system used during actual testing.

Total temperature information during the concentration measurement tests

was provided by wiring the thermocouples directly to the EXP-16 expansion multiplexer. This unit is equipped with an on-board cold junction temperature sensor and amplification. The Labtech Notebook data acquisition software package converted the thermocouple voltage directly into temperature readings.

The hot-film concentration probe was calibrated before and after the tests by exposing it to gas samples with a known helium/air composition. The calibration hardware setup is shown in Figure 17. Calibration gas samples were obtained by filling a pressure vessel with air and helium from compressed gas cylinders. A Heise Model CMM-1112C analog pressure gage was used to monitor the tank pressure. The composition of the mixture was determined by noting the partial pressure of each gas during the filling process. To simulate the actual probe operation, the vacuum system (see Section 3.2.4) was used to draw the calibration samples through the probe, which was connected to the vessel with plastic tube. Calibration was done at seven levels of helium concentration, from zero to 60 percent mole fraction helium, in increments of 10 percent. To simulate test conditions, calibration was performed at a constant temperature of 290 K over a range of pressures from 2.0 to 4.0 atm.

Because the sensor pressure developed in the main supersonic tunnel is much lower than that in the free jet facility, previous calibrations were performed over a much lower pressure range than those performed for the free jet experiments. Past calibration curves were generated based on the following semi-empirical equation relating the hot film voltage to the Reynolds number:

$$\mathrm{V}^2 = \frac{(R_s + R_w)^2}{R_w} \pi l k (a Re^m + b)(T_w - T_T) \tag{3.2}$$

where R_s, R_w, l and T_w were known, and k was a function of the gas composition [31]. The set of constants a, b and m was derived from the

calibration data obtained at each helium concentration level. Using these constants, a logarithmic curve was generated by a least-squares-fit computer code. Figure 18 shows a typical set of calibration curves used for experiments in the main supersonic tunnel. As this plot shows, the agreement between the calibration data points and the generated curve begins to deteriorate slightly at pressures above 2 atm. This trend was more pronounced when calibration was performed at higher pressures. Figure 19 shows a plot of the data points from the calibration performed for the free jet tests and the corresponding curves over a pressure range from 2.0 to 4.0 atm. These curves had an error that often exceeded 10 percent. To reduce the calibration error, a second curve fit method was employed. This method used Proplot, a commercially available software package, to fit an n^{th} order polynomial to the data. Integer values for n ranged from 2 to 5, with the quadratic fit (n = 2) producing the smoothest curve. Figure 20 shows the same calibration data points from Figure 19 plotted with the set of quadratic curves. The error in these curves did not exceed one percent.

By using this completely empirical method, equation (3.2) is no longer necessary. This eliminates the need to generate the constant sets for a, b and m, and also greatly simplifies the data reduction process. However, this simplicity does not come without a cost: this method has no compensation for any temperature change in the flow around the sensor. This point is minor, though, because the temperature of the flow in the sensor plane varies by no more than 5 percent during the tests, leading to an estimated maximum error of 10 percent helium mole fraction.

The potentiometer used to measure the lateral (y direction) probe position was calibrated immediately before concentration data were taken. The process

involved positioning the probe at six different lateral positions and recording the corresponding voltages. The distances from the axial centerline to the calibration points were measured using calipers, and these data were used to generate a linear curve describing the probe position as a function of voltage. The voltage was amplified, filtered and digitized with the same system used during actual tests.

3.4.2 Injector Expansion Ratio

The injectant total pressures used during testing were chosen to correspond to various values of the expansion ratio. The expansion ratio is defined as the ratio of injectant static pressure to the minimum injectant static pressure required to choke the injector ($\frac{P_j}{P_{jCH}}$). P_{jCH} was determined experimentally by varying the injectant pressure and recording the corresponding mass flow rate measured by the flowmeter. This was done while running the free jet. The mass flow rate of a compressible, ideal gas through the injector is given by:

$$\dot{m} = P_j A_j M_j \sqrt{\frac{\gamma}{RT_j}} \tag{3.3}$$

If the injectant temperature, T_j, is held constant and the injector is choked, the ratio of the mass flow rate to the injectant pressure ($\frac{\dot{m}}{P_j}$) is a constant. Using this result, P_{jCH} was determined graphically by plotting $\frac{\dot{m}}{P_j}$ as a function of P_j. This procedure was done for unheated helium injection through the uninsulated circular injector. The value of P_{jCH} was found to be 1.49 atm. This value was assumed to be the same after the injector was insulated. Since only the injectant total pressure was measured, it is more convenient to express the expansion ratio in terms of the total pressures as $\frac{P_{Tj}}{P_{TjCH}}$. P_{TjCH} is calculated using the isentropic static to total pressure ratio for choked flow, which resulted in values of 3.06 atm for helium injection and 2.82 atm for air injection.

For the infrared imaging, both heated and unheated helium were injected at a total pressure of 4.44 atm. This corresponds to an expansion ratio of 1.45, which is the same value used by Barber [31]. For the oil flow and nanoshadowgraph photographs and the concentration measurement tests, unheated helium was injected at total pressures of 3.67, 4.44 and 5.20 atm, which correspond to expansion ratios of 1.20, 1.45 and 1.70. Additionally, for the concentration measurement experiments, air was also injected, as a benchmark for zero helium concentration. The air was injected at the same pressures as the helium, which correspond to expansion ratios of 1.30, 1.57 and 1.85.

The flow rate of injectant was measured by taking the flowmeter reading and multiplying by the pressure, temperature and specific gravity scale factors. The discharge coefficients were calculated by dividing the actual mass flow rate by the theoretical mass flow rate calculated from Equation (3.3). These mass flow parameters are listed in Section 3.1 for both air and helium injectant.

3.4.3 Data Acquisition Procedures

Due to the lack of space and equipment, the free jet operation was an entirely manual process. For the flow visualization tests, all data acquisition, which included monitoring the free jet and injectant conditions, was also a manual process. The sequence for the flow visualization experiments is as follows: First, the optical hardware (light sources, cameras, etc.) was set up and properly aligned. The injectant pressure was then set, using an analog pressure gage. In the case of the heated injection tests, the welder was set and turned on three to five minutes prior to the test, to allow the injection coil to pre-heat. In the case of the oil flow tests, the oil drops were placed on the test section prior to the test. In the case of the nanoshadowgraph tests, a camera operator had to be secured

inside the sound insulation room. This was necessary to prevent any light from exposing the film upon opening the sound room door, since the camera was not equipped with a shutter. In all cases the utility door was securely fastened. When the storage tank pressure reached at least 38 atm, the operator opened the injectant valve, followed by the free-jet on/off valve. During the tests the operators had various tasks, which included recording the infrared images, monitoring the free-jet conditions, monitoring the injectant conditions and recording the flowmeter reading. The nanoshadowgraph photographs were taken approximately five seconds after the free-jet main valve was opened. Because the surface oil flow patterns were not distorted during free jet shutdown, these photographs were taken after the test was complete. The oil flow and nanoshadowgraph tests lasted about 10 seconds, while the infrared imaging runs lasted up to 20 seconds.

Fortunately, for the concentration measurements, all data acquisition was automated. However, because of the additional equipment that was necessary, at least two operators were needed for a successful test. Before the test, the probe was placed in position and calibrated as outlined in Section 3.4.1, and the injectant pressure was set before the test using an analog pressure gage. The vacuum pump was turned on several minutes before the experiment, to allow complete evacuation of the tank. At the time of the test, one operator was assigned to open the injection valve, turn on the traverse and record flow meter readings. The second operator triggered the data acquisition system, controlled the free jet main valve, monitored the oscilloscope, which displayed the hot film signal, and observed the probe movement along the test surface during the test. Concentration measurement tests lasted between 20 and 25 seconds. The time

needed between tests to refill the storage tanks was roughly five minutes.

3.4.4 Data Reduction

During the flow visualization tests, the test conditions were monitored to insure proper operation, thus no data reduction was necessary. The data recorded during the concentration tests was divided into two groups: the data to insure proper test operation and the data necessary to determine the local helium concentration. The data needed to determine the helium concentration was written to a single data file, and included the probe position, the sensor voltage, pressure and temperature. Before any reduction, the data was smoothed using a routine that employed a standard Hamming window, with a window size of 10 data points. This method produced smoother data sets than the conventional method of using an unweighted boxcar average over 10 data points. The computer code used to smooth the data was written as a part of this project and is included in the Appendix A.

As was mentioned in Section 3.4.1, the hot film calibration curves were produced using two very different methods. One procedure was semi-empirical, and involved generating three constant sets from the calibration data. The second method was purely empirical and employed a quadratic curve fit to the calibration data. Hot film data was reduced using both calibrations. Surprisingly, the trends in helium concentration were very similar for the two methods, although the magnitudes had a difference of up to 10 percent mole fraction helium. Because the calibration error using the curve fit method was much less, the final data reduction was performed using these calibration curves.

The data reduction program read the coefficients describing the calibration curves from a data file. The hot film data was also read from a file. The program

used interpolation between appropriate calibration curves to determine the local helium concentration. This FORTRAN code is listed in the Appendix A.

3.4.5 Nondimensionalization Methods

All distances were nondimensionalized by the jet diameter. This method is different from that used by Barber [31], who used an effective radius defined as:

$$R_b = \sqrt{\frac{\dot{m}_j}{\rho_\infty u_\infty}} \tag{3.4}$$

The effective radius was abandoned in this work for reasons of simplicity, since the primary goal of the research is the evaluation of various techniques. All pressures and temperatures were nondimensionalized by their respective free stream quantities. The exception to this is the injection pressure, which was nondimensionalized by the minimum jet pressure required to choke the injector. This ratio is defined as the expansion ratio. The free stream Mach number was determined from the ratio of the exit static pressure to the total pressure, and had a value of $M_\infty = 1.95$.

4 Results and Discussion

4.1 Free-Jet Facility

Since the major goal of this research was to develop a supersonic free-jet facility, it is appropriate that a discussion of the effectiveness of the facility be included. Many tests were conducted that were not formally documented, to determine the characteristics and capabilities of the facility. Additionally, free-jet conditions were closely monitored during the normal injection experiments. Under this scrutiny, the free-jet facility proved that it was capable of providing repeatable test runs, with the exit static pressure varying by no more than three percent. Other advantages of the free jet, as compared to the main supersonic tunnel, were its simple operation procedure, longer available test durations (up to 25 seconds) and less time needed between tests for the storage tanks to be pressurized (typically less than five minutes). The facility was tested for its durability by running the free jet continuously, although not at stable test conditions, for extended periods of time (up to three minutes) at various total pressure levels. These tests showed some areas, especially in the sound room and traverse system, that were susceptible to failure. As the design was revised, the facility has proven itself to be very durable.

Figure 21 shows nanoshadowgraph photographs of two cases of the undisturbed free jet flow over the test section (the effectiveness of nanoshadowgraph photography will be discussed in Section 4.3). The Mach 1.95

free jet runs from left to right, with the test surface located at the bottom and ambient air at the top of the photograph. These pictures clearly show the shear layer between the free jet and ambient atmosphere, the exit shocks, and the boundary layer on the test surface. The photographs show that the boundary layer grows from about 2 mm (0.5 injector diameters) at the injection point to about 3 mm (0.8 injector diameters) at an axial position of $\frac{x}{d} = 5.3$. The boundary layer is much smaller than that observed in the main supersonic tunnel. These photographs demonstrate the repeatability of the free jet facility from run to run.

Because of the newness of the facility, much time was spent evaluating three methods of flow visualization. The surface flow patterns for helium injection were visualized by both oil flow photography and infrared imaging. Nanoshadowgraph photography was used to visualize the flow field at three injection pressures. In addition to these qualitative methods, the effectiveness of an existing hot-film concentration probe was examined. Plots of the helium concentration at the test surface were made for selected test cases, for both air and helium injection at various injection pressures. To help interpret the concentration results, plots of the hot-film voltage and sensor pressure for the test cases were also made.

4.2 Oil Flow Photographs

Figure 22 (a-c) shows the oil flow photographs for helium injection at expansion ratios of 1.20, 1.45 and 1.70. The flow is from left to right in these photographs. These photographs show a boundary layer separation zone in front of the injector, that extends from 1.0 to 1.2 injector diameters upstream of the

injector, increasing in size as the expansion ratio is increased. This trend was also noted by Barber [31]. The photographs also show a separated region downstream of the injector, in the jet core region, the size of which appears to increase with an increase in the expansion ratio. The bow shock region, indicated by the dark regions around the injector, also shows an increase in size and definition as the expansion ratio increases.

Oil flow surface visualization is a very effective technique in the free-jet facility for two main reasons: the photographs are taken normal to the test surface and the surface oil patterns are not destroyed upon facility shutdown. Because of the restrictions imposed by the enclosed test section in the main supersonic tunnel, oil flow photographs in this facility are taken at an angle of about 60 degrees to the test section. This prevents direct scaling of the photographs, which can be accomplished with photographs taken normal to the test surface, such as those from the free-jet facility. Because the free-jet exit static pressure is equal to the local atmospheric pressure, the surface oil flow patterns are not destroyed by a large pressure fluctuation upon facility shutdown, as they are in the main supersonic tunnel. This permits the photographs to be taken after shutdown, which allows more versatility and time to take good photographs. Best results were obtained using ASA 1000 color film, an aperature setting of 2.0 and an exposure time of 1 to 2 seconds, with an ultraviolet lamp as the only light source.

4.3 Nanoshadowgraph Photographs

Figures 23 through 25 are nanoshadowgraph photographs of helium injection at three different expansion ratios. The Mach 1.95 free jet runs from left

to right, with the test surface located at the bottom and ambient air located at the top of the photographs. Nanoshadowgraph photography was chosen over schlieren photography mainly because the optical set up was less complicated. Because of the extremely short exposure times, this method allows for rapidly moving flow structures to be captured. However, because this method senses second order density gradients, as opposed to the first order gradients detected by schlieren photography, some sensitivity was sacrificed. Schlieren photography, which typically has longer exposure times, also captures time-averaged phenomena better than the nanoshadowgraph method.

Figure 23 shows a composite photograph of helium injection at an expansion ratio of 1.20. The boundary layer, although hard to detect, is of comparable size to that seen in the undisturbed flow cases. Injection causes a strong shock that is located just upstream of the injector and extends across the free stream. Previous experiments [1,31] have shown an abrupt turn in this jet shockwave at the edge of the boundary layer near the point of injection. Because of the much smaller boundary layer, a sharp direction change is not evident in these experiments. Instead, the shockwave exhibits a more gradual change from an angle of 49 degrees near the test surface to 34 degrees in the free stream, as measured counterclockwise from the test surface. The photograph also shows that the shockwave has a lambda structure near the test surface caused by the injection.

Figure 24 shows the case of unheated helium injection at an expansion ratio of 1.45. The features in this photograph are very similar to those seen in Figure 23. Once again, the jet shockwave turns gradually from 49 degrees near

the test surface to 36 degrees in the free stream. The lambda shock upstream of the injector is evident in this photograph. Qualitatively, there appears to be greater jet penetration in this case, especially near the injector.

Figure 25 shows the case of helium injection at an expansion ratio of 1.70. This case differs from the previous two in that the jet shockwave turns rather abruptly from 59 degrees near the surface to 36 degrees in the free stream. The turn is located about two injector diameters above the surface ($\frac{z}{d} = 2$), which is well above the upstream boundary layer. Also, the lambda shock structure is much more distinct in this case. As expected, this photograph shows greater jet penetration near the injector than the previous two cases.

Nanoshadowgraph photography is more difficult in the free-jet facility than in the main supersonic tunnel for two main reasons: the vertical orientation of the test section and the need for a camera operator to be inside the sound room during tests. The test section orientation requires that the nanoshadowgraph optical set up be in the vertical plane, rather than the horizontal plane, which is a difficulty because it required the system components to be positioned at different levels from the floor. Since the camera was not equipped with a shutter, an operator positioned in the sound room was necessary to prevent light from ruining the film, by processing the film before the sound room door was opened. Even at night, there was sufficient light in the surroundings to ruin the exposed film. The main disadvantage of this requirement is that the camera operator is exposed to extremely unpleasant conditions during the free jet operation. The requirement of an additional operator is also an inconvenience. In spite of these difficulties, high quality nanoshadowgraph photographs are obtainable in the free-jet facility.

4.4 Infrared Imaging

Figures 26 through 29 are infrared images of several different flow conditions. The Mach 1.95 flow in these photographs runs from right to left. All of these photographs are for test cases using the insulated injector with an expansion ratio of 1.45. Since this was a study of the effectiveness of infrared imaging in the free jet facility, many different instrument settings were experimented with. Perhaps the two most crucial settings were the temperature range and the color scale. All of the images presented used a gray scale, with darker images being colder and lighter images being hotter. This scale produced images that were easier to interpret and reproduce than the color scales. The temperature ranges available with the system were 5, 10, 20, 50, 100 and 200 degrees Kelvin. The two ranges that provided the best images were 10 and 20 degrees Kelvin. The upper and lower temperature limits were set during each test to give the best image. The photographs in Figures 26 through 29 were taken directly from the color monitor with a Nikon F Series 35 mm camera. Best results were obtained using ASA 100 film, an aperature setting of 5.6 and an exposure time of $\frac{1}{4}$ second.

Figure 26 shows two cases of heated helium injection. The injectant total temperature was 315 Kelvin in both cases, with the temperature range set at 20 degrees Kelvin. Both images clearly show the injector insert and the four screws securing it in place. A set screw also appears as a small, dark circle in the lower right side. The circular injector appears as a very light circle in the center, indicating a relatively high local temperature. The dark region that runs axially downstream of the injector in the jet core region indicates a region with a cooler

surface temperature. An interesting feature that appears in both cases is the locally warm region that bisects the jet core region axially. It is also important to note that there are no significant surface temperature differences upstream of the injector. When interpreting these images, it is important to realize that many surface temperature differences were caused by filling putty on the surface, and not necessarily by the flow characteristics. The putty, which has different heat transfer properties than the aluminum surface, was used to create a smooth surface. This procedure has typically been used in the main supersonic tunnel.

Figure 27 shows two cases of unheated helium injection. The injectant total temperature was 300 Kelvin in both cases. The temperature range was 10 degrees, spanning 289.2 to 299.2 degrees Kelvin in the top image and 288.2 to 298.2 degrees Kelvin in the bottom image. The lower range allows for greater resolution than that achieved in Figure 26. The basic trends are similar to those seen in Figure 26, with the dark jet core region being much more pronounced using these camera settings. One possible reason for the greater contrast is that the lower injectant temperature caused the surface downstream of the injector to be cooler. Another difference from Figure 26 is that there is no visible warm region axially bisecting the cool jet core region. This may have also been the result of the lower injectant temperatures. Another possible explanation is that the reduced temperature range does not allow for the detection of this warmer region. These images also show no significant surface temperature differences upstream of the injector.

When monitoring the infrared images in real time, some transient patterns were observed at the instant the injection was turned on or off. By viewing the

recordings at one-third speed, these patterns were captured and are shown in Figure 28. Figure 28(a) shows heated helium injection at the instant the injectant was turned on. The injectant total temperature was 310 Kelvin. The temperature range for this image was 10 degrees, spanning from 288.2 to 298.2 degrees Kelvin. In contrast to the previous images, this image shows a locally warm region downstream of the injector in the jet core region. This transient trend lasted only a fraction of a second before the region became cooler than its surroundings. This phenomenon may have been the result of an initially lower convective heat transfer coefficient, causing locally warmer surfaces in the areas with high helium concentration. The convective heat transfer coefficients may have been lower because of the initially lower axial velocity of the injectant. This pattern was not observed during tests with unheated injection.

Figure 28(b) shows unheated helium injection at the instant the injectant was turned off. The helium total temperature was 300 Kelvin. The temperature range was 20 degrees, spanning from 285.3 to 305.3 degrees Kelvin. This photograph captures a period of rapid cooling downstream of the injector as the injectant is turned off. Although this surface area is cooler than its surroundings during steady state operation, it became noticeably cooler as the injectant was turned off. This rapid cooling may have resulted from a sudden pressure expansion caused by shutting off the injectant valve. Evaluating the Joule-Thomson coefficient, which is a measure of the change in temperature corresponding to a change in pressure for a constant enthalpy process, reveals that the helium temperature will drop during such a pressure expansion. This trend lasted about one second before disappearing, and was seen in both heated and

unheated injection tests.

Test cases where no injection occured and at the instant of free jet shutdown are included in Figure 29. Figure 29(a) shows a test case where a cylindrical rod was placed protruding from the injector orifice, to examine the flow around a solid body. The temperature range was 20 degrees, spanning from 285.3 to 305.3 degrees Kelvin. This photograph does not show a significantly cooler region downstream of the injector, as was seen in Figures 26 and 27. The features in this photograph are very similar to the undisturbed flow cases. Figure 29(b) shows the surface immediately following facility shutdown. Upon shutdown, the entire surface underwent a rapid cooling followed by a slow heating back to ambient conditions. Evaluating the Joule-Thomson coefficient for air shows that a pressure expansion will cause an increase in temperature, which is the opposite of what is experienced, leaving this phenomenon unexplained. However, since studying the transient effects of injection was not a goal of this research, no further investigation was done. The transient cooling lased for only a fraction of a second. This image shows the surface as it was returning to ambient conditions.

It was hoped that these images would provide some information about the injectant flow patterns in the boundary layer, especially in areas away from the jet core region. Unfortunately, the infrared images did not show conclusive evidence of any injectant flow around the jet core region. One reason for the inconclusiveness of the images is the test procedure, which aimed to produce locally higher surface temperatures in areas with high helium concentration by heating the helium. This procedure was not effective because the differences in

surface temperature caused by the temperature difference between the free stream and the injectant was not significant compared with the differences in surface temperature caused by the difference in convective heat transfer coefficients between helium and air. The result was that areas with higher helium concentration actually produced lower surface temperatures than the surroundings, even though the helium was considerably hotter than the free stream. This is shown by the locally cool region seen downstream of the injector in Figures 26 and 27. A heat transfer analysis of the injector block will quantify this effect and demonstrate that it may be possible in the future to use infrared imaging to quantitatively measure local helium concentration, with some modifications to the experiment. Figure 30 will assist in the following analysis.

The one-dimensional conduction through the injector block is given by:

$$q = \frac{k}{t}(T_i - T_o) \tag{4.1}$$

where q can be determined given information about T_i and T_o. Local values for T_o can be obtained from the infrared images and values for T_i can be obtained by instrumenting the inside surface of the block with thermocouples. The convection heat transfer away from the surface is given by:

$$q = h(T_o - T_\infty) \tag{4.2}$$

Having determined q from equation (4.1), the local convective heat transfer coefficient, h, can be determined, given values for T_∞. The heat transfer coefficient is related to the Nusselt number:

$$Nu = \frac{hx}{k} \tag{4.3}$$

where x is the axial distance and k is the thermal conductivity of the fluid. For a

turbulent flat plate flow, the local Nusselt number is given by:

$$Nu = 0.0296 Pr^{\frac{1}{3}} Re^{0.8} \tag{4.4}$$

Knowing that the Prandtl number is roughly the same for helium and air, and assuming that the local Reynolds number is a constant, h is reduced to a function of the local thermal conductivity, k, of the fluid. Since the thermal conductivity of helium is about six times as great as that for air, it is possible that differences in the local values of h could actually be used to determine the local helium concentration. A more complete analysis of the problem, including instrumentation considerations and calibration procedures, would be required to determine the feasibility of this idea.

This analysis shows that the surface temperature is affected by the difference in the convective heat transfer coefficients, as well as by the temperature difference between the fluid and the surface. As a result, heating and cooling the injectant is not necessarily a requirement to qualitatively, or possibly quantitatively, determine the injectant flow patterns within the boundary layer. The effects of increased turbulence, separation and vortices caused by the injection should also be more carefully considered in future work with the infrared imaging technique.

As Figures 26 through 29 show, infrared imaging has great potential as a means to qualitatively, and possibly quantitatively, investigate normal injection. The images produced were clear, and since they were taken normal to the test surface, could be directly scaled. The test set up for the experiments was relatively simple and versatile. Another advantage of this method is that it allows for near real-time flow visualization, which captures the transient, as well as

steady-state flow patterns. The major deficiency of this method is that the images are extremely sensitive to the physical nature of the test surface. Objects such as screws, scratches and filling putty all affect the images, distorting what are interpreted as flow effects on the surface temperature. By implementing a test surface and injector constructed of one homogeneous material and utilizing the results of the previous heat transfer analysis, better results may be obtained.

4.5 Concentration Measurements

Helium concentration measurements were taken for test cases with both air and helium injection at total pressures of 3.67, 4.44 and 5.20 atm. These injectant pressures correspond to expansion ratios of 1.20, 1.45 and 1.70 for helium injection and 1.30, 1.57 and 1.85 for air injection. All injectant was unheated, with the injectant total temperature being 300 Kelvin. Concentration measurements were taken at two axial positions, $\frac{x}{d} = 10.9$ and $\frac{x}{d} = 6.9$. The center of the probe tip was located at $\frac{z}{d} = 0.1$. At each axial position, the probe was traversed laterally, ranging from $\frac{y}{d} = +5$ to $\frac{y}{d} = -9$ (the test section coordinate system is shown in Figure 7). At each test point two runs were made, one with the probe traversing upward and one with the probe traversing downward. This was done to verify the results and to see if the traverse direction had any bearing on the data. Due to physical and operational limits, the actual lateral range traversed varied from run to run. All data was reduced by the the two methods discussed in Section 3.4.1. Because the empirical curve fit method produced a lower calibration error, all of the data presented herein was reduced using the empirical calibration curves.

Figures 31 and 32 are plots of helium concentration versus lateral position for the air injection tests. Similar plots for test cases with helium injection and no

injection are provided in Appendix B. The air injection tests were done to test the validity of the concentration results. Since no helium was present in the flow, all concentration levels should be zero, within some level of uncertainty, regardless of any selective sampling that may occur. This is a common practice, and past results have shown that the probe detects no helium, within a small uncertainty range, as expected. The plots are characterized by what appears to be a central peak in helium concentration, with two peaks on either side. Similar characteristics were noted in the concentration data from all of the air and helium injection cases. All test cases also showed an unrealistic trend of increasing helium concentration as the lateral position increased past $\frac{y}{d}$ = -7. These trends were consistent regardless of the traverse direction during the tests.

These results are definitely not factual, since no helium was present anywhere in the flow field, and show that there was a problem with this concentration probe operating in the free-jet facility. Based on these results, the uncertainty of the concentration data is no less than 25 percent mole fraction helium. The high peak-to-peak variance and repeatability of the general trends seen in Figures 31 and 32 eliminate the possibility that a zero offset calibration error or high random noise levels in the hot-film signal are the causes of the unusually high uncertainty. Another trend contributing to the uncertainty of the results was the lack of repeatability of the apparent helium concentration levels at the same test point, which varied by as much as 15 percent mole fraction helium in the air injection cases and up to 20 percent mole fraction helium in the helium injection cases. Such high uncertainty and lack of repeatability have not been encountered in past experiments using the same probe.

Since the concentration data were determined from only the probe pressure and the sensor voltage, plots of these data were made and are presented in Figures 33 and 34 for the air injection cases. Similar plots for test cases with helium injection and no injection are provided in Appendix B. The probe pressure is nondimensionalized by the free stream total pressure, which had a value of 6.67 atm. All of the pressure data for the injection cases showed similar trends, which are characterized by two high pressure peaks separated by a central low pressure area. The plots also show two secondary areas of high pressure on either side of the two central peaks, with the probe pressure dropping rapidly as the lateral position increases away from the centerline past $\frac{y}{d}$ = -7 and $\frac{y}{d}$ = +4. The location of the low pressure areas in these plots correspond exactly to the areas in Figures 31 and 32 that show apparent peaks in helium concentration. Likewise, the areas of high pressure correspond to the areas that show lower helium concentration. This result indicates that either the pressure measurements were erroneous or the probe calibration and data reduction process, which determined local helium concentration using the probe pressure, was not valid.

The hot-film voltage plots are characterized by two central voltage peaks, separated by a low voltage region. The plots show a fairly level signal from $\frac{y}{d}$ = -3 outward, before dropping significantly around $\frac{y}{d}$ = -8. The data, in general show a steady decline on the positive side of the centerline. The peak-to-peak variance in the signal was as high as 0.5 volts. Although significant variations in the trends and magnitudes of the hot-film voltage were often seen, the signal does not appear to have unusual characteristics when compared with the signals from past experiments.

There are several factors that may have contributed to the ineffectiveness of the concentration probe. The probe was used very differently than in previous experiments, in that it was positioned with the tip in direct contact with the test surface. This positioning most likely had an effect on whether or not the probe swallowed the bow shock, if one existed at all. Failure to capture an undistorted sample may have lead to poor results. Also, the probe was positioned at an angle of incidence of about 18.5 degrees to the free stream, which allowed the probe tip to be as close to the test surface as possible. Ng, et al. [8] studied the effects of probe angle on the concentration results. They concluded that measured helium concentration was about three percent less than the actual helium concentration when the probe was positioned at a 15 degree angle. No conclusions were made concerning the uncertainty of the probe results as the angle was increased. Since the probe was designed to operate in two-dimensional flow, large angles of incidence may lead to an increase in the uncertainty of the results [37]. This hypothesis is supported by a previous study of slot injection into a supersonic flow. In this study, which used a similar concentration probe, results at the axial position nearest to the slot showed high levels of uncertainty. This may have been the result of a highly vortical flow at the probe tip, caused by the slot injection [38]. Other slot injection experiments have shown no such effects.

While the previous two considerations may have affected the results, they still do not satisfactorily explain why helium concentration levels as high as 30 percent mole fraction appeared in cases known to have no helium present in the flow field. Since the modified data reduction method (Section 3.4.4) does not account for the temperature of the flow through the probe, this was investigated

as a possible source of error. The probe temperature typically dropped steadily from about 300 to about 280 degrees Kelvin during tests, causing this data to be dependent on the traverse direction. Based on the semi-empirical hot-film relationship (Section 3.4.1) and past experiments, such a temperature drop will have some effect on the concentration results. However, because the shape of the concentration plots is repeatable regardless of the traverse direction, while the temperature data are very dependent on the traverse direction, the probe temperature does not appear to have a significant effect on these concentration results. Since the concentration data were determined from only the probe pressure and sensor voltage, the source of error most likely lies in either erroneous measurements of these data or in the calibration and data reduction process. Because probe calibration was performed over a much higher pressure range than past experiments have required, this is the most likely source of error. As mentioned in Section 3.4.1, calibration results over the higher pressure range exhibited a vastly different behavior, and thus required the abandonment of the semi-empirical calibration curve fitting technique in favor of a purely empirical method. These changes in calibration and data reduction techniques are the most likely cause for the ineffectiveness of the concentration probe.

5 Conclusions and Recommendations

The development of a Mach 1.95 free-jet facility for the experimental investigation of normal injection through a circular injector was inspired by the need to investigate the injectant flow patterns in the boundary layer. Previous studies of transverse injection have indicated the possibility that a small amount of injectant might be escaping around the jet core region within the boundary layer. To facilitate further investigation, the goal of the project was to build a free-jet facility, in which injection tests could be performed with much greater optical and spatial access, using as much existing hardware as possible. The use of nanoshadowgraph and oil flow photography, as well as infrared imaging, for flow visualization were investigated as a part of development. The second major goal was to evaluate the effectiveness of using an existing hot-film concentration probe in the facility. This examination involved taking quantitative measurements of the local helium concentration, using both air and helium as the injectant.

The Mach 1.95 free-jet facility produced a relatively shock free and repeatable flow. The facility proved to be durable, easy to operate and versatile for implementing various tests. The improved optical access led to the successful implementation of various flow visualization techniques. Oil flow photographs taken in the free-jet facility were superior to those taken in the main supersonic tunnel, because they were taken normal to the test surface, allowing them to be

directly scaled. While nanoshadowgraph photography was a slightly more complicated procedure in the free-jet facility, high quality photographs were obtainable. The use of infrared imaging as a flow visualization technique was also successfully implemented in the facilty. Although this technique did not yield conclusive evidence about the injectant flow patterns in the boundary layer, it did show great promise for future work.

The evaluation of the hot-film concentration probe revealed that the results had an uncertainty of no less than 25 percent mole fraction helium. Additionally, the probe data suggested that up to 30 percent mole fraction helium existed in flow fields known to have no helium present. These erronous results were most likely the result of improper probe calibration and data reduction processes, which had to be modified for tests in the free-jet facility.

Although the concentration probe was ineffective in the facility, this project has shown promise for future work. There are many improvements that should be made to enhance the performance of the free-jet facility for future experiments. The addition of automated control of the injectant valve and traversing system would eliminate the need for a second operator during concentration measurement tests. Additionally, automating the nanoshadowgraph photography process would eliminate the need for a camera operator to be positioned in the sound room during tests and lead to more efficient and safer operation of the free jet facility. This could be accomplished by adding a shutter, that is remotely triggered, to the camera. Although the set up for schlieren photographs is more complicated than the nanoshadowgraph set up, it would be beneficial to use this technique to capture the time-averaged phenomena in the flow. Eventually, automation of the free-jet on/off valve, in conjunction with the

injectant and traversing systems, would result in more efficient and repeatable tests. This has been proven by the recent advances in the automation of the main supersonic facility. In addition to these hardware improvements, local mean flow quantities, such as pressure and temperature, should be measured to more accurately characterize the free jet flow. These properties have typically been measured with intrusive sampling probes.

The study of injectant flow patterns in the boundary layer should be continued to provide more conclusive results. The first priority in the continuation of these experiments is to investigate the lack of effectiveness of the concentration probe. This will most likely involve a detailed analysis of the calibration and data reduction methods, and how they change at the higher pressures experienced in the free-jet facility. This may also involve redesigning some aspects of the probe or test section. The work with infrared imaging should also be continued, as this flow visualization method may provide important information about the injectant flow patterns on the test surface. More conclusive results may be obtained by using a flow surface and injector made of a solid, homogeneous material. Results may also be enhanced by more carefully considering the results from the heat transfer analysis performed in section 4.4. The possibility of using the infrared imaging system as a quantitative means of measuring the local helium concentration should also be investigated further.

Appendix A: Computer Programs

The computer programs used to smooth and reduce the data are given on the following pages. Program 1 was the smoothing routine and Program 2 is the code used to reduce the data using the curve fit calibration data. Both programs were written in FORTRAN 77 on an IBM Personal Computer.

```
c*****************************************************************
c    PROGRAM  HAMMING.FOR

     written by John R. Mills,  August 1991

c    This program inputs the data from XRUN.RUN# and smooths the
c    position, voltage, temperature and pressure data using a
c    HAMMING window smoothing technique.  This method is a biased
c    averaging technique that uses a weighted average, rather than
c    the arithmetic mean to smooth the data.  The program allows for
c    the size of the window to be varied.

c*****************************************************************

     CHARACTER*15 FILEIN, FILEOUT

     REAL HAMMING(200), POS(1250), YNONDIM, VOLT(1350), PNONDIM
     REAL SUMPOS1, TEMP(1350), SUMPRES1, PRES(1350)
     REAL AMP, A, I1, N1, POS1, SUMPOS, VOLT1, SUMVOLT
     REAL TEMP1, SUMTEMP, PRES1, SUMPRES
     INTEGER I, J, J1, PTS, N, HALFN, HALFN1, PTS1

c************ Open files ***********************************************

     WRITE(*,*)
     WRITE(*,*) '     Input data file name ... '
     READ(*,5) FILEIN
     WRITE(*,*)
     WRITE(*,*) '     Output data file name ... '
     READ(*,5) FILEOUT
     WRITE(*,*)
5    FORMAT(A15)

     OPEN(1, FILE = FILEIN, STATUS = 'OLD')
     OPEN(2, FILE = FILEOUT,STATUS = 'NEW')

c************ Input size of window and data file **********************
     WRITE(*,*)
     WRITE(*,*) '     Size of HAMMING window (even no. of pts) = '
     READ(*,*) N
     WRITE(*,*)
     WRITE(*,*) '     Size of input data file (no. of pts) = '
     READ(*,*) PTS
     WRITE(*,*)
c************ Input the nondimensional parameters *********************
     WRITE(*,*) '     Nondimensional pressure parameter (psi) = '
     READ(*,*) PNONDIM
     WRITE(*,*)
```

Program 1: Data Smoothing Program

```
      WRITE(*,*) '    Nondimensional position parameter (mm) = '
      READ(*,*) YNONDIM
      WRITE(*,*)

c************ Initialization ****************************************

      PI    =   3.141593
      AMP   =   0.0
      HALFN =   N / 2
      HALFN1 =   HALFN + 1
      PTS1  =   PTS + HALFN
      N1    =   REAL(N)

c************ Data input and wrap ***********************************

      WRITE(*,*) '    Loading data '
      DO  10  I  =  HALFN1, PTS1

      READ(1,*) POS(I), VOLT(I), PRES(I), TEMP(I)

10    CONTINUE
      WRITE(*,*)

      DO  20  I  =  1, HALFN

      POS(I)  =  POS(N+1-I)
      VOLT(I) =  VOLT(N+1-I)
      TEMP(I) =  TEMP(N+1-I)
      PRES(I) =  PRES(N+1-I)

     J  =  HALFN1 - I
     J1 =  PTS1 + I

     POS(J1) =  POS(PTS+J)
     VOLT(J1)=  VOLT(PTS+J)
     TEMP(J1)=  TEMP(PTS+J)
      PRES(J1)=  PRES(PTS+J)

20    CONTINUE

c************ Calculate total amplitude of window *********************

      DO  30  I  =  1, N

      I1    =   REAL(I)
      A     =   0.54 - 0.46*COS(2.*PI*I1/N1)
      AMP   =   AMP + A
```

Program 1: Data Smoothing Program

```
30   CONTINUE
     DO 40 I = 1, N

     I1   =  REAL(I)
     HAMMING(I) =  (0.54 - 0.46*COS(2.*PI*I1/N1)) / AMP

40   CONTINUE

c************ Loop to smooth data ************************************
     WRITE(*,*) '     Smoothing data '

     DO 60 I = HALFN1, PTS1

     SUMPOS = 0.0
     SUMVOLT = 0.0
     SUMTEMP = 0.0
     SUMPRES = 0.0

     DO 50 J = 1, N

     POS1 = POS(I+J-HALFN-1) * HAMMING(J)
     VOLT1 = VOLT(I+J-HALFN-1)* HAMMING(J)
     TEMP1 = TEMP(I+J-HALFN-1)* HAMMING(J)
     PRES1 = PRES(I+J-HALFN-1)* HAMMING(J)

     SUMPOS  =  SUMPOS + POS1
     SUMVOLT =  SUMVOLT + VOLT1
     SUMTEMP =  SUMTEMP + TEMP1
     SUMPRES =  SUMPRES + PRES1

50 CONTINUE

     SUMPOS1 = SUMPOS / YNONDIM
     SUMPRES1 = SUMPRES/ PNONDIM

     WRITE(2,70) SUMPOS1, SUMVOLT, SUMPRES1, SUMTEMP

60   CONTINUE

70   FORMAT (F10.3,F10.4,F10.3,F10.2)
     CLOSE (1)
     CLOSE (2)

     WRITE(*,*)
     WRITE(*,*) '     Program finished '
     END
```

Program 1: Data Smoothing Program

```
c**********************************************************************

c  Program :  XREDUCE2.FOR

c      This program reduces the hot film voltage, total
c      pressure and total temperature into helium
c      concentration at each traverse location.  This
c      program differs from XREDUCE1.FOR in that it does
c      not calculate the calibration voltages from the
c      Nusselt number correlation (using constants A & B).
c      Instead this program uses a predetermined curve fit
c      for the voltage vs. pressure calibration curves
c      and uses these fits to determine the voltage limits.
c      This was done because at higher pressures the routine
c      used to determine the constants A & B is not accurate.
c      Because of the method of this routine, temperature
c      variations are not accounted for.


c  For new TSI sensor-20

c  Input file = xrun.run#     which is of the form:

c ylvdt - Sensor voltage - sensor P (psia) - sensor T (K)

c  Output file = xrunout.run#   which is of the form:

c Xhe (mole fracation He)  -  ylvdt

c  by:    Joel C. Rosson   begun       2/19/85
c     Fei T. Kwok      modified    10/20/88
c     Eric J. Fuller   Modified     1/19/90
c     Eric J. Fuller   Modified     5/10/90
c     John R. Mills    Modified     8/05/91

c**********************************************************************
c      File open and data input section
c**********************************************************************

      character*3 run
      Character*15 calfile,filein,fileout,limitout

      DIMENSION TT(2000),PT(2000),AP1(2000),XHE(2000),YLVDT(2000)
      DIMENSION A(10,10)
      INTEGER ORDER, JRUN, L, I, ILIMS, J, NUM

c  Set Calibration file name, input file name and output file name
```

Program 2: Data Reduction Program

```
      WRITE(*,*)
      WRITE(*,*) '  Calibration file name = '
      READ(*,5) calfile
5     FORMAT(a15)

c   open hfrun.num  containing the Hot film run numbers to be reduced
c   which is of the form (by column):  NUMRUN  RUN#  RUN#  RUN# ...

      OPEN (1,file='hfrun.num',status='old')
      READ (1,*)
      READ (1,*) numrun

c   Big loop for each run #

      DO  9999  JRUN  =  1, NUMRUN
        READ (1,'(a3)') run


c       open files

      filein = 'finl.'//run
      fileout = 'xrunout2.'//run
      limitout = 'limit.'//run

      OPEN(2,FILE=calfile)
      OPEN(3,FILE=filein)
      OPEN(7,FILE=fileout)
      OPEN(8,FILE=limitout)

c    Read in the calibration file containing the
c    calibration constants for different temperatures.
c   -- NR     =  1
c   -- L      =  number of data values from experimental run
c   -- NCONST =  number of concentration levels per calibration
c   -- # of curve fit constants sets
c   -- DELX   =  Increment of Xhe between Calibration levels
c   -- ORDER  =  Order of pressure / voltage curve fit


      READ(2,*) NR,L,NCONST,DELX,ORDER
      NUM  =  ORDER + 1

      DO  2  I = 1, NCONST
   DO  1 J  =  1, NUM

      READ(2,*) A(I,J)

1     CONTINUE
2     CONTINUE
      CLOSE (2)
```

Program 2: Data Reduction Program

```
c   Read in the data values from XRUN.RUN#

c  ylvdt  = lvdt location
c  ap1    =  sensor voltage
c  pt     =  sensor pressure (psia)
c  tt     =  sensor temperature (deg K)

      WRITE(*,*)
      WRITE(*,*)' LOADING DATA VALUES . . .'
      WRITE(*,*)
      DO  10  I = 1 ,L
  READ(3,*) YLVDT(I),AP1(I),PT(I),TT(I)
  PT(I)  =   PT(I)*6.6667
10     CONTINUE
      CLOSE (3)


c**********************************************************************
c      Reduction section
c**********************************************************************

c   input shift voltage to correct for drift (shift ideally = 0.0)


 WRITE(*,*)
  WRITE(*,*)' INPUT SHIFT VALUE IN VOLTS (EXP-CALC)'
 WRITE(*,*)
 READ(*,*) SH
 WRITE(8,*) SH
 WRITE(*,*) SH

     NCOUNT = 0
     NC0 = 0
     NC1 = 0

c    Loop to interpolate for XHe according to calculated
c    bounds from the curve fit.

     DO 1000  I = 1, L

c   Loop to compute upper and lower concentration bounds
c   and then to interpolate to get XHe

      XLOW = 0.0
      XUP = DELX
      DO 250 ILIMS = 1 , NCONST-1
```

Program 2: Data Reduction Program

```
c     Calculate lower bound

 VLOW = A(ILIMS,1) + A(ILIMS,2)*PT(I) + A(ILIMS,3)*PT(I)**2 +
    +       A(ILIMS,4)*PT(I)**3 + A(ILIMS,5)*PT(I)**4 +
    +       A(ILIMS,6)*PT(I)**5 + SH

c     Calculate upper bound


 VUP = A(ILIMS+1,1) + A(ILIMS+1,2)*PT(I) + A(ILIMS+1,3)*PT(I)**2
    +     + A(ILIMS+1,4)*PT(I)**3 + A(ILIMS+1,5)*PT(I)**4 +
    +       A(ILIMS+1,6)*PT(I)**5 + SH

c     Account for values that fall below XHe=0. and exceed
c  XHe =1. due to exprimental errors

   IF(ILIMS.EQ.1.AND.AP1(I).LT.VLOW)THEN
       XHE(I) = 0.0
       NC0 = NC0 + 1
       WRITE(8,*) I,XHE(I),AP1(I)-VLOW
       GO TO 1600
    ELSE IF(ILIMS.EQ.NCONST-1.AND.AP1(I).GT.VUP)THEN
       XHE(I) = 1.0
       NC1 = NC1 + 1
       WRITE(8,*) I,XHE(I),AP1(I)-VUP
       GO TO 1600
   END IF

c     Interpolate to get XHe

  IF(AP1(I).EQ.VLOW)THEN
      XHE(I) = XLOW
     GO TO 1600
  ELSE IF(AP1(I).EQ.VUP)THEN
     XHE(I) = XUP
     GO TO 1600
  ELSE IF(AP1(I).GT.VLOW.AND.AP1(I).LT.VUP) THEN
     XM = (XUP - XLOW) / (VUP - VLOW)
     XHE(I) = XM * (AP1(I) - VLOW) + XLOW
     GO TO 1600
  END IF
  XLOW = XUP
  XUP = XLOW + DELX

250   CONTINUE
```

Program 2: Data Reduction Program

```
c      Write data to output file

1600   WRITE(7,1610) XHE(I),ylvdt(i)
       NCOUNT = NCOUNT + 1

1610  FORMAT(F10.5, F10.4)

     IF (I/50 * 50 .EQ. I)  WRITE(*,*) I

1000  CONTINUE

     WRITE(*,*)' Number of pts used = ',NCOUNT,' out of ',L
     WRITE(*,*)
     WRITE(*,*)' Number of pts. forced to 1.0 = ',NC1
     WRITE(*,*)
     WRITE(*,*)' Number of pts. forced to 0.0 = ',NC0

     CLOSE(7)
     CLOSE(8)

9999  CONTINUE
     CLOSE (1)

999    STOP
      END

c**************************************************************************
```

Program 2: Data Reduction Program

Appendix B: Additional Plots

Additional plots of the helium concentration, hot-film voltage and probe pressure for test cases with helium injection and no injection are given on the following pages.

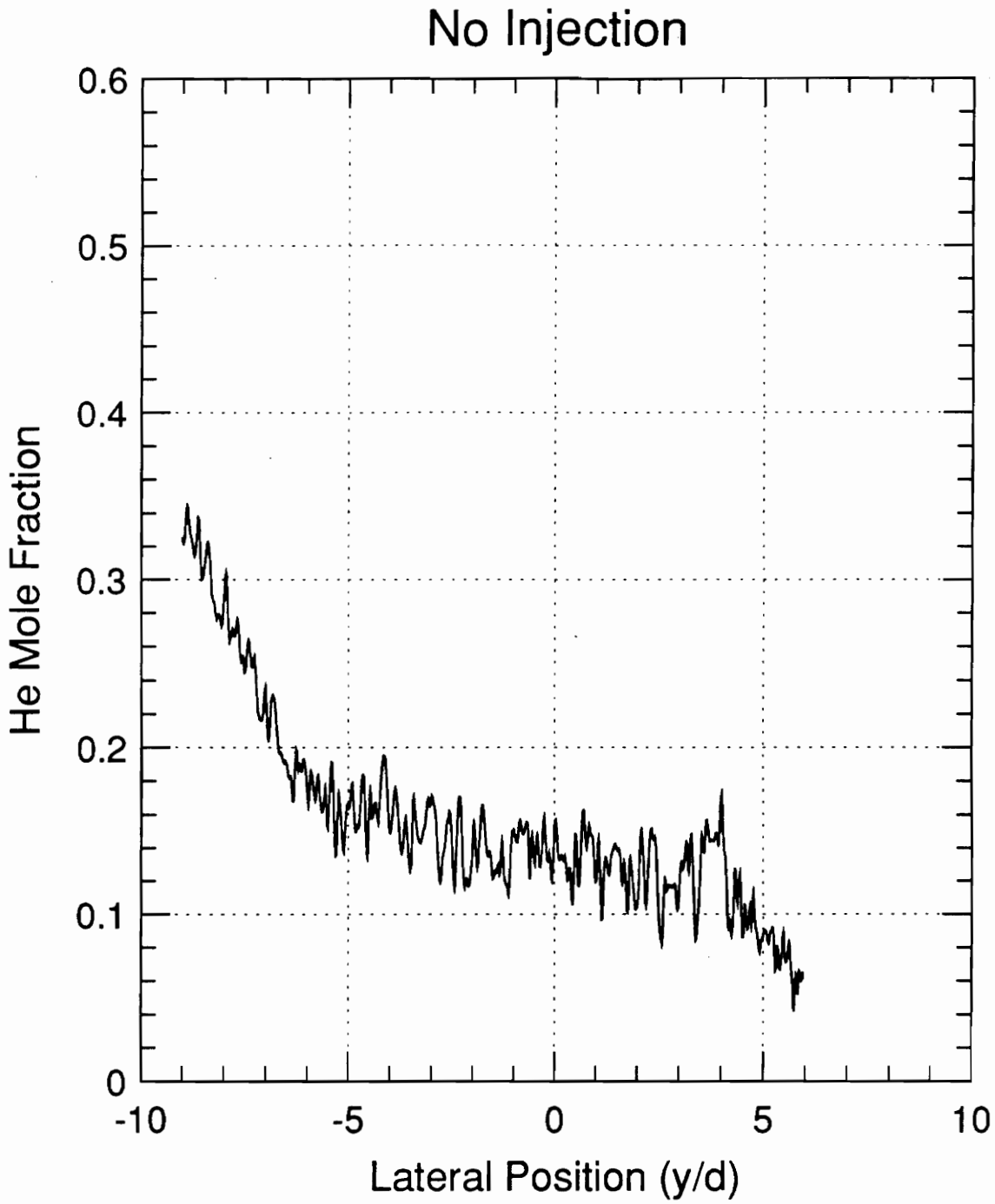

Helium Concentration Measurements
No Injection, $\frac{x}{d} = 10.9$

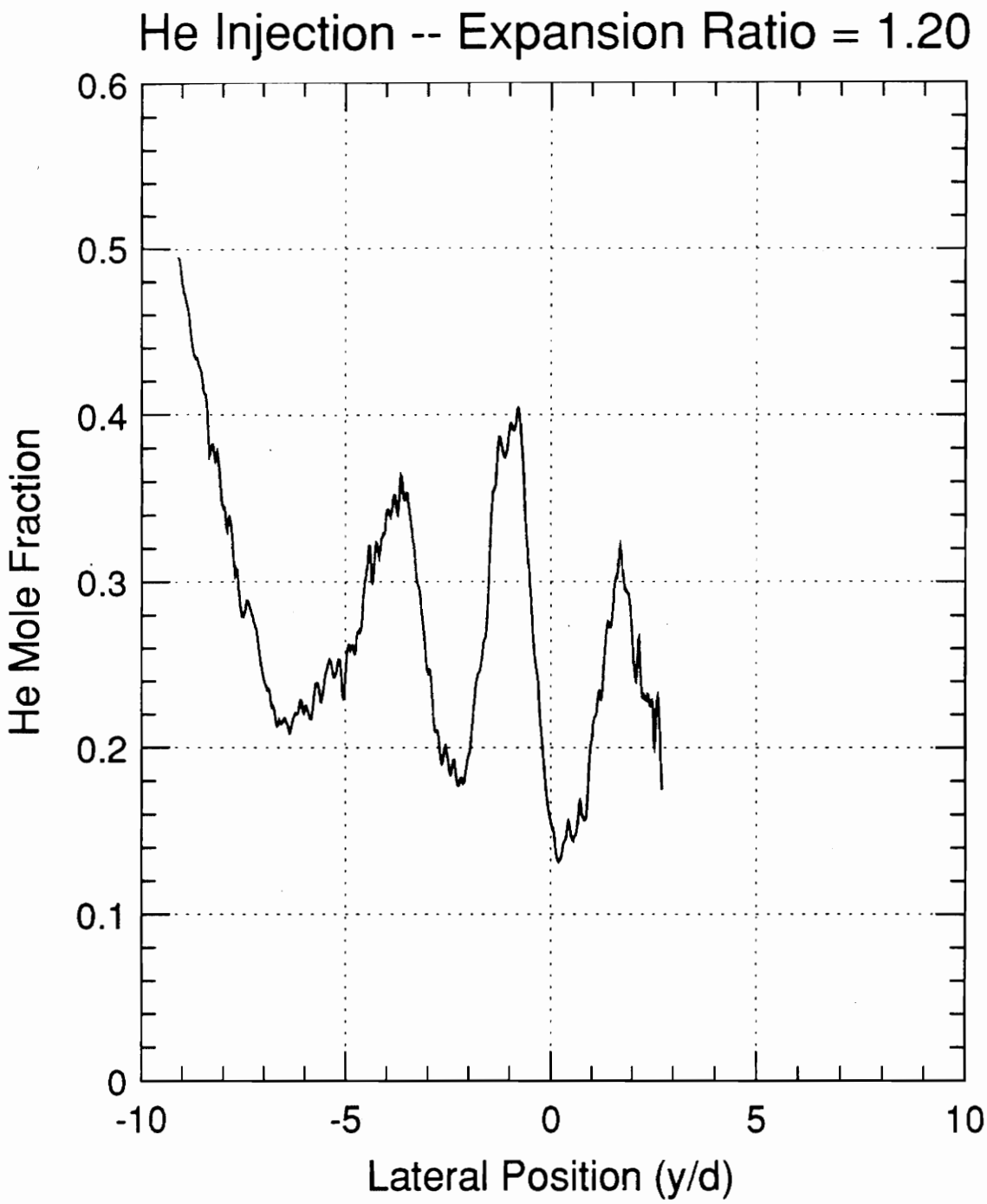

Helium Concentration Measurements, Helium Injection
Expansion Ratio = 1.20, $\frac{x}{d} = 6.9$

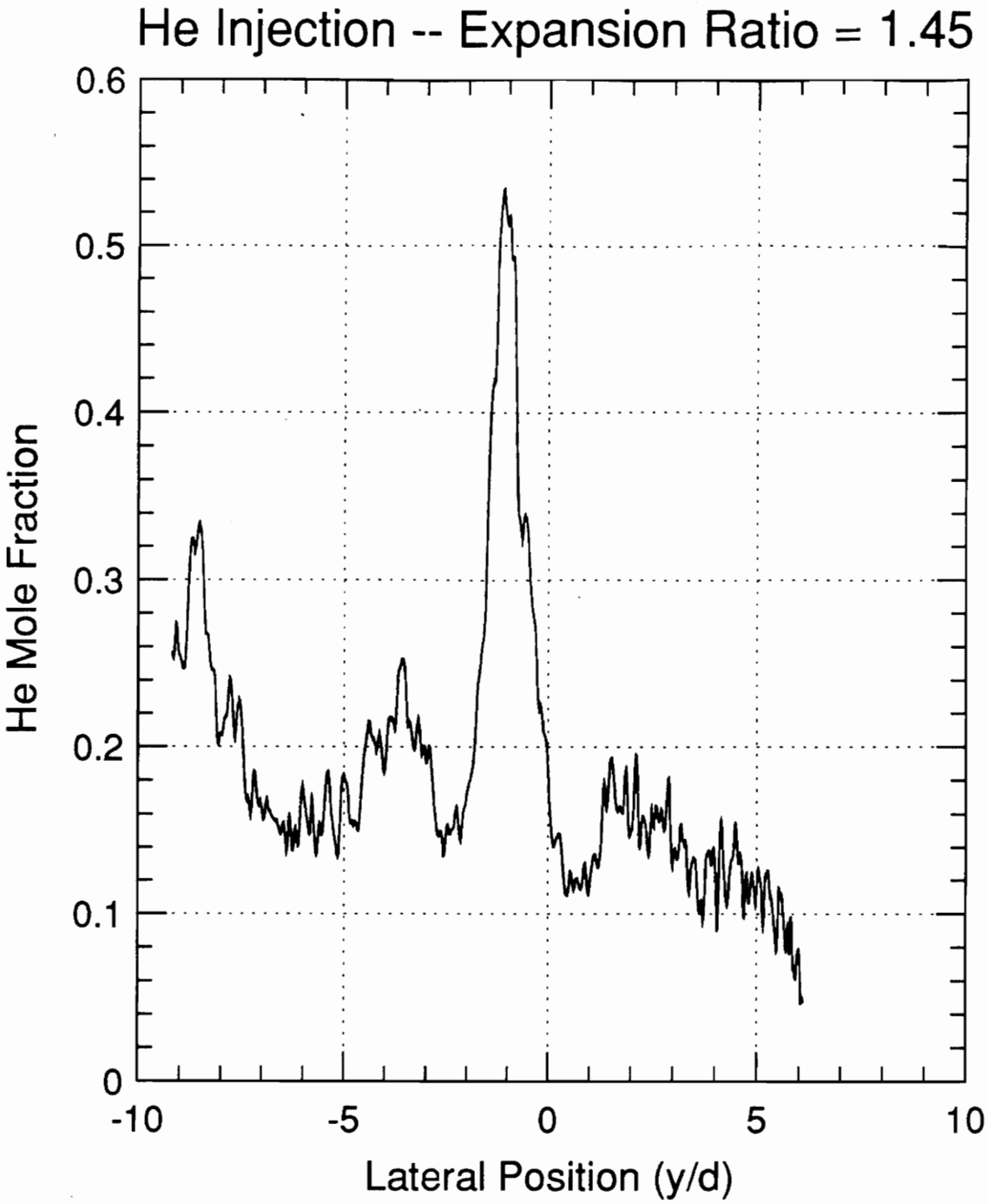

Helium Concentration Measurements, Helium Injection
Expansion Ratio = 1.45, $\frac{x}{d} = 10.9$

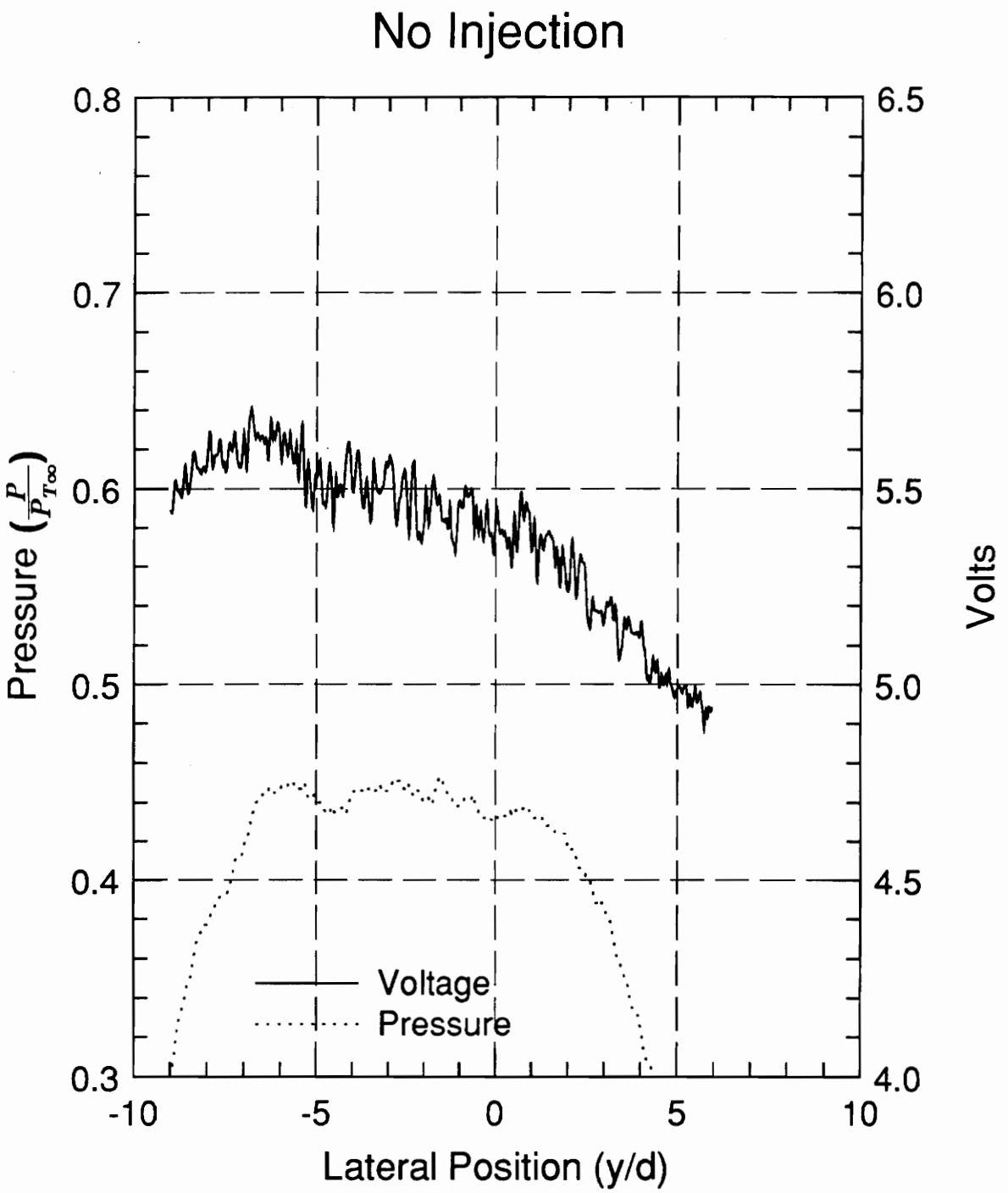

Probe Pressure, Sensor Voltage
No Injection, $\frac{x}{d} = 10.9$

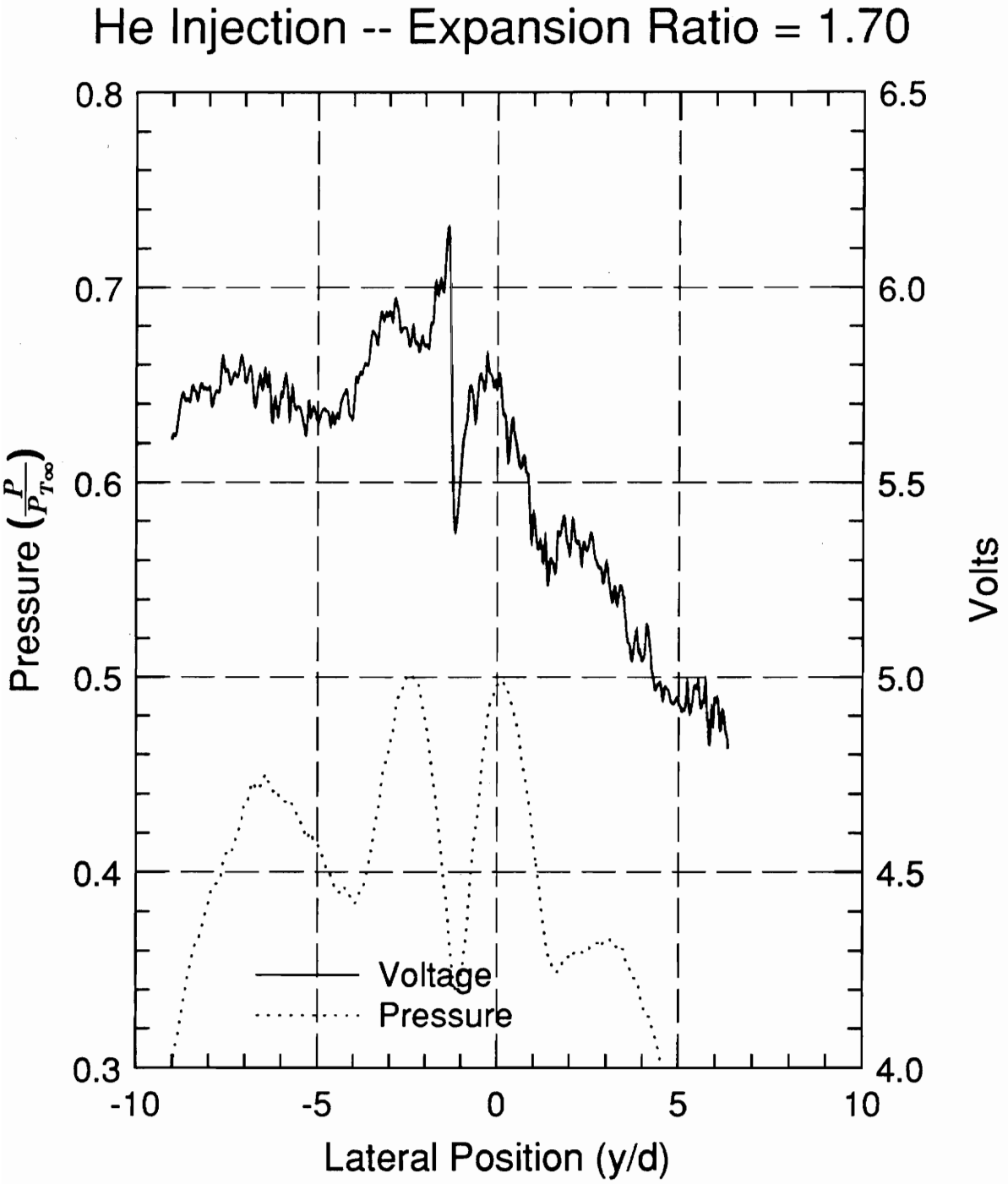

Probe Pressure, Sensor Voltage, Helium Injection
Expansion Ratio = 1.70, $\frac{x}{d} = 6.9$

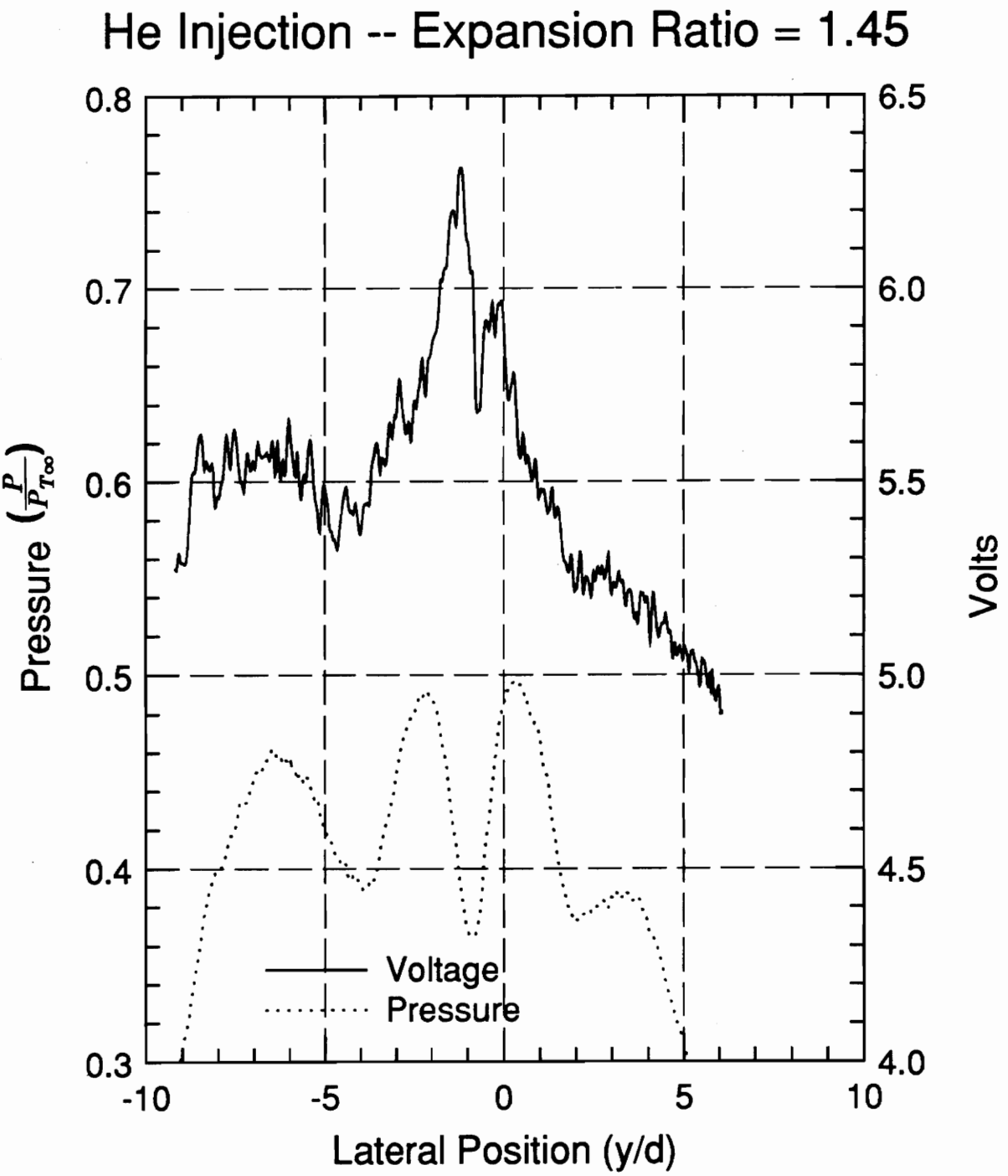

Probe Pressure, Sensor Voltage, Helium Injection
Expansion Ratio = 1.45, $\frac{x}{d} = 10.9$

References

[1] Mays, R.B., "Experimental Investigation of Sonic Helium Injection at a Low Downstream Angle into Supersonic Flow," M.S. Thesis, Virginia Polytechnic Institute and State University, June 1990.

[2] Thomas, R.H., Schetz, J.A. and Billig, F.S., "Gaseous Injection in High Speed Flow," Presented at the Ninth International Symposium on Airbreathing Engines, Athens, Greece, September 1989.

[3] Rogers, R.C., "A Study of the Mixing of Hydrogen Injected Normal to a Supersonic Airstream," NASA TN D-6114, Langley Research Center, March 1971.

[4] Rogers, R.C., "Mixing of Hydrogen Injected from Multiple Injectors Normal to a Supersonic Airstream," NASA TN D-6476, Langley Research Center, September 1971.

[5] Torrance, M.G., "Effect of Injectant Molecular Weight on Mixing of a Normal Jet in a Mach 4 Airstream," NASA TN D-6061, Langley Research Center, January 1971.

[6] Cohen, L.S., Coulter, L.J. and Egan, W.J., "Penetration and Mixing of Multiple Gas Jets Subjected to a Crossflow," *AIAA Journal*, Vol. 9, No. 4, April 1971, pp. 718-724.

[7] Reis, V.H. and Fenn, J.B., "Separation of Gas Mixtures in Supersonic Jets," *The Journal of Chemical Physics*, Vol. 19, No. 12, December 1963, pp. 3240-3250.

[8] Ng, W.F., Kwok, F.T. and Ninnemann, T.A., "A Concentration Probe for the Study of Mixing in Supersonic Shear Flows," AIAA Paper 89-2459, July 1989.

[9] Wood, C.W., "Oscillating Shock Impingement on Low-Angle Gas Injection into a Supersonic Flow," PhD Dissertation, Virginia Polytechnic Institute and State University, April 1991.

[10] Schetz, J.A., Personal Communication, May 1991.

[11] Schetz, J.A. and Billig, F.S., "Penetration of Gaseous Jets Injected into a Supersonic Stream," *Journal of Spacecraft and Rockets*, Vol. 3, No. 11, November 1966, pp. 1658-1664.

[12] Schetz, J.A., Hawkins, P.F. and Lehman, H., "Structure of Highly Underexpanded Transverse Jets in a Supersonic Crossflow," *AIAA Journal*, Vol. 5, No. 5, May 1967, pp. 882-884.

[13] Weidner, E.H. and Drummond, J.P., "Numerical Study of Staged Fuel Injection for Supersonic Combustion," AIAA Paper 81-1468, July 1981.

[14] Shuen, J.S. and Yoon, S., "Numerical Study of Chemically Reacting Flows Using an LU Scheme," NASA CR-180882, Lewis Research Center, 1988.

[15] Harloff, G.J. and Lytle, J.K., "Three-Dimensional Viscous Flow Computations of a Circular Jet in Subsonic and Supersonic Crossflows," NASA CR-182153, Lewis Research Center, July 1988.

[16] McDonough, J. and Catton, J., "Calculation of a Lateral Jet in a Hypersonic Cross-Flow," AIAA Paper 89-2459, July 1989.

[17] Uenishi, K. and Rogers, R.C., "Three-Dimensional Computation of Mixing of Traverse Injector in a Ducted Supersonic Airstream," AIAA Paper 86-1423, June 1986.

[18] Uenishi, K., Rogers, R.C. and Northam, G.B., "Three-Dimensional Computations of Transverse Hydrogen Jet Combustion in a Supersonic Airstream," AIAA Paper 87-0089, January 1987.

[19] Mao, M., Riggins, D.W., and McClinton, C.R., "Numerical Simulation of Transverse Fuel Injection," Presented at the CFD Symposium on Aeropropulsion, Lewis Research Center, April 1990.

[20] Carpenter, M.H., "Three-Dimensional Computations of Cross-Flow Injection and Combustion in a Supersonic Flow," AIAA Paper 84-0041, January 1984.

[21] Thomas, R.H. and Schetz, J.A., "Distributions Across the Plume of Transverse Liquid and Slurry Jets in Supersonic Airflow," AIAA Paper 84-0041, January 1984.

[22] Hollo, S.D., Hartfield, R.J. and McDaniel, J.C., "Injectant Mole Fraction Measurements of Transverse Injection in Constant Area Supersonic Ducts," AIAA Paper 90-1632, June 1990.

[23] Abbitt, J.D.,III, Hartfield, R.J. and McDaniel, J.C., "Mole Fraction Imaging of Transverse Injection in a Ducted Supersonic Flow," AIAA Paper 89-2550, July 1989.

[24] Marvin, J.G., "Future Requirements of Wind Tunnels for Computational Fluid Dynamics Code Verification," Presented at the AIAA 14^{th} Aerodynamic Testing Conference, W. Palm Beach, FL, March 1986.

[25] Gartenberg, E., Roberts, A.S., Jr. and Selby, G.V., "Infrared Surface Imaging as a Flowfield Diagnostic Tool," Presented at the International Congress on Instrumentation in Aerospace Simulation Facilities, 1987.

[26] Brandon, J.M., Manuel, G.S., Wright, R.E., Jr. and Holmes, B.J., "In-Flight Flow Visualization Using Infrared Imaging," AIAA Paper 88-2111, May 1988.

[27] Crowder, J.P., "Infrared Cameras for Detection of Boundary Layer Transition in Transonic and Subsonic Wind Tunnels," AIAA Paper 90-1450, June 1990.

[28] Schetz, J.A., Cannon, S.C. and Baranovsky, S., "Ignition of Liquid Fuel Jets in Supersonic Airstream," *AIAA Journal*, Vol. 18, No. 9, September 1980, pp. 1101-1102.

[29] Collier, A.S., Lafferty, J.F., Swinford, S.S. and Witte, D.W., "Aerodynamic Heat Transfer Testing in Hypersonic Wind Tunnels Using an Infrared Imaging System," AIAA Paper 90-0189, January 1990.

[30] Nelson, D.J., Personal Communication, June 1990.

[31] Barber, M.J., "Experimental Investigation of Normal, Sonic Injection Through a Wedge-Shaped Nozzle into Supersonic Flow," M.S. Thesis, Virginia Polytechnic Institute and State University, January 1991.

[32] Schetz, J.A., Personal Communication, July 1990.

[33] Grove Valve and Regulator Co., Product Catalog, Bulletin #12/88-P-9.

[34] Beranek, L., *Noise and Vibration Control*, McGraw-Hill, Inc., New York, NY, 1971.

[35] Ninnemann, T.A., "Aspirating Probes for Measurement of Mean Concentration and Fluctuating Quantities in Supersonic Air/Helium Shear Layers," M.S. Thesis, Virginia Polytechnic Institute and State University, December 1990.

[36] Liepmann, H.W. and Roshko, A., *Elements of Gasdynamics*, John Wiley and Sons, Inc., New York, NY, 1967.

[37] Ninnemann, T.A., Personal Communication, August 1991.

[38] Ninnemann, T.A., Personal Communication, August 1991.

[39] Inframetrics, "Installation and Operation of the Inframetrics Model 600 IR Imaging Radiometer," Manual 04625-000 Rev. B.

Figures

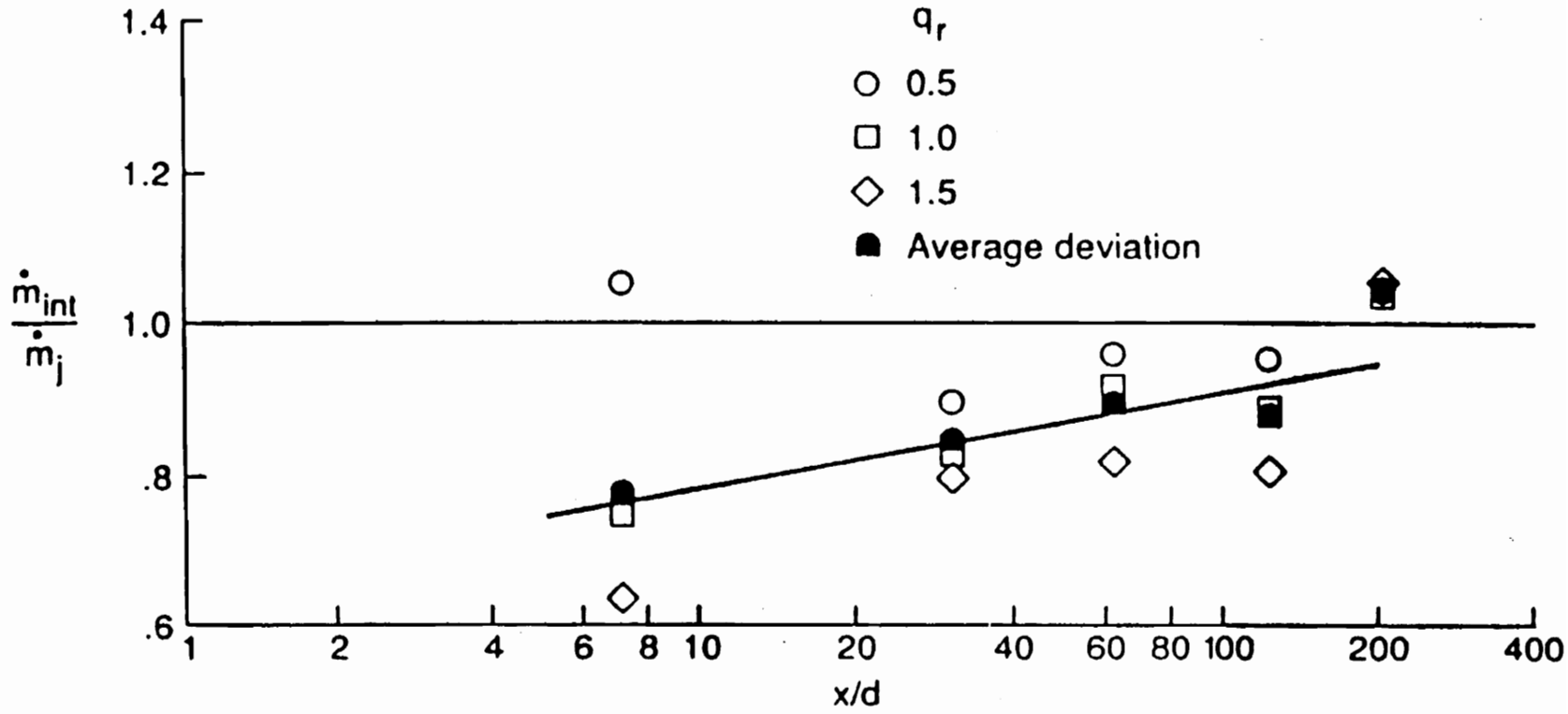

Figure 1. Integrated Mass Flow Results (Rogers)

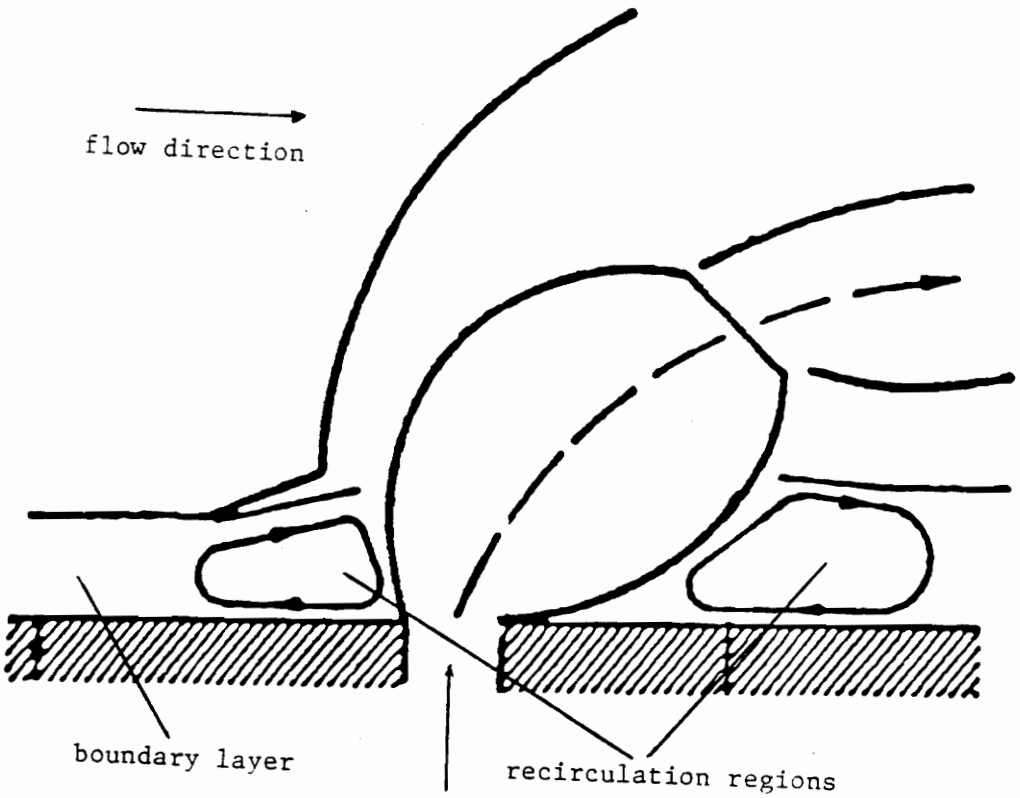

Figure 2. Illustration of Normal Injection

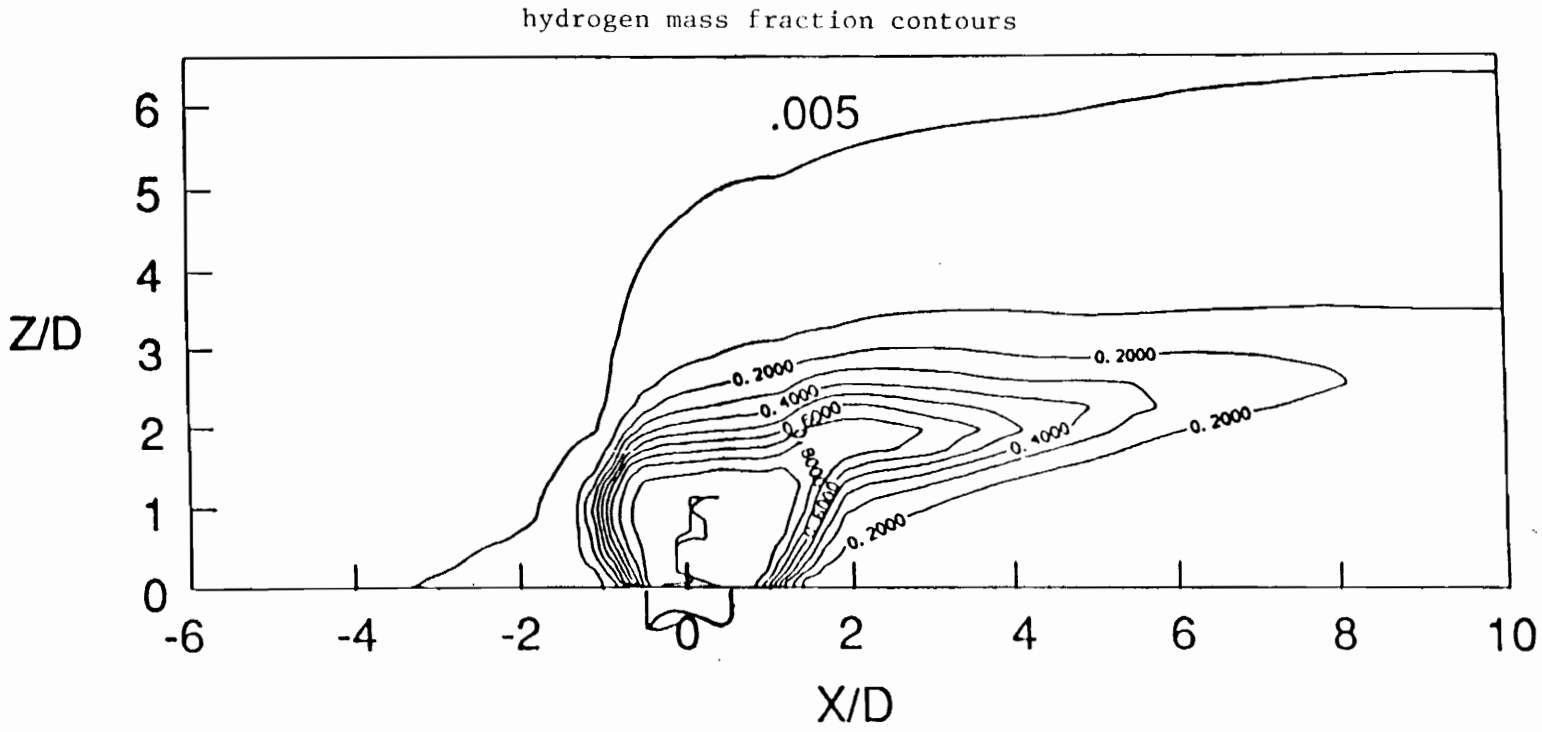

Figure 3. Simulation of Normal Injection of Hydrogen into a Mach 4.05 Free Stream [3]

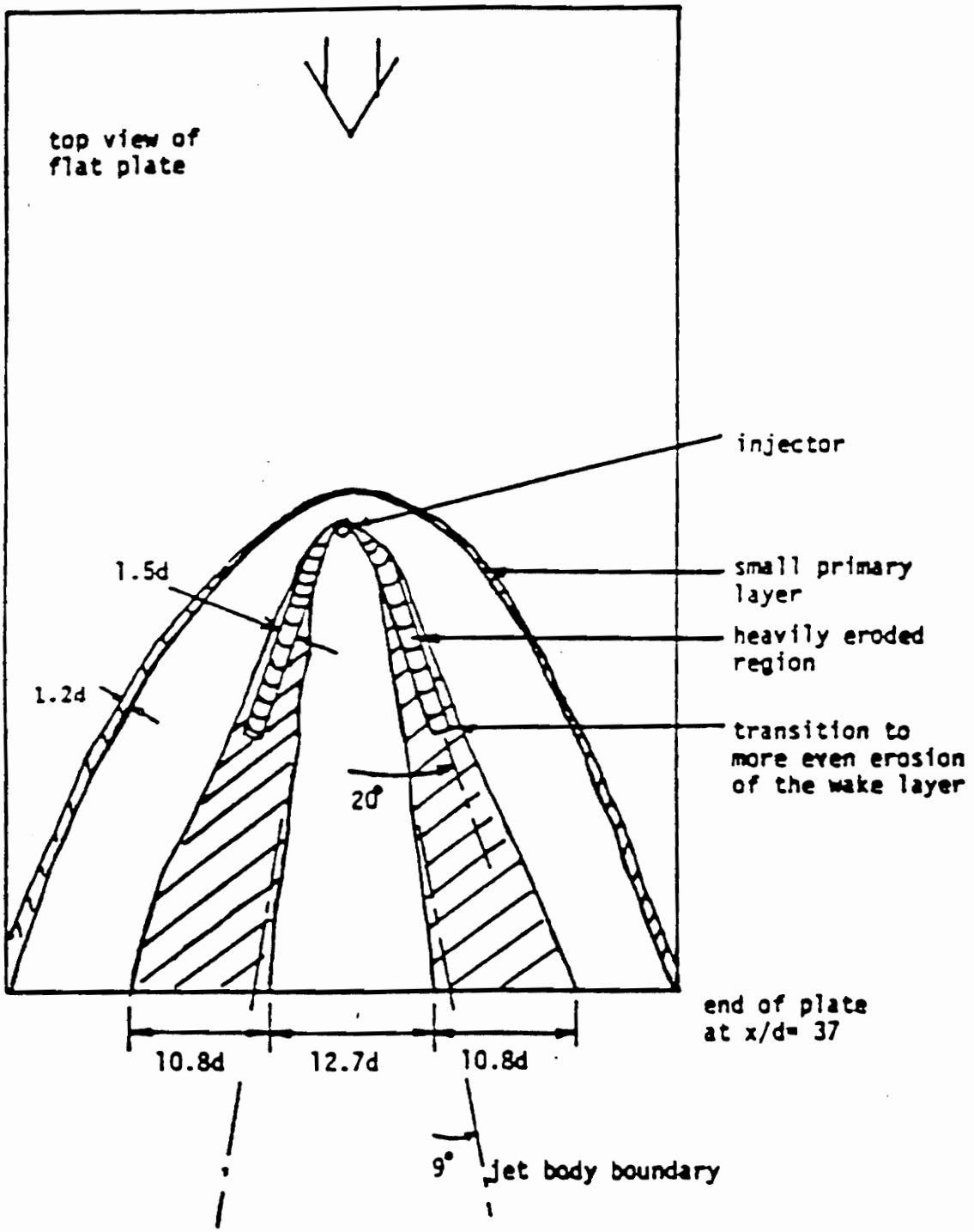

Figure 4. Surface Erosion Pattern of Liquid Slurry Injection into a Mach 3 Free Stream [2]

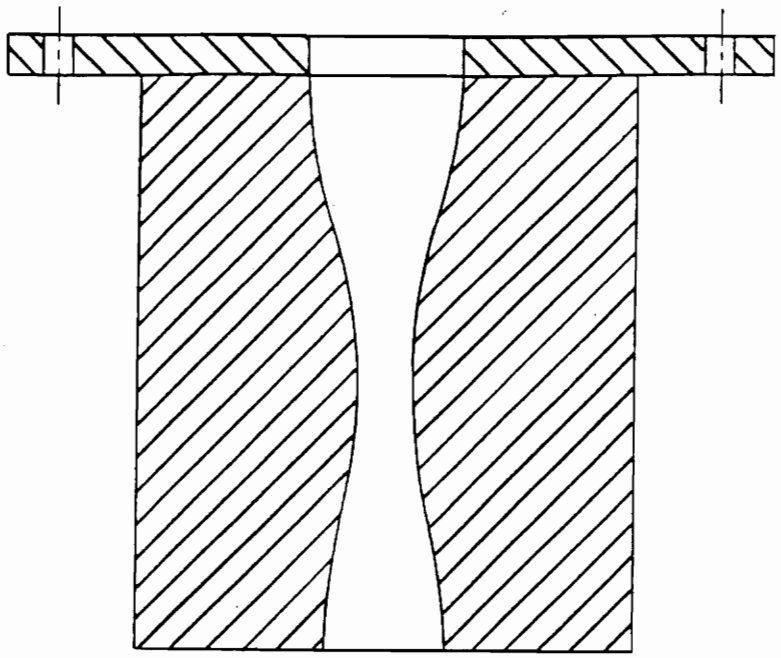

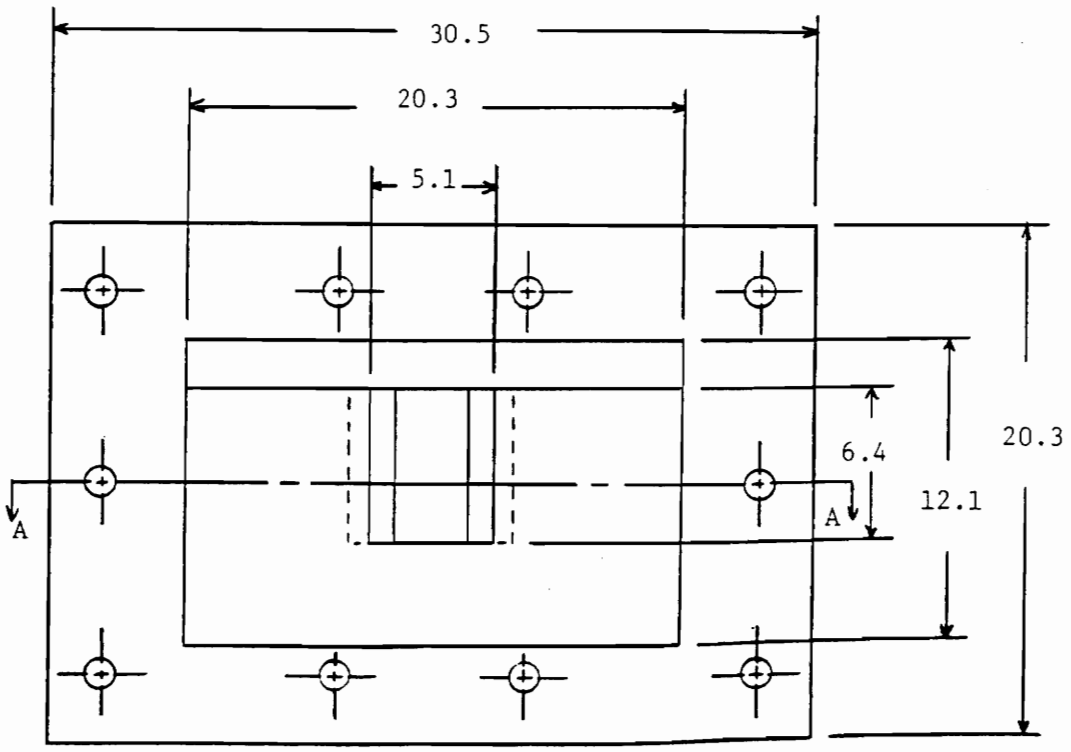

Figure 5. Mach 1.95 Nozzle (all dimensions in cm)

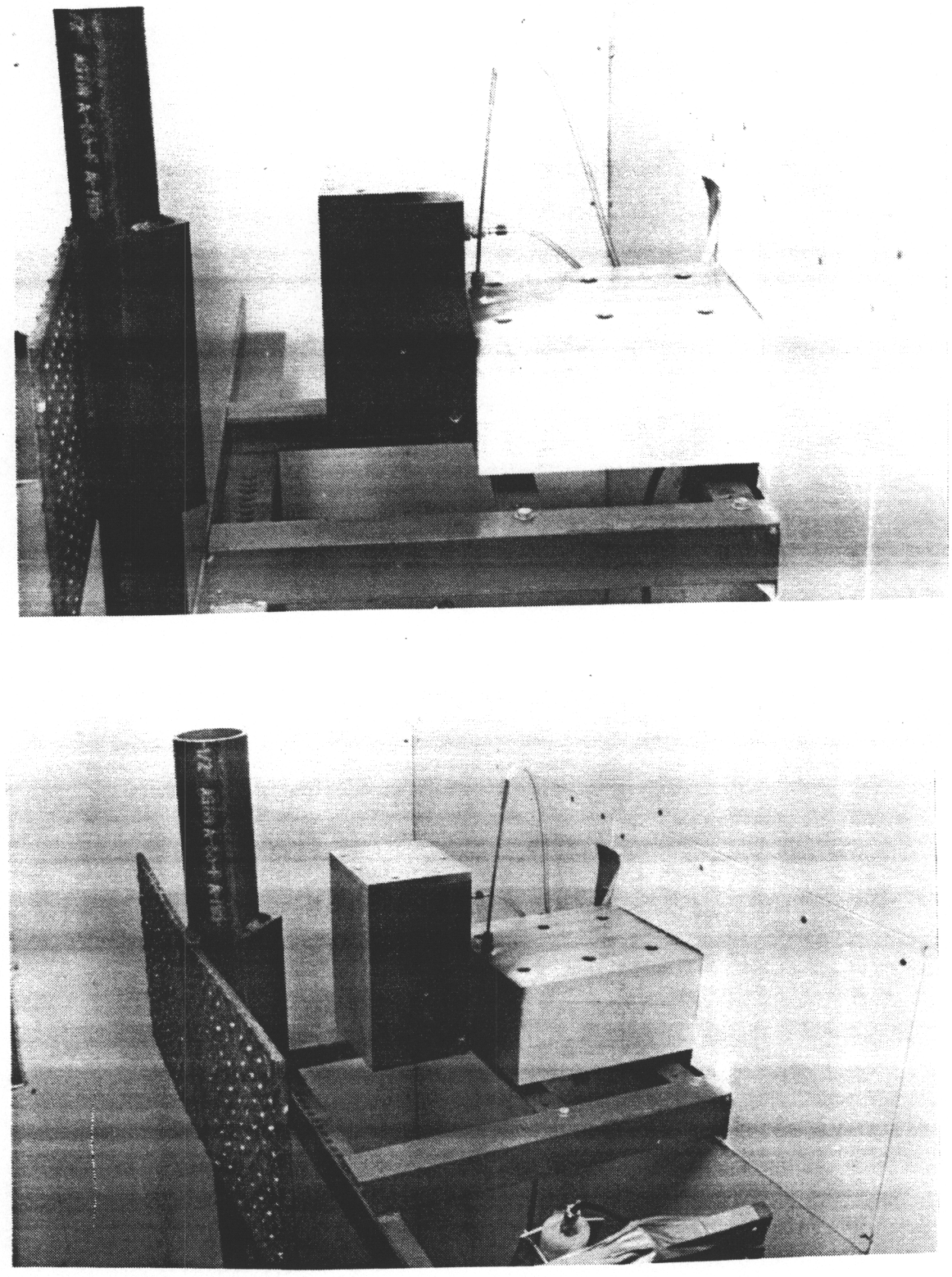

Figure 6. Free Jet Test Section

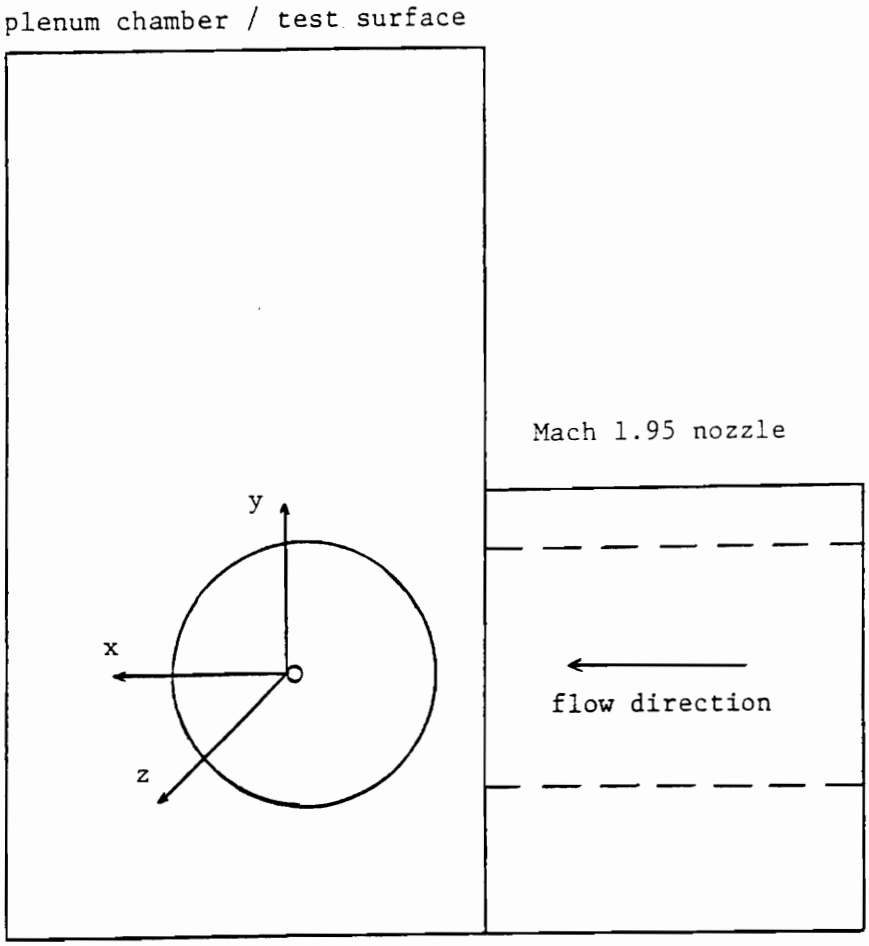

Figure 7. Test Section Coordinate System

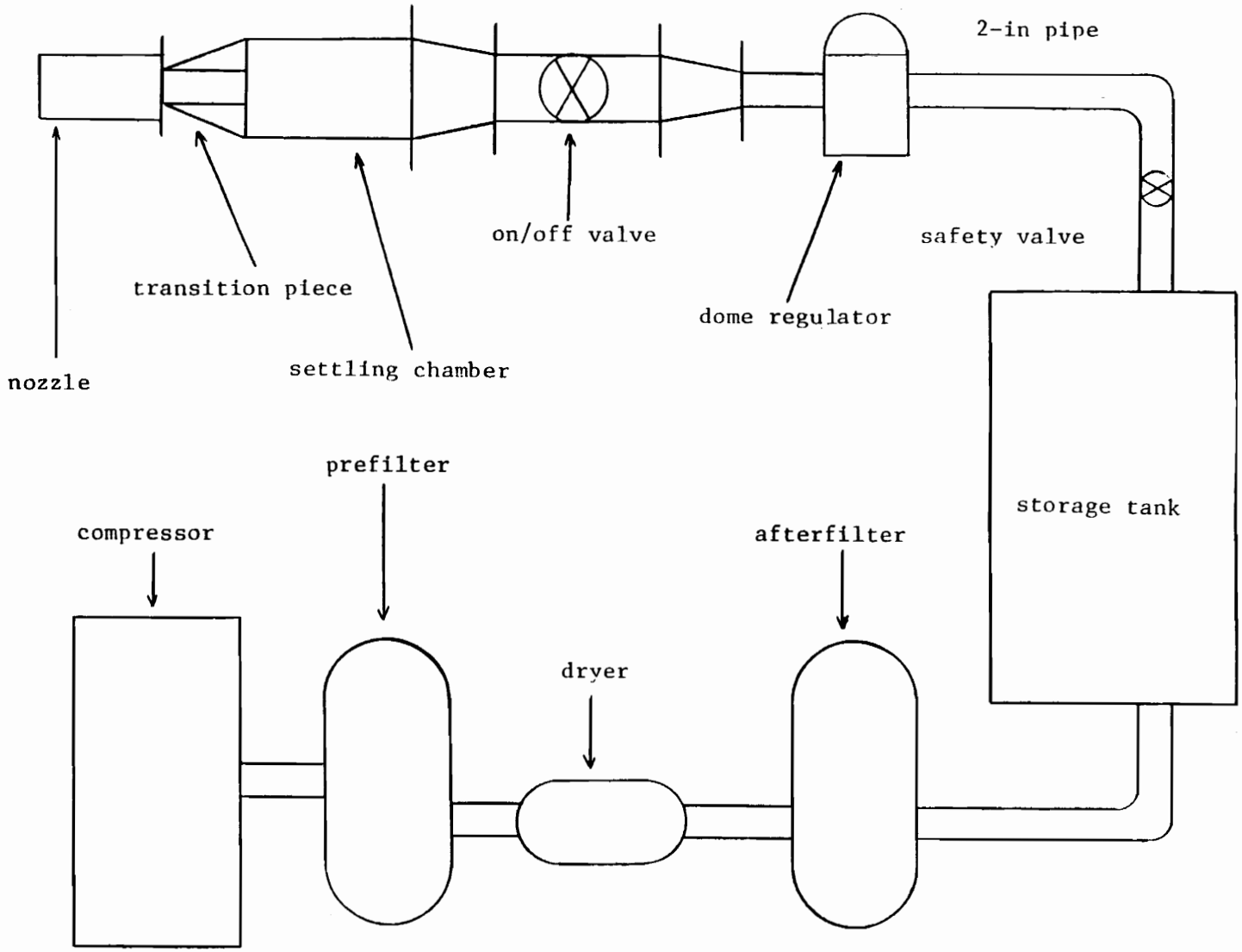

Figure 8. Free Jet Plumbing

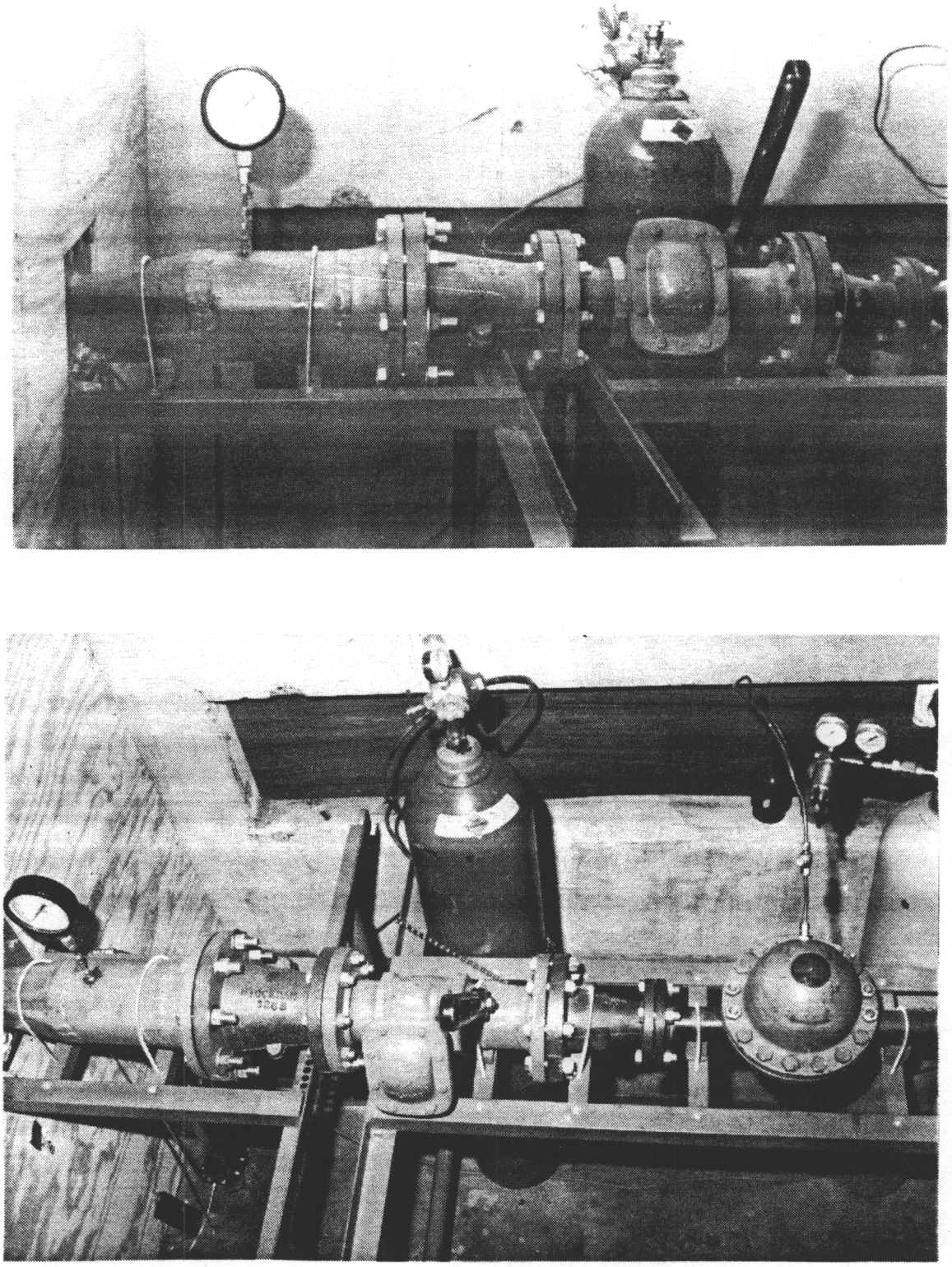

Figure 9. Free Jet Plumbing - Photograph

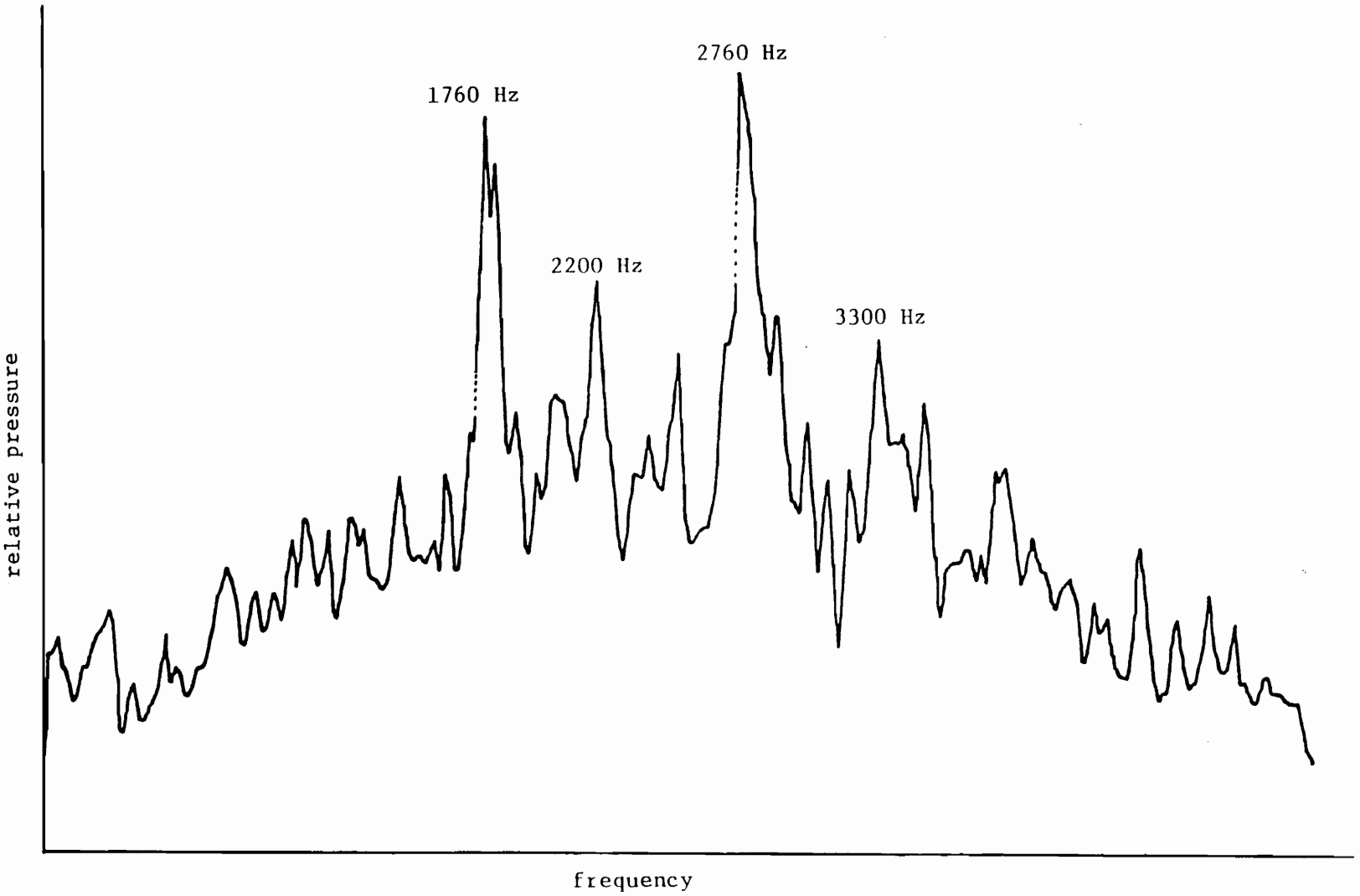

Figure 10. Free Jet Noise - Spectral Analysis

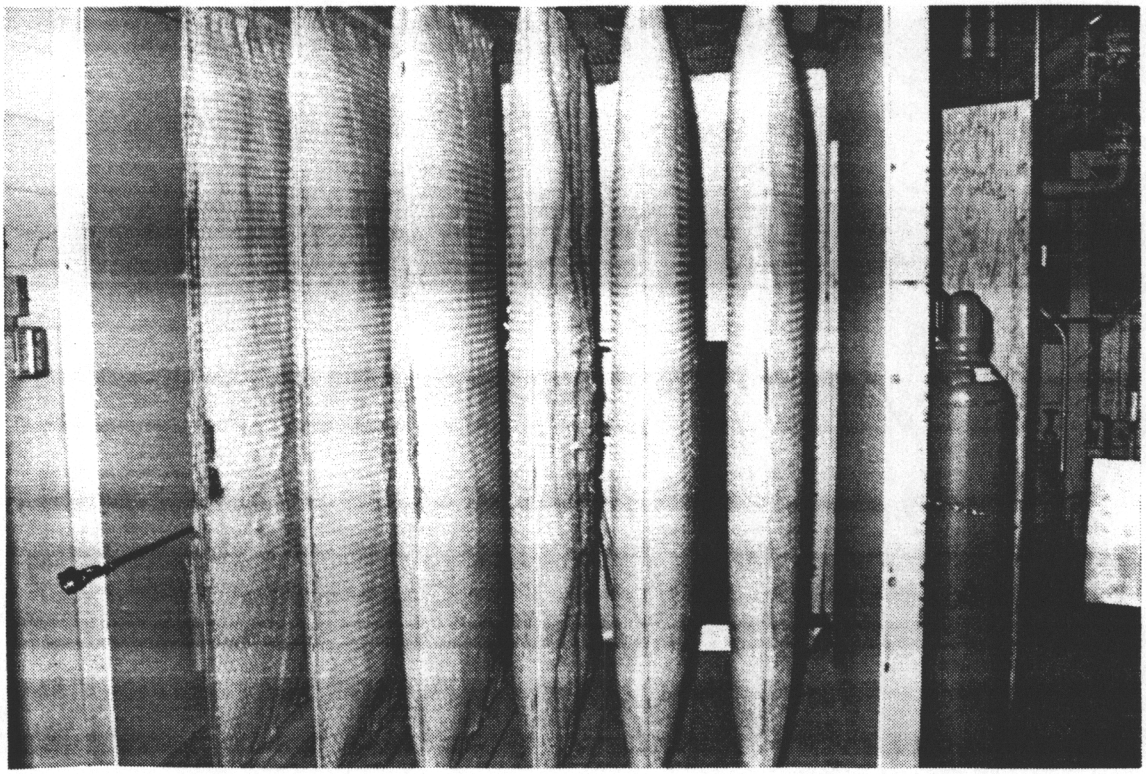

Figure 11. Sound Room Baffle Structure

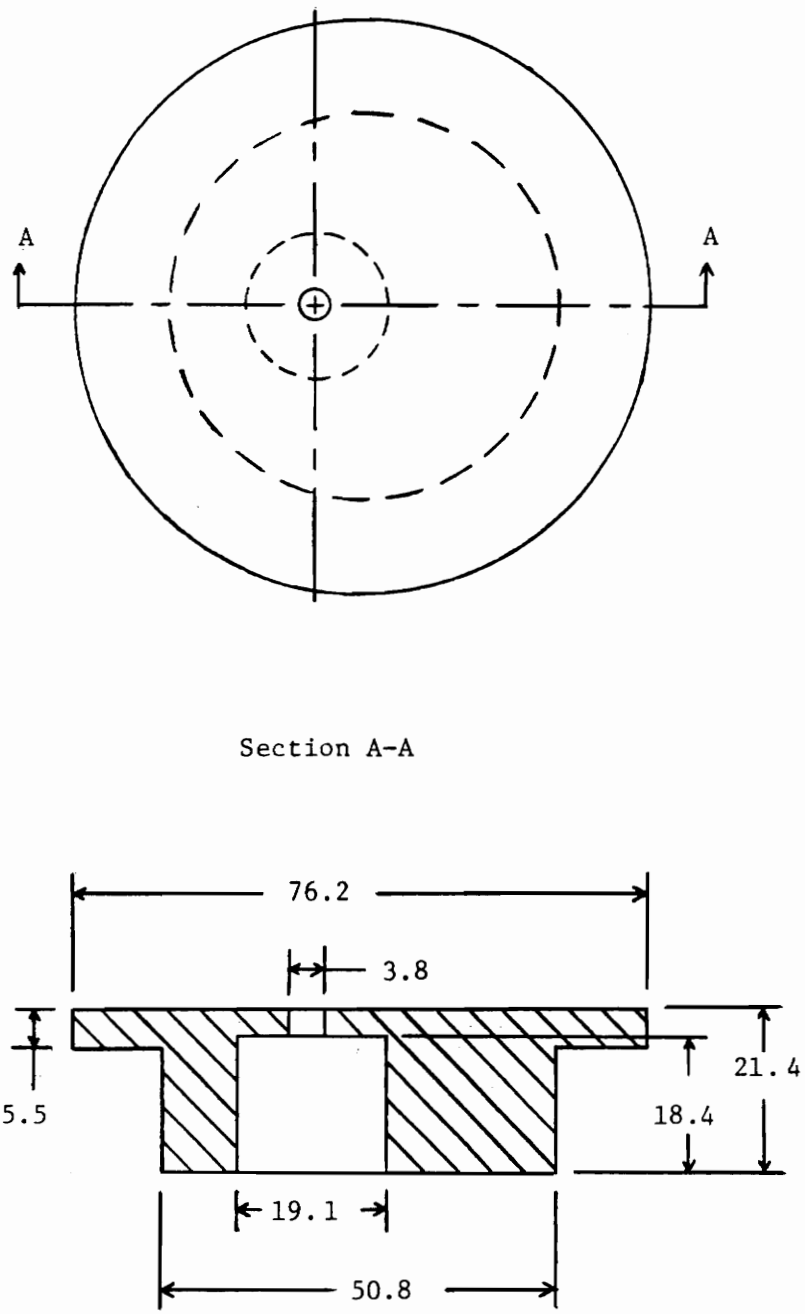

Figure 12. Circular Injector Model (all dimensions in mm)

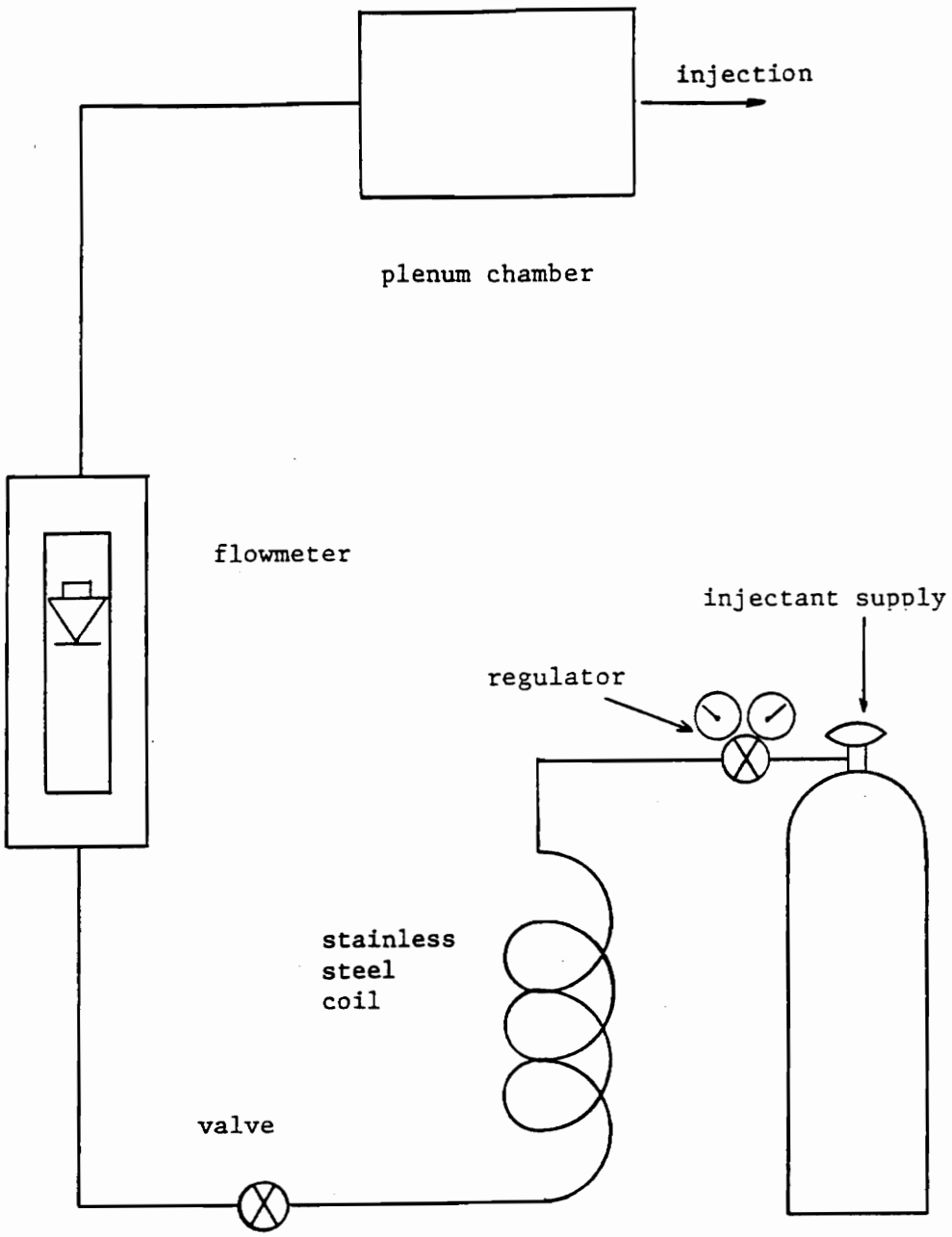

Figure 13. Injectant Supply System

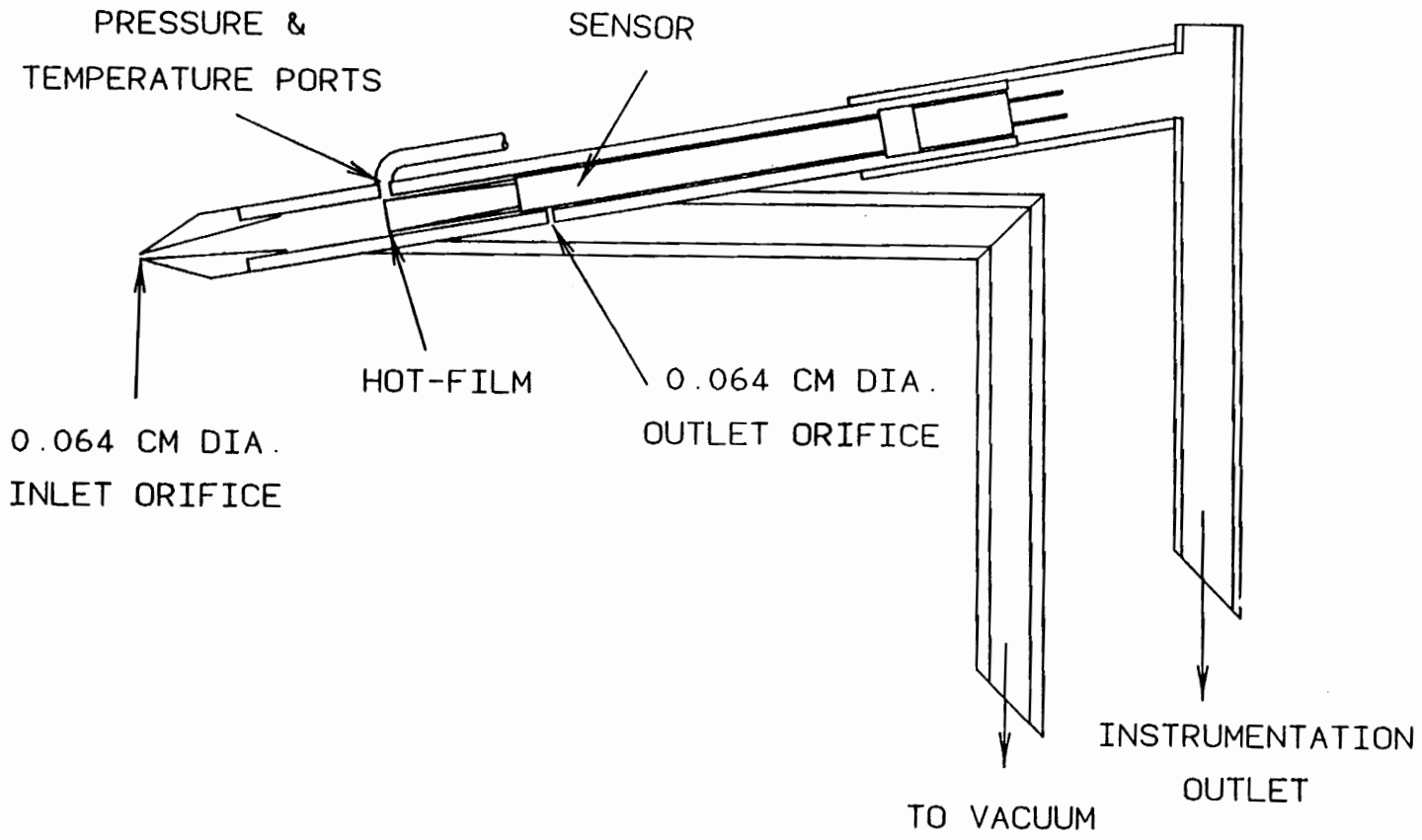

Figure 14. Concentration Probe

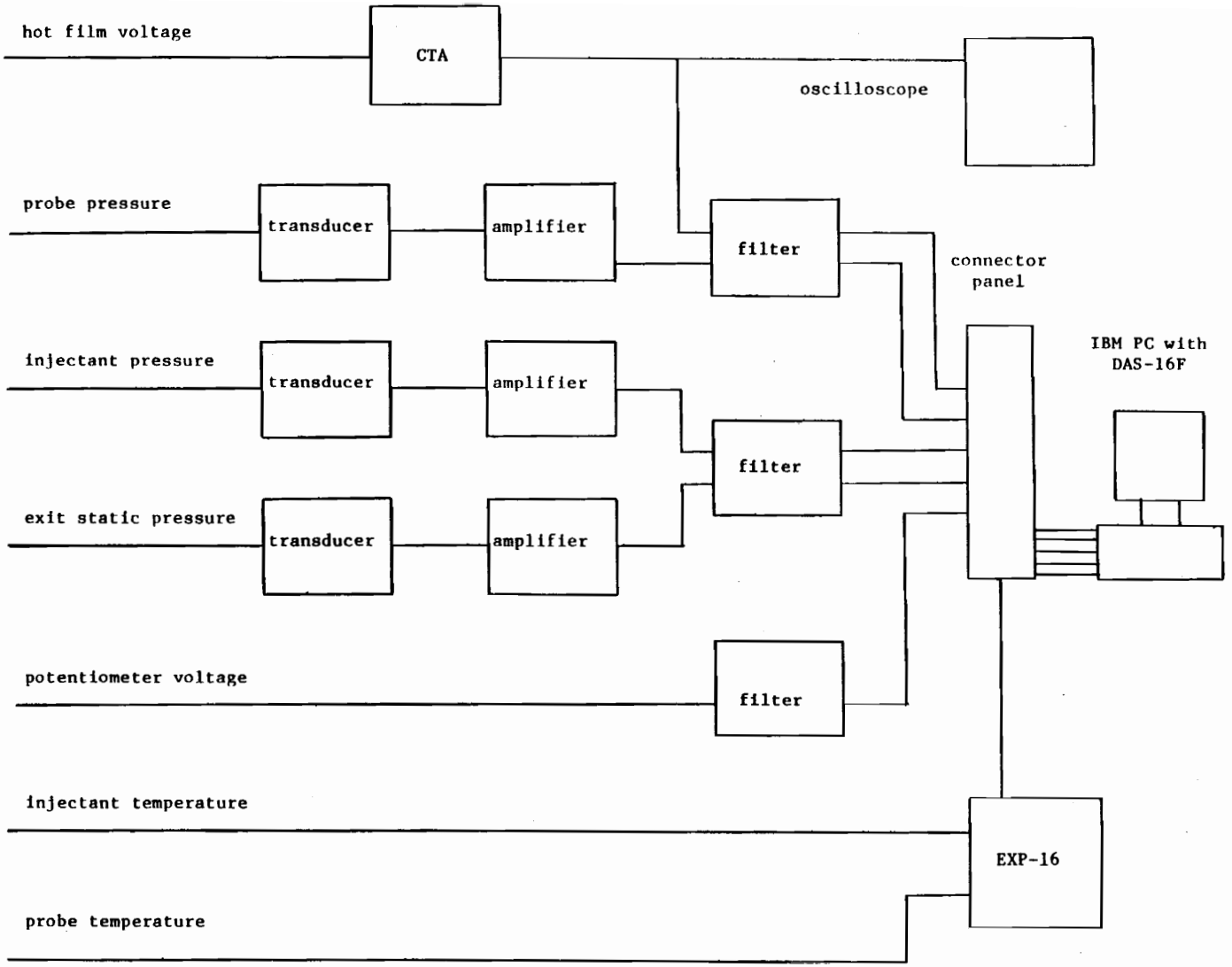

Figure 15. Data Acquisition System

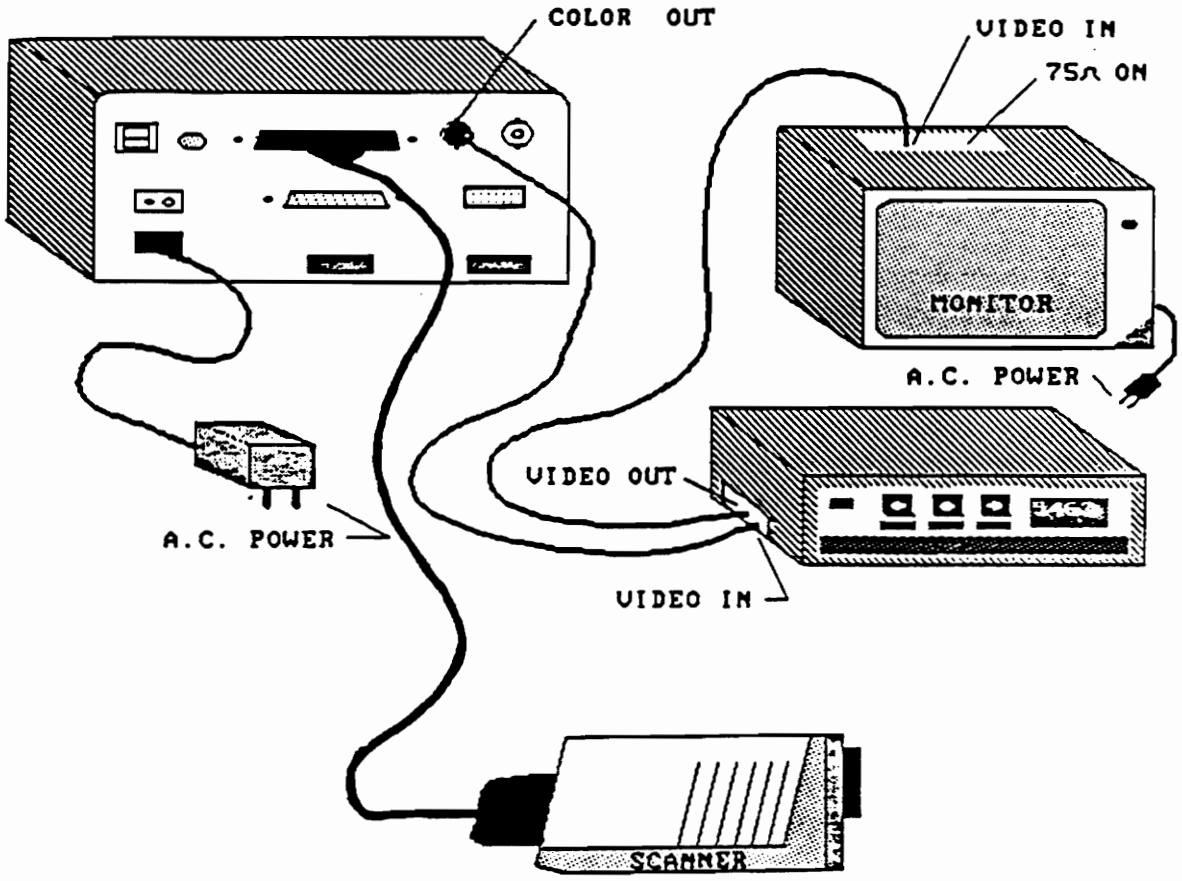

Figure 16. Infrared Imaging System [39]

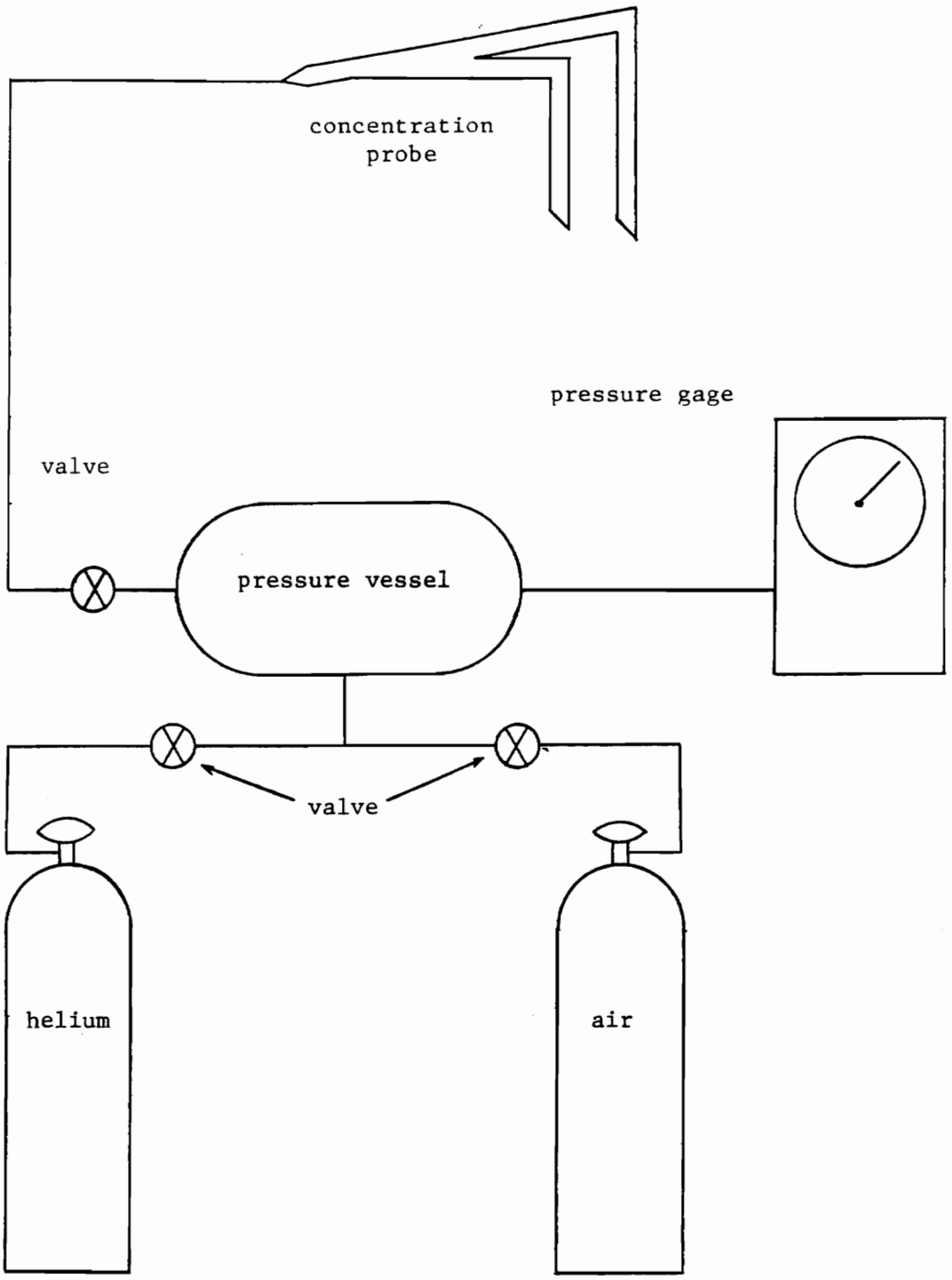

Figure 17. Concentration Probe Calibration Hardware

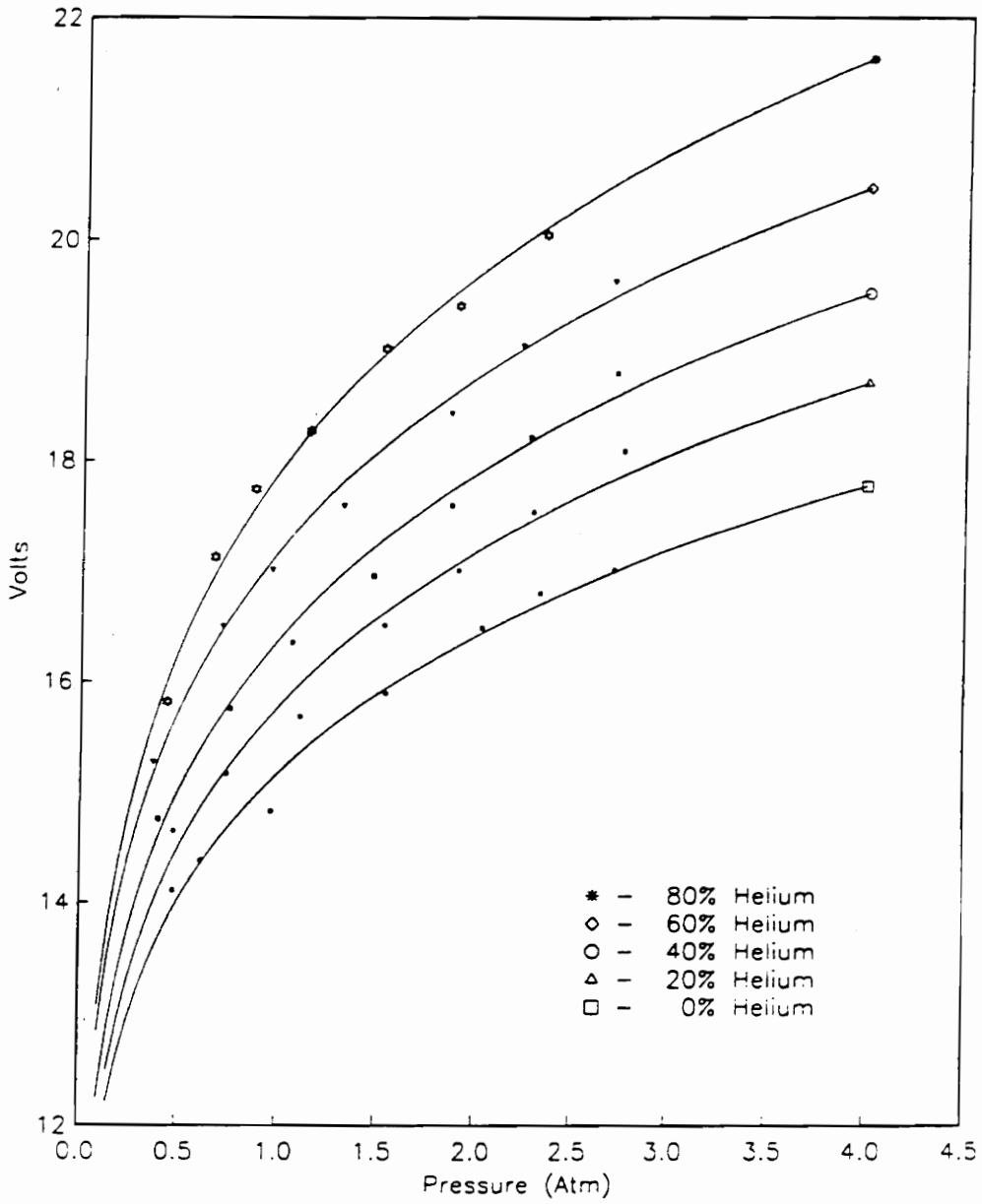

Figure 18. Typical Concentration Probe Calibration Curves [1]

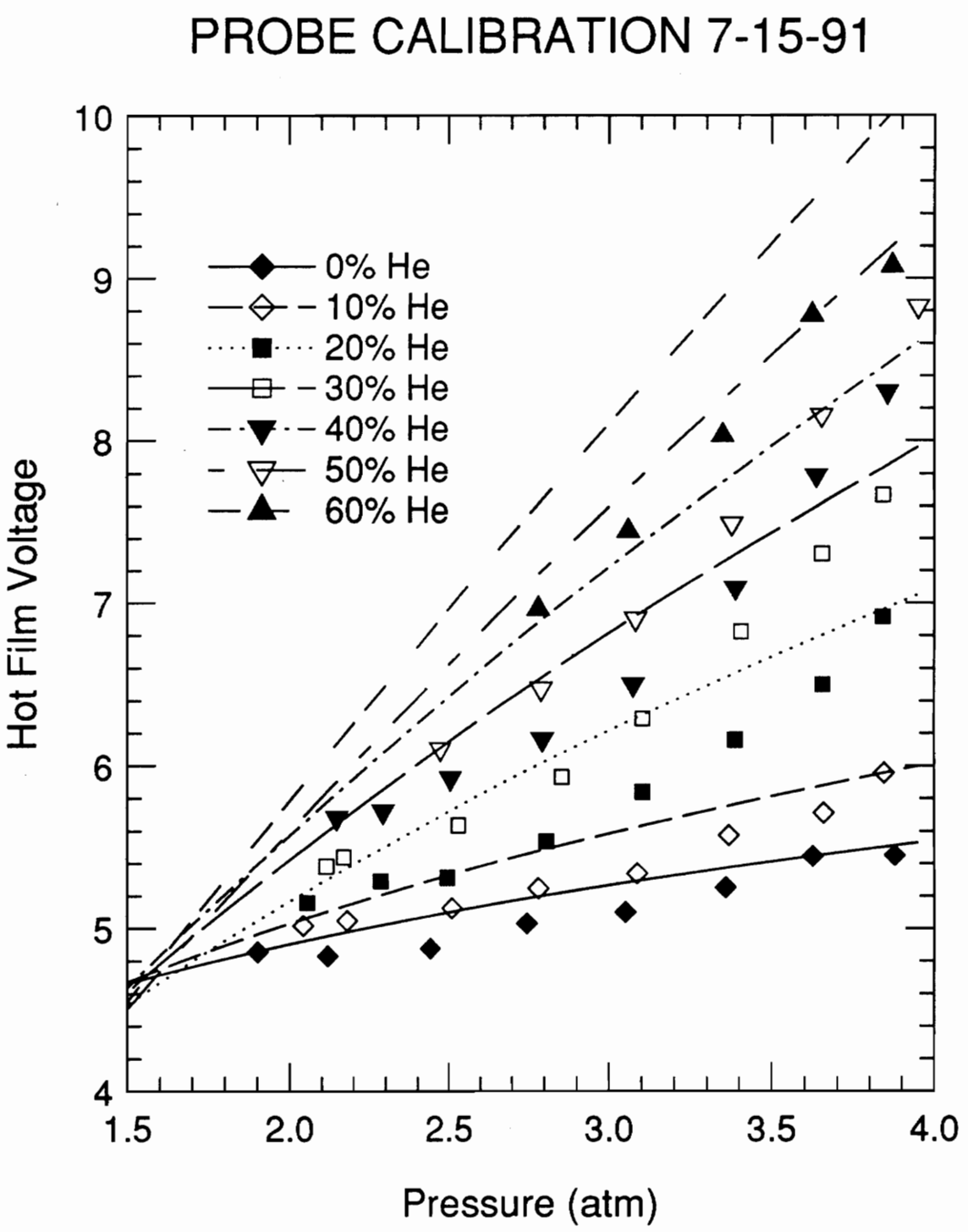

Figure 19. Concentration Probe Calibration Curves - High Pressure Range

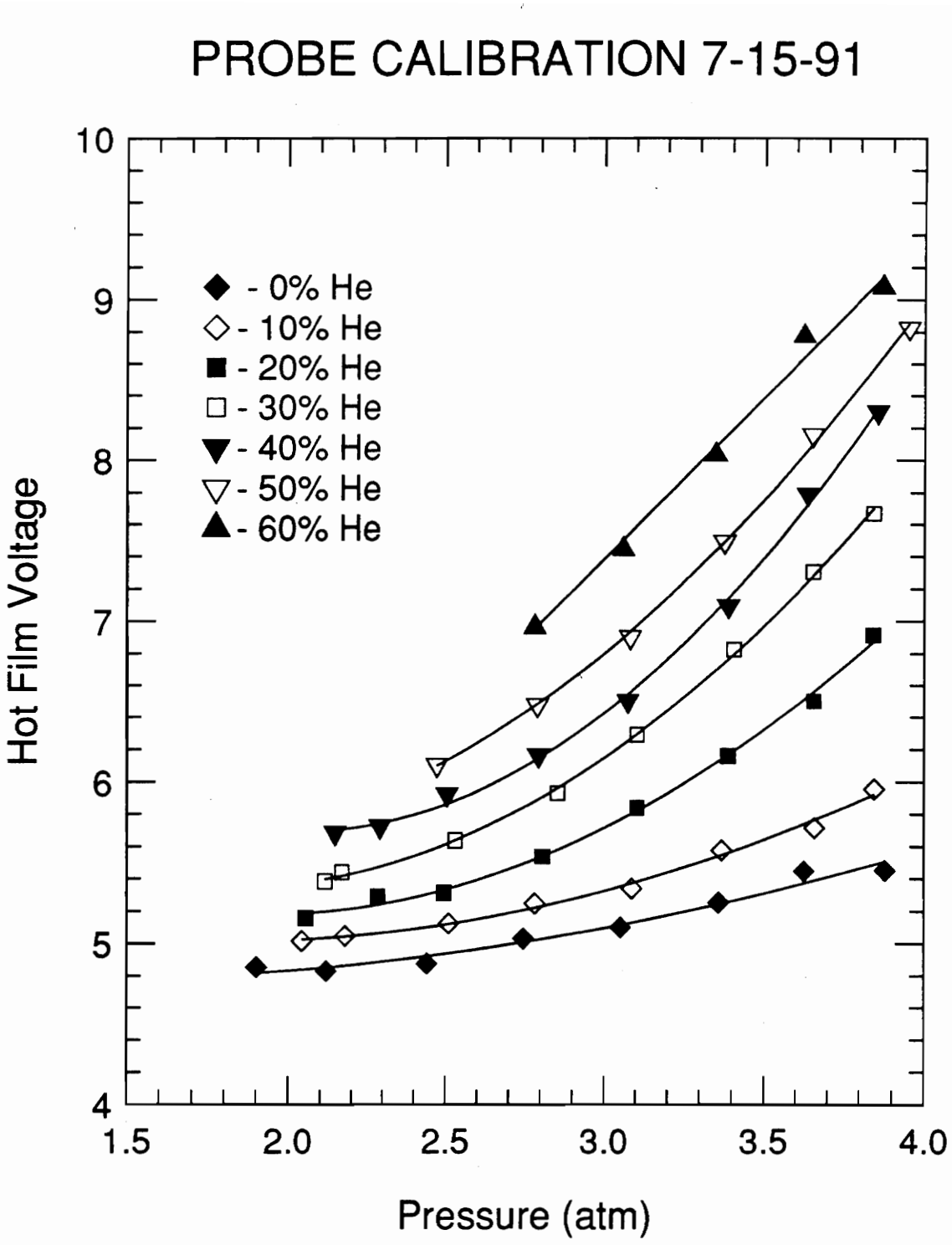

Figure 20. Concentration Probe Calibration Curves - Empirical Method

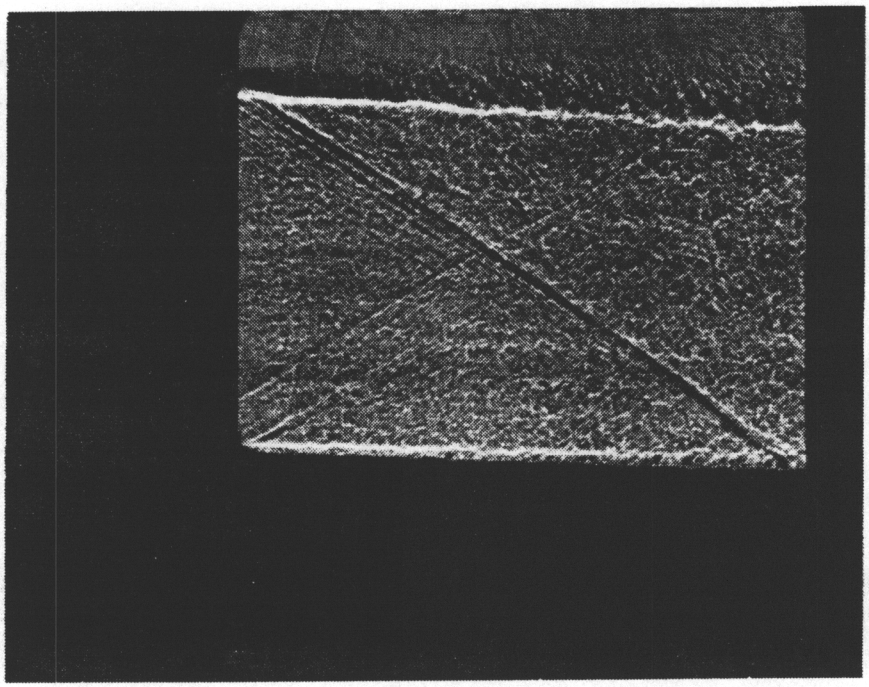

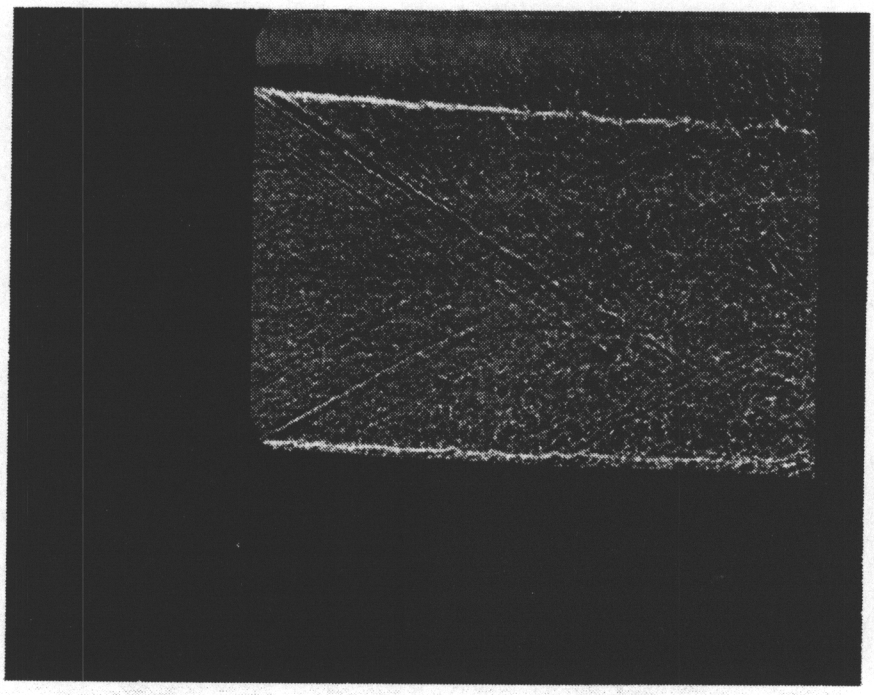

Figure 21. Nanoshadowgraph Photographs, No Injection

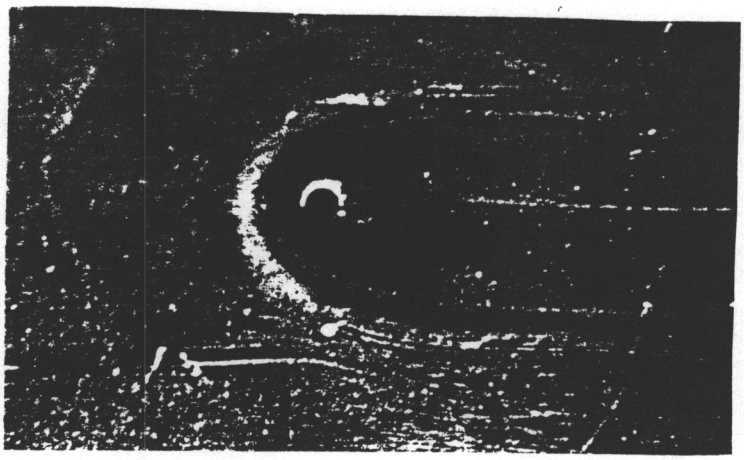

a. Expansion Ratio = 1.20

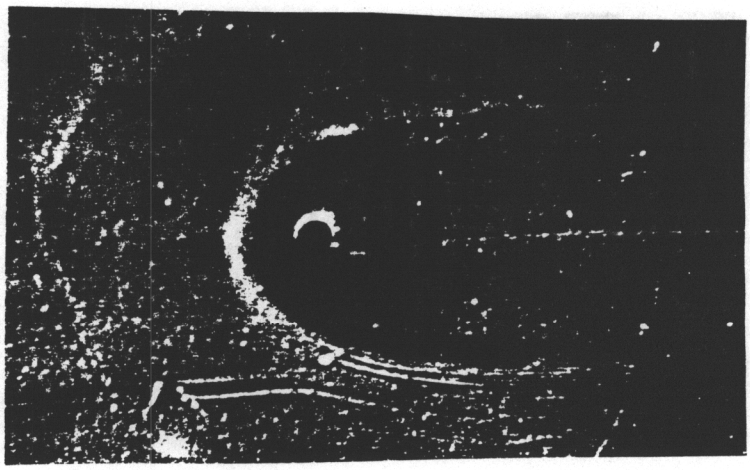

b. Expansion Ratio = 1.45

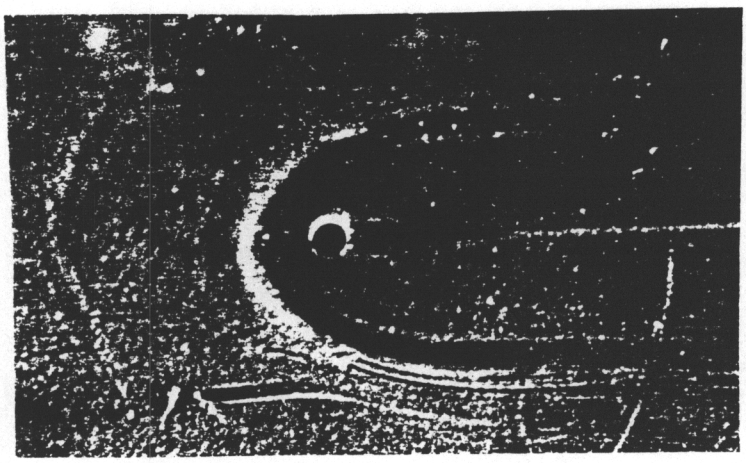

c. Expansion Ratio = 1.70

Figure 22. Oil Flow Photographs, Helium Injection

Figure 23. Nanoshadowgraph Photograph, Expansion Ratio = 1.20

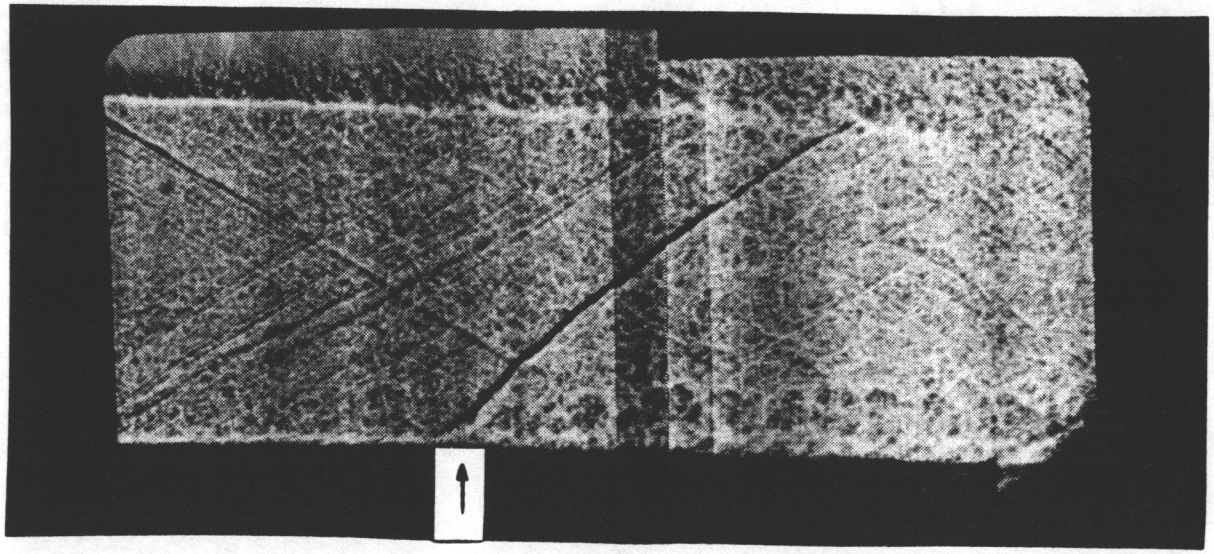

Figure 24. Nanoshadowgraph Photograph, Expansion Ratio = 1.45

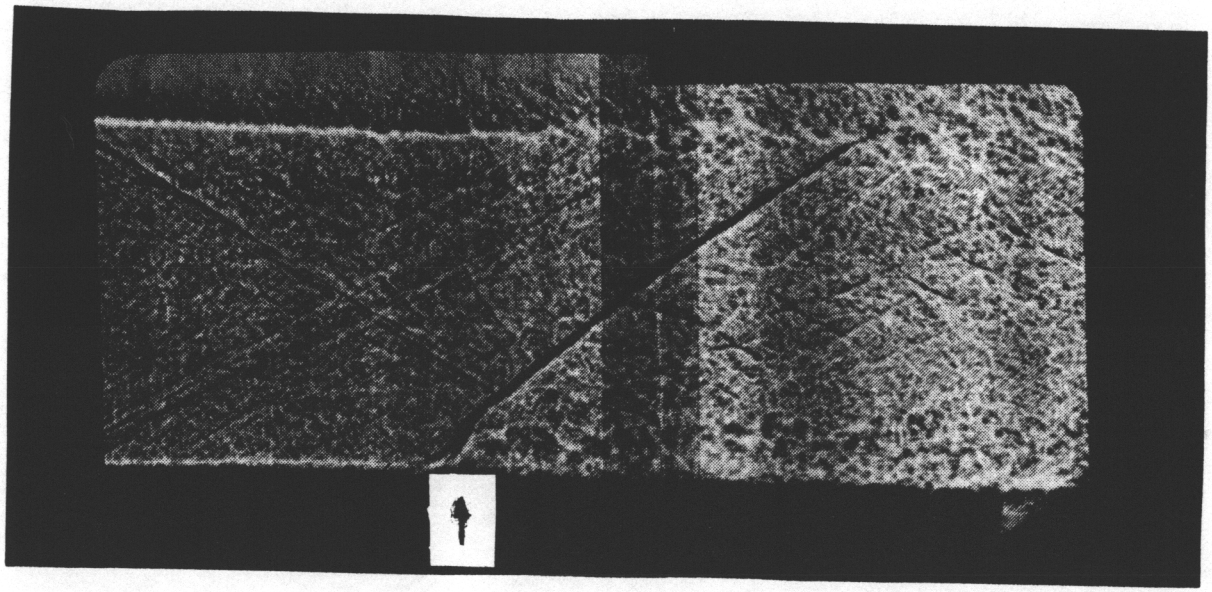

Figure 25. Nanoshadowgraph Photograph, Expansion Ratio = 1.70

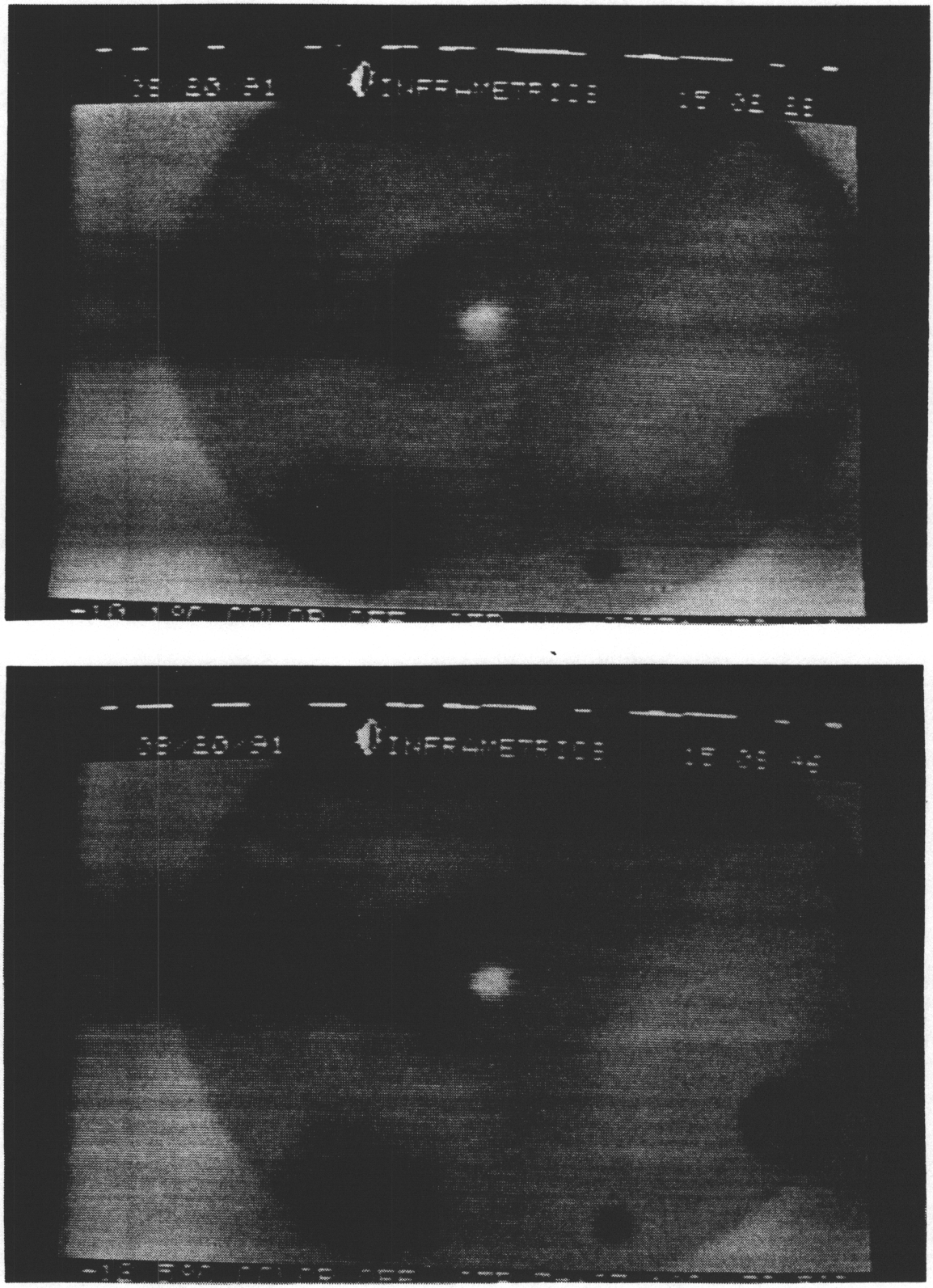

Figure 26. Infrared Images, Heated Injection

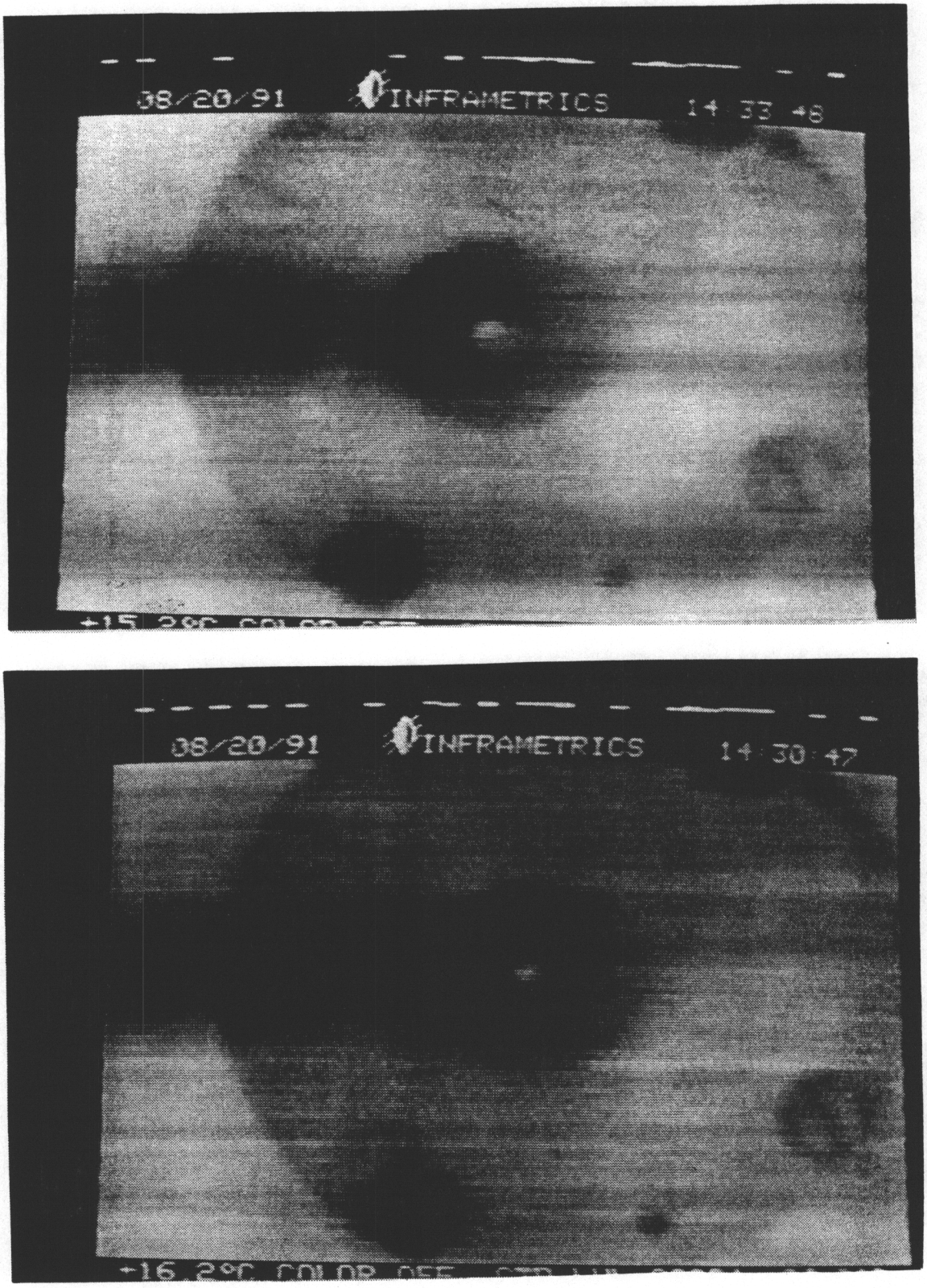

Figure 27. Infrared Images, Unheated Injection

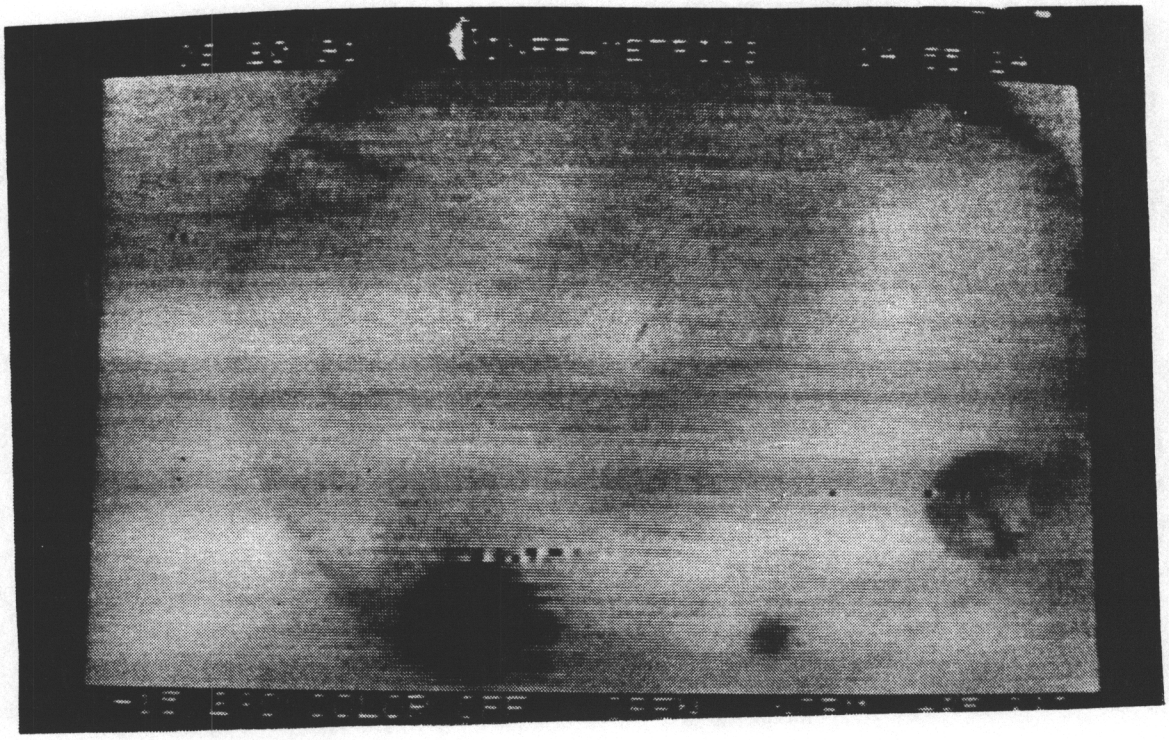

a. Photograph as Injectant is Turned On

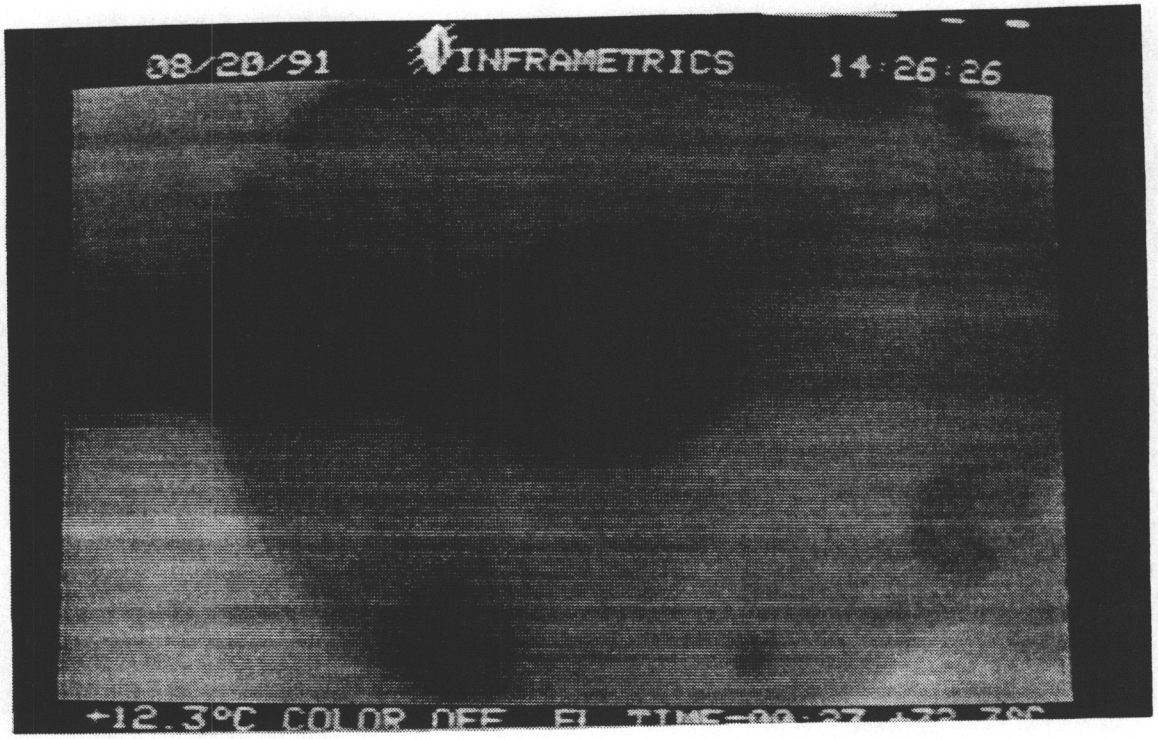

b. Photograph at Free Jet Shutdown

Figure 28. Infrared Images, Transient Flow Patterns

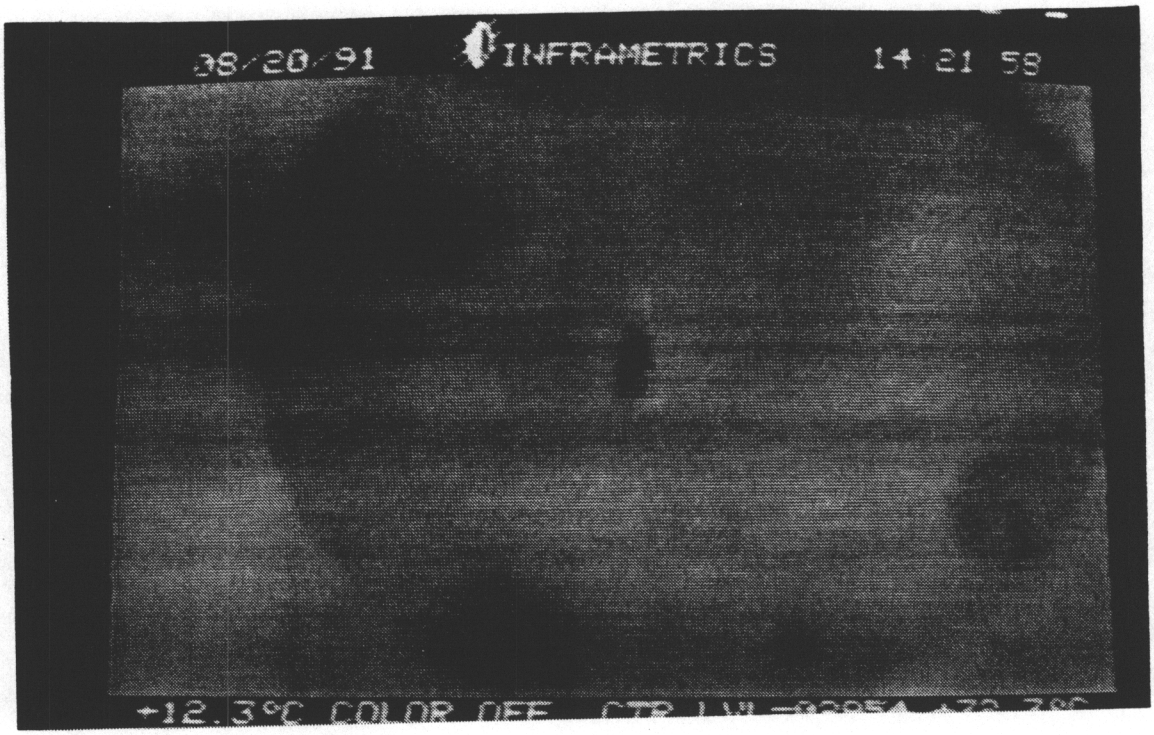

a. No Injection

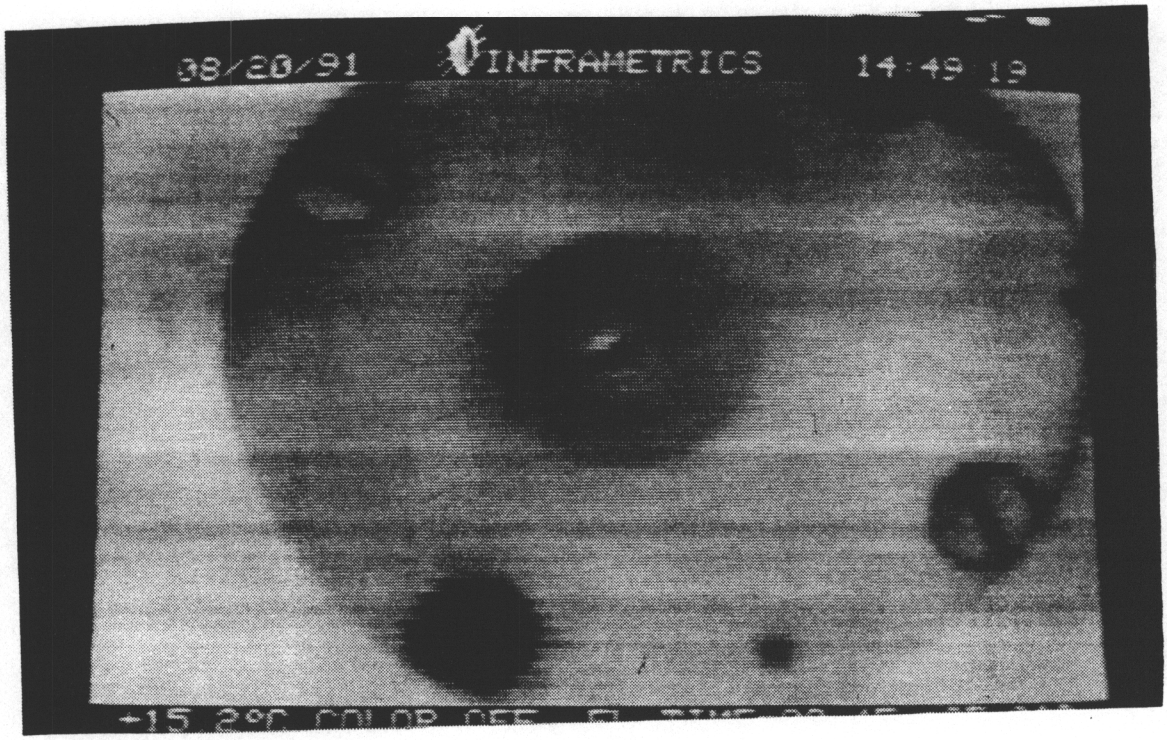

b. Facility Shutdown

Figure 29. Infrared Images

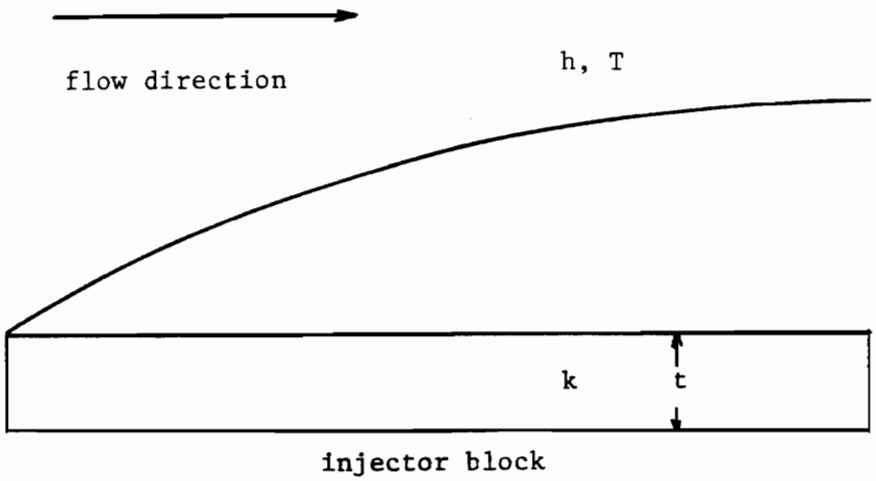

Figure 30. Heat Transfer Analysis of Injector Block

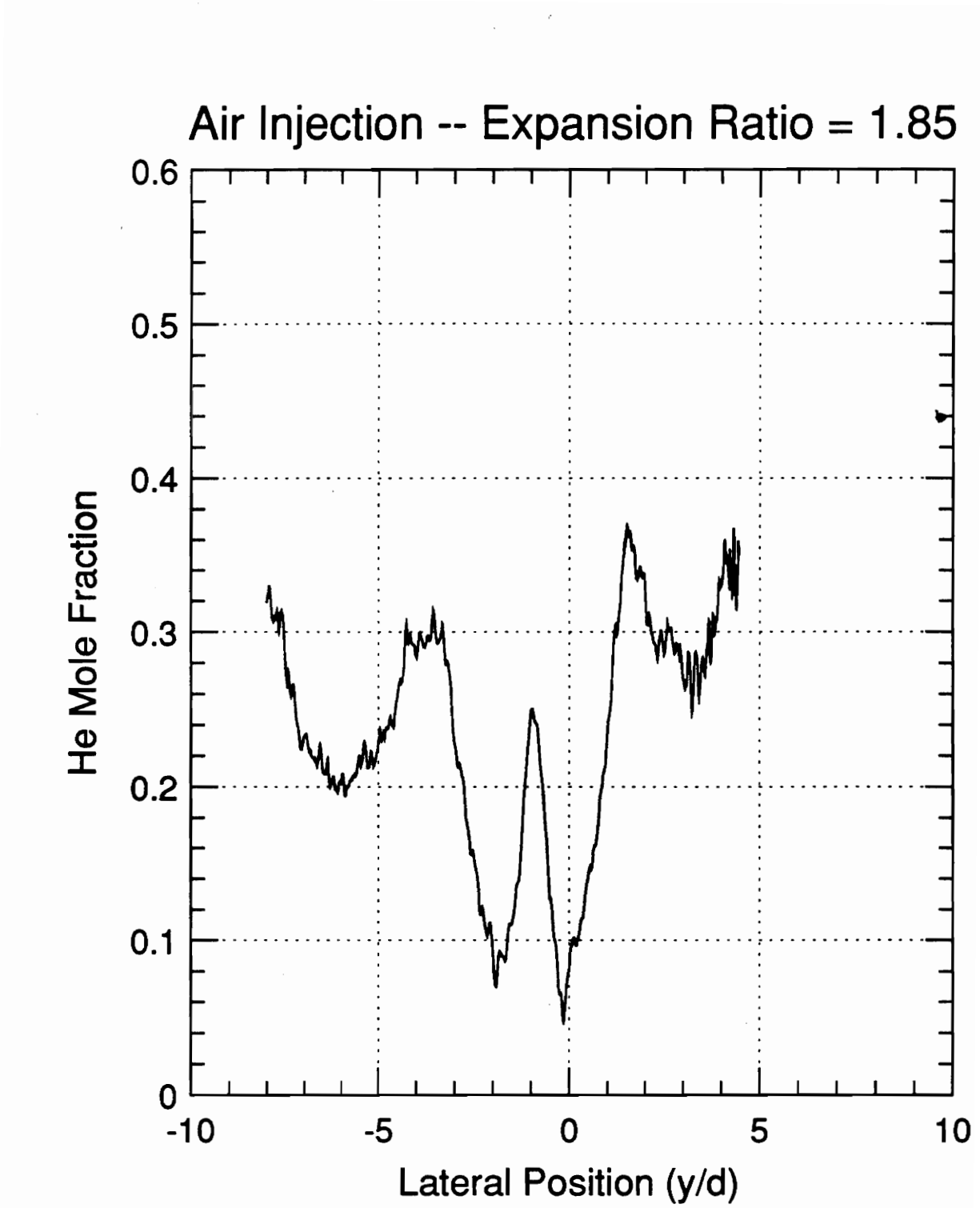

Figure 31. Helium Concentration Measurements, Air Injection Expansion Ratio = 1.85, $\frac{x}{d} = 6.9$

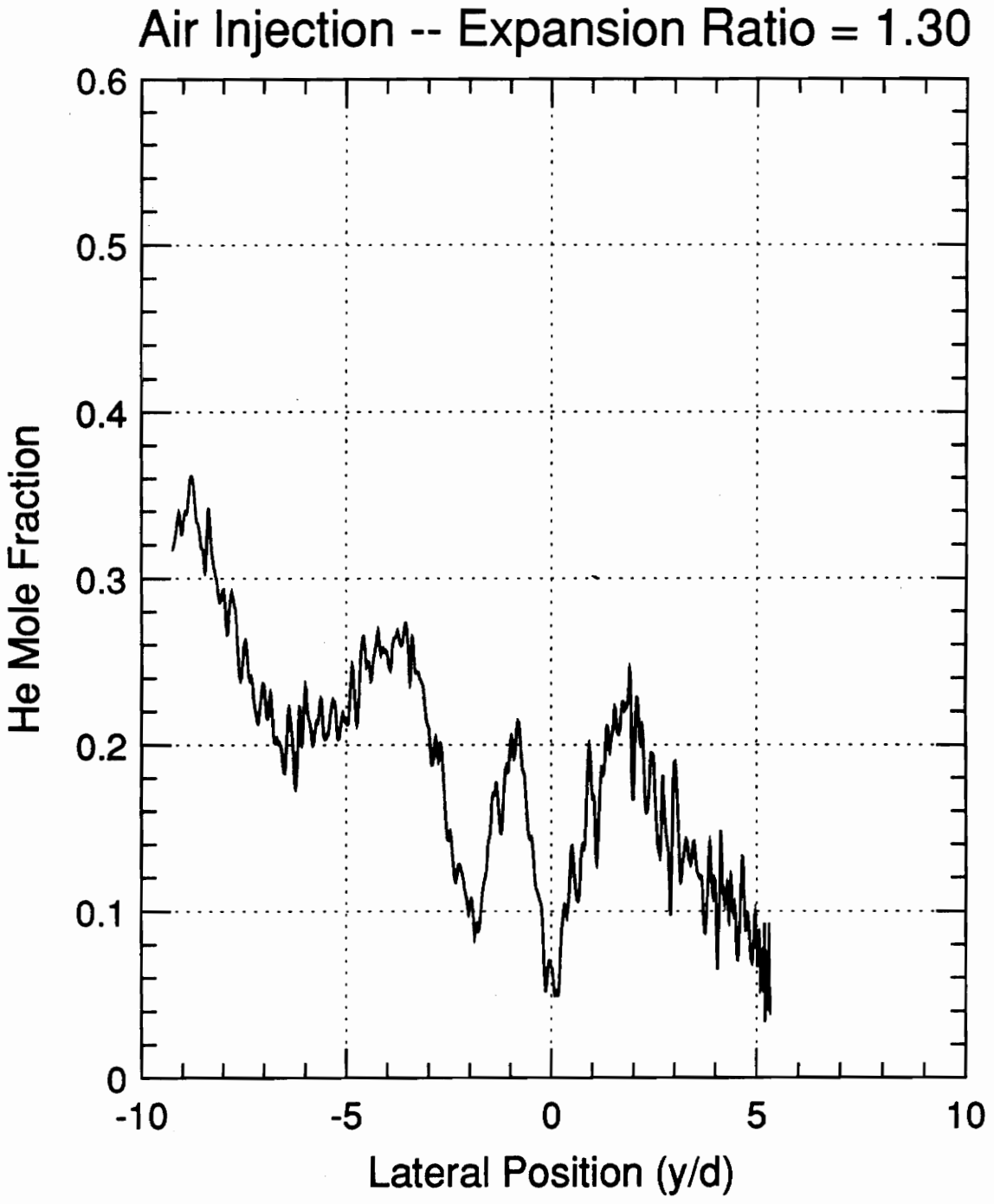

Figure 32. Helium Concentration Measurements, Air Injection Expansion Ratio = 1.30, $\frac{x}{d} = 10.9$

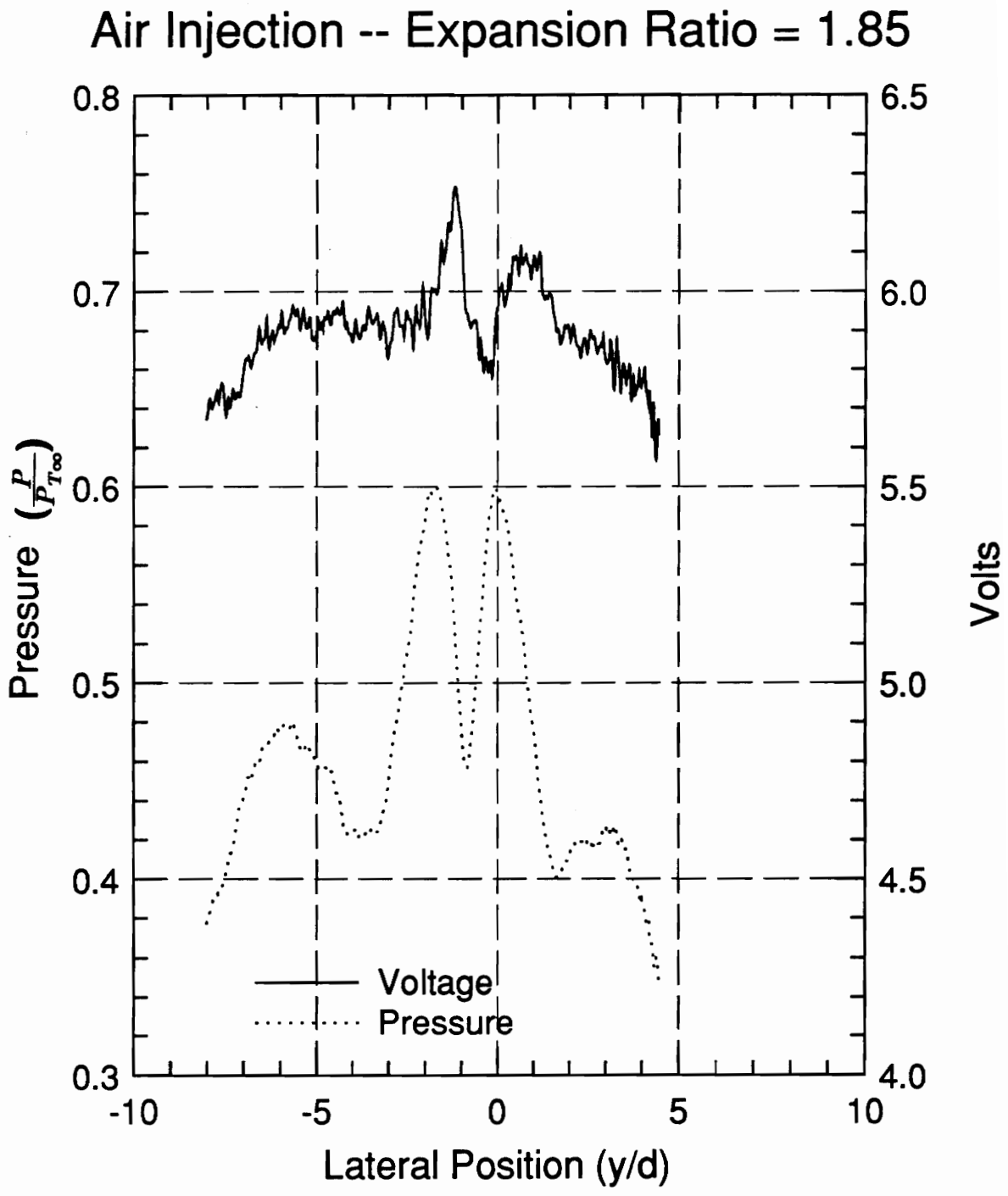

Figure 33. Probe Pressure, Sensor Voltage, Air Injection Expansion Ratio = 1.85, $\frac{x}{d} = 6.9$

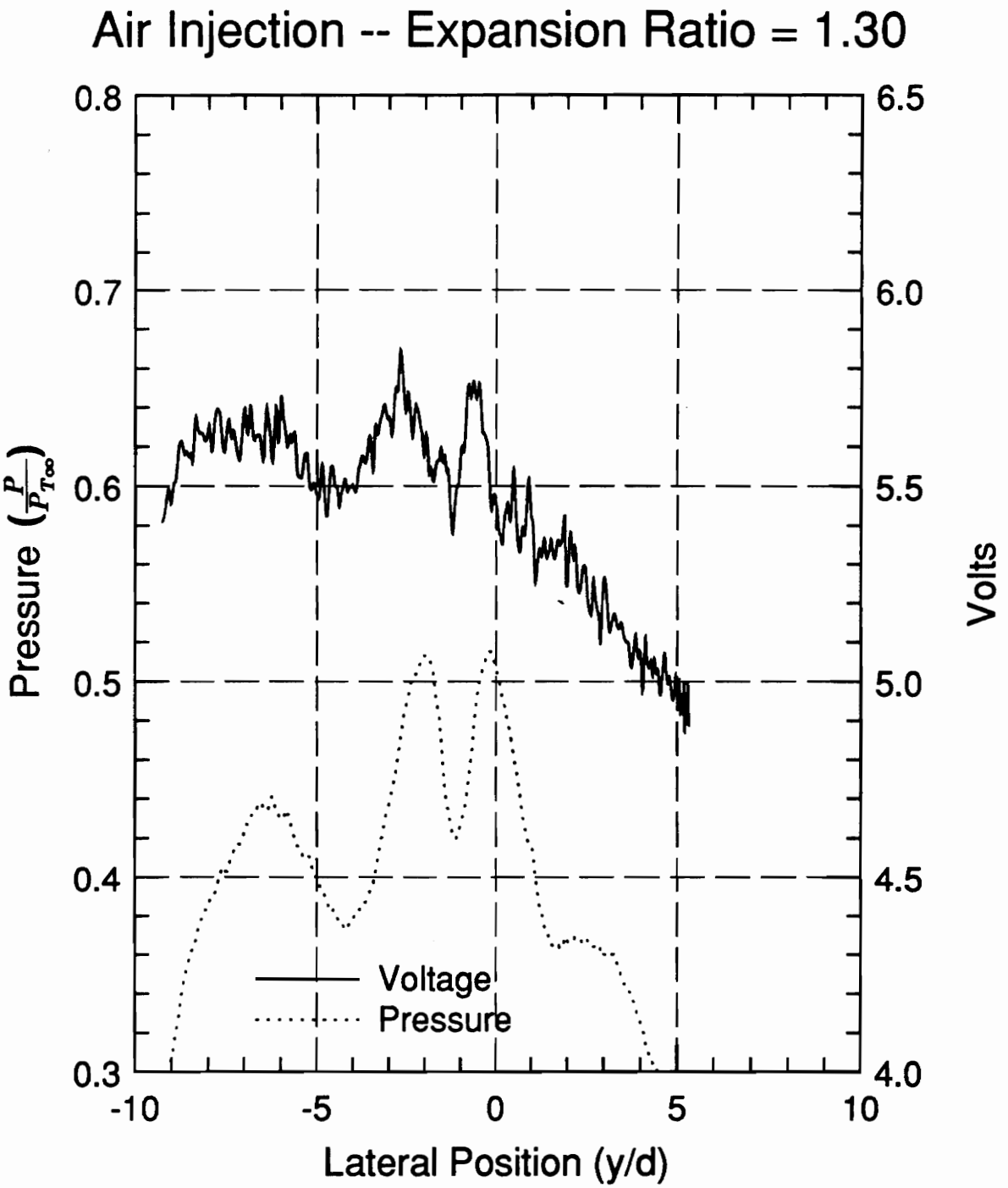

Figure 34. Probe Pressure, Sensor Voltage, Air Injection Expansion Ratio = 1.30, $\frac{x}{d} = 10.9$

Vita

John Richard Mills was born on May 10, 1967 in Newport News, Virginia. He graduated from Tabb High School in June 1985 and enrolled in Virginia Polytechnic Institute and State University in September 1985. He worked as a Cooperative Education Student at IBM, Corp. in Manassas, Virginia, where he served in many capacities. He received a Bachelor of Science Degree in Mechanical Engineering in May 1990. He stayed at VPI & SU to pursue graduate studies in Mechanical Engineering. His primary areas of interest include gas dynamics, turbomachinery and combustion. Mr. Mills is a member of Pi Tau Sigma, SAE and ASME.